In vivo magnetic resonance imaging reveals the effect of gonadal hormones on morphological and functional brain sexual dimorphisms in adult sheep. Order of Authors

David Barrière, Arsène Ella, Hans Adriaensen, Charles Roselli, Philippe Chemineau, Matthieu Keller

In vivo magnetic resonance imaging reveals the effect of gonadal hormones on morphological and functional brain sexual dimorphisms in adult sheep. Order of Authors

David Barrière, Arsène Ella, Hans Adriaensen, Charles Roselli, Philippe Chemineau, Matthieu Keller, Tracy Melzer, Kevin Whittingstall, Gerard Thompson, Lance Kriegsfeld

Manuscript Details

Manuscript number	PNEC_2019_79_R3
Title	In vivo magnetic resonance imaging reveals the effect of gonadal hormones on morphological and functional brain sexual dimorphisms in adult sheep.
Article type	Research Paper

Abstract

Sex differences in brain and behavior are produced by the perinatal action of testosterone, which is converted into oestradiol by the enzyme aromatase in the brain. Although magnetic resonance imaging (MRI) has been widely used in humans to study these differences, the use of animal models where hormonal status can be properly manipulated are necessary to explore the mechanisms involved. We used sheep, a recognized model in the field of neuroendocrinology, to assess brain morphological and functional sex differences and their regulation by adult gonadal hormones. To this end, we performed a voxel-based morphometry and a resting state functional MRI approach to assess sex differences in gonadally intact animals. We demonstrated significant sex differences in grey matter concentration (GMC) at the level of the gonadotropic axis; i.e. not only within the hypothalamus and pituitary, but also within the hippocampus and the amygdala of intact animals. We then performed the same analysis one month after gonadectomy and found that some of these differences were reduced following gonadectomy, especially in the hypothalamus and amygdala. By contrast, we found few differences in the organization of the functional connectome between males and females either before or after gonadectomy. As a whole, our study identifies brain regions that are sexually dimorphic in sheep brain at the resolution of MRI and highlights the role of gonadal hormones in the maintenance of these differences.

Keywords	sex differences; sheep; voxel-based morphometry; resting state fMRI; gonadectomy.
Manuscript category	Preclinical studies

Corresponding Author	Matthieu Keller
Corresponding Author's Institution	CNRS
Order of Authors	David Barrière, Arsène Ella, Hans Adriaensen, Charles Roselli, Philippe Chemineau, Matthieu Keller

Suggested reviewers	Tracy Melzer, Kevin Whittingstall, Gerard Thompson, Lance Kriegsfeld

Submission Files Included in this PDF

File Name [File Type]

Cover Letter.docx [Cover Letter]

Letter_to_the_editor_PNE_DAB_CER.doc [Response to Reviewers]

Highlights.docx [Highlights]

SexDiff_final.docx [Manuscript File]

Figure_1.jpg [Figure]

Figure_2.jpg [Figure]

Figure_3.jpg [Figure]

Figure_4.jpg [Figure]

Figure_5.jpg [Figure]

Figure_6.jpg [Figure]

Figure_7.jpg [Figure]

Supplementary_Data_FigureS1.jpg [Figure]

Supplementary_Data_FigureS2.jpg [Figure]

Supplementary_Data_FigureS3.jpg [Figure]

Supplementary_Data_FigureS4.jpg [Figure]

Table 1.pdf [Table]

Table 2.pdf [Table]

Table 3.pdf [Table]

Table 4.pdf [Table]

Table 5.pdf [Table]

Table 6.pdf [Table]

Table 7.pdf [Table]

Table 8.pdf [Table]

Conflict of interest.docx [Conflict of Interest]

R5FX83BH-9AD2-968E-8BFA-F291-9D32.pdf [Author Statement]

To view all the submission files, including those not included in the PDF, click on the manuscript title on your EVISE Homepage, then click 'Download zip file'.

Research Data Related to this Submission

There are no linked research data sets for this submission. The following reason is given:
Data will be made available on request

Highlights :

- Brain sex differences can be observed by using MRI in sheep, a well-recognized model in neuroendocrinology.

- Adult male and female brains show important sexual dimorphisms.

- Gonadectomy reduces these differences, showing their dependence on adult circulating hormone levels.

In vivo magnetic resonance imaging reveals the effect of gonadal hormones on morphological and functional brain sexual dimorphisms in adult sheep.

David André Barrière[1,2], Arsène Ella[1,3], Hans Adriaensen[1], Charles E. Roselli[4], Philippe Chemineau[1] & Matthieu Keller[1,*]

[1]UMR Physiologie de la Reproduction et des Comportements, INRA/CNRS/Université de Tours/IFCE, Nouzilly, France.

[2]Neurospin, CEA, Université Paris-Saclay, Gif-sur-Yvette, France.

[3]MRC Cognition & Brain Science Unit, University of Cambridge, UK.

[4]Oregon Health & Science University, Portland, USA.

***Corresponding Author:** Matthieu Keller, Laboratoire de Physiologie de la Reproduction et des Comportements, UMR 7247 INRA/CNRS/Université de Tours/IFCE, 37380 Nouzilly, France; Phone: +33 (0)2 47 42 72 75; Email: Matthieu.Keller@tours.inra.fr

Abstract

Sex differences in the brain and behavior are produced by the perinatal action of testosterone, which is converted into estradiol by the enzyme aromatase in the brain. Although magnetic resonance imaging (MRI) has been widely used in humans to study these differences, the use of animal models, where hormonal status can be properly manipulated, is necessary to explore the mechanisms involved. We used sheep, a recognized model in the field of neuroendocrinology, to assess brain morphological and functional sex differences and their regulation by adult gonadal hormones. To this end, we performed voxel-based morphometry and a resting-state functional MRI approach to assess sex differences in gonadally intact animals. We demonstrated significant sex differences in gray matter concentration (GMC) at the level of the gonadotropic axis, *i.e.,* not only within the hypothalamus and pituitary but also within the hippocampus and the amygdala of intact animals. We then performed the same analysis one month after gonadectomy and found that some of these differences were reduced, especially in the hypothalamus and amygdala. By contrast, we found few differences in the organization of the functional connectome between males and females either before or after gonadectomy. As a whole, our study identifies brain regions that are sexually dimorphic in the sheep brain at the resolution of the MRI and highlights the role of gonadal hormones in the maintenance of these differences.

Key words: sex differences, sheep, voxel-based morphometry, resting state fMRI, gonadectomy.

Highlights:

- Brain sex differences can be observed by using MRI in sheep, a well-recognized model in neuroendocrinology.
- Adult male and female brains show important sexual dimorphisms.
- Gonadectomy reduces these differences, showing their dependence on adult circulating hormone levels.

Introduction

Males and females show various sexually dimorphic traits in adulthood at the behavioral level that relate to the structure and function of the brain (McCarthy et al., 2015). Characterizing these sexual differences is of importance not only to gain a global understanding of the normal brain but also to gain insights into various brain disorders that are of differential prevalence and progression between males and females (Miller et al., 2017). Sex differences related to reproductive function are one of the most prominent types of sexual dimorphism, as both the neuroanatomical and functional organization of the gonadotropic axis differ widely between males and females.

In mammalian species, the classic view of sexual differentiation holds that these sex differences develop under the perinatal influence of testosterone and/or estradiol derived from the neural aromatization of testosterone (Alexander et al., 2011; Bakker and Baum, 2008). The brain develops as male in the presence of these hormones, and testicular testosterone in male embryos is necessary for the expression of male-typical hormonal and associated behavioral responses later in life, a process known as masculinization. Testosterone exposure not only masculinizes the brain but also actively defeminizes it so that males are unable to exhibit female-typical behavioral or physiological responses. By contrast, the absence of hormonal exposure predisposes animals to display female-typical adult sexual behaviors and hormone responses, a process known as feminization. While the early actions of sex steroids are necessary for the maturation and/or organization of several brain structures and neural circuits (Arnold, 2009), the differentiated neural circuits in adults are then responsible for sex-typical responses when sex steroids are synthesized by the mature gonad. Thus, the permanent developmental effects of sex steroids are usually referred to as “organizational”, while the transient or reversible effects observed during adulthood are referred to as “activational”.

While these effects have been studied mostly in rodents, similar mechanisms exist in many other mammalian species. The sheep is an animal model that offers a unique opportunity to study brain mechanisms underlying sexual differentiation for several reasons, including the ability to perform long-term blood or cerebrospinal fluid sampling (Clarke and Cummins, 1982), the ability to manipulate the hormonal milieu in the fetus or adult (Clarke and Cummins, 1982; Perkins and Roselli, 2007) and the abundance of information that exists characterizing reproductive physiology and behavior in this species (for review Roselli and Stormshak, 2010, 2009). Sexual differentiation of the sheep brain is dependent on testosterone and androgen receptor signalling during gestation (Cheng et al., 2010; Foster et al., 2002; Robinson et al., 1999; Roselli and Stormshak, 2010). While these studies, performed at the cellular or molecular levels, are very informative, they only examined a limited number of hypothalamic nuclei. Thus, information about other possible sexually dimorphic brain regions is lacking.

Magnetic resonance imaging (MRI) allows investigation at the level of the whole brain and has been widely used in humans to study sex differences in the function and organization of the brain (Burke et al., 2016, 2012). MRI is now a routine approach in neuroscience due to several advantages, including its noninvasive nature and the ability to perform longitudinal studies that allow changes within the same individuals to be tracked over time. However, due to ethical considerations, it is not possible to experimentally manipulate the hormonal milieu in humans, thus highlighting and reinforcing the usefulness of animal models such as sheep.

Some evidence suggests that gray and white matter content in sheep brain are sexually dimorphic, but because of the suboptimal resolution of the images and the lack of the appropriate neuroinformatic tools (namely, a brain template and atlas), the data could not be analyzed properly (Nuruddin et al., 2013). We recently established the tools necessary for conducting MRI experiments in sheep (Ella et al., 2017; Ella and Keller, 2015). In this study, we employed these tools to map and compare sexually dimorphic brain structures and

connectivity in rams and ewes. This comparison was performed by using voxel-based morphometry (VBM) to assess neuroanatomical differences in gray matter concentrations (GMC) according to sex. We also validated resting-state functional MRI to assess basal dynamic activity differences between sexes. Finally, we tested which sex differences are programmed during sexual differentiation (organizational effect) or due to adult gonadal hormones (activational effect) by analyzing the effect of gonadectomy.

Materials and Methods

Animals. Experiments were performed at the National Institute for Agronomic Research (Institut national pour la recherche agronomique, INRA) in Nouzilly, France (latitude 47°, 32N and longitude 0°, 46E) on adult Ile-de-France sheep (*Ovis aries*). A total of 24 animals (4 years old) were used: 12 ewes (50.33 ± 0.71 kg) and 12 rams (70.91 ± 0.92 kg). Animals were maintained indoors during the experiment and were fed daily with barley straw, Lucerne hay and commercial concentrate and had access to water and mineral blocks *ad libitum*. All procedures were performed in accordance with the European directive 2010/63/EU for animal protection and welfare used for scientific purposes and approved by the local ethical committee for animal experimentation (CEEA VdL, Tours, France, authorization N° 10465).

Experimental protocol. Animals were scanned twice in October and November 2017 at the CIRE platform (INRA Nouzilly, France, http://www.val-de-loire.inra.fr/cire). One week before the first scan, progesterone vaginal sponges (flugestone acetate, Chronogest CR 20 mg, MSD, Beaucouze, France) were placed in ewes to induce and maintain a luteal-like phase until the first day of the scan. On the day of the scan, sheep were weighed, and a blood sample was collected by jugular venipuncture to check the hormonal status of the animal. After the first scan, vaginal sponges were retrieved from the ewes, and both ewes and rams were gonadectomized following established procedures. To this end, the sheep were fasted 24 h before surgery. Following premedication with an i.v. injection of thiopental (14 mg/kg body weight, BW; Nesdonal, Merial, Villeurbanne, France), the sheep were intubated and maintained under anesthesia with a closed circuit of 3 to 4 % isoflurane (Vetflurane, Virbac, Carros, France) and 100 % oxygen. Castration and ovariectomy were conducted under sterile surgical conditions. Local anesthesia with lidocaine (4 %, Lurocaïne, Vétoquinol, Luré, France) was given prior to scrotal incision in males and laparotomy in females. Testicles or ovaries were

surgically extracted, and the tissues were sutured. The entire procedure was performed within 20 minutes. Postoperative ventilation with oxygen was maintained until the first signs of awakening appeared. The sheep were then housed individually for 6 hours in a padded stall before being put back with congeners. They received an anti-inflammatory drug for 2 days (2 mg/kg BW flunixin meglumine, Finadyne®, Intervet, Beaucouzé, France), an antiedema medication: (1 mg/kg BW of furosemide, Dimazon®, Intervet, Beaucouzé, France) at the end of surgery and 3 mg/kg BW hydrochlorothiazide with 0.03 mg/kg BW dexamethasone (Diurizone®, Vétoquinol, Luré, France) for 2 days. One month after the surgery, a second scan session was performed; the sheep were again weighed, and blood samples were collected as described above to assess the efficiency of the surgery (**Figure 1A and Figure S1**).

Testosterone and progesterone assays. Plasma was obtained from heparinized blood after 30 min of centrifugation at 3500 g. The concentration of testosterone was determined in duplicate samples using a radioimmunoassay as previously described (Hochereau-de Reviers et al., 1990). The sensitivity of this assay was 0.1 $ng.mL^{-1}$. The concentration of plasma progesterone was determined in duplicate samples using an immunoenzymatic assay as previously described (Chasles et al., 2016). The sensitivity of the progesterone assay was 0.25 $ng.mL^{-1}$ (**Figure 1A**).

Anesthesia protocol. Before scanning, the sheep were first anesthetized by an intrajugular administration of a ketamine/xylazine mix (1 $mg.mL^{-1}$ ketamine/0.1 $mg.mL^{-1}$ xylazine, volume of injection 6.5 mL). After induction, the animal was intubated (8.5 mm probe, SON612, Centravet, France) and ventilated manually. The jugular vein was catheterized for a continuous infusion of 0.1 $mg.mL^{-1}$ ketamine/xylazine mix (1.5 $mL.min^{-1}$), which permits preservation of both pupillary and palpebral reflexes and of the regular spontaneous respiratory rate.

Since MRI investigation in animals requires that animals be sedated, we developed a specific protocol of anesthesia for both functional and morphometric acquisition. Indeed, functional connectivity is highly sensitive to the pharmacological class of anesthetics used, and numerous studies have demonstrated that the widely used isoflurane gas obscures the naturally occurring functional connectivity by inducing synchronous cortico-striatal fluctuations and silencing subcortical activity (Kalthoff et al., 2013; Liu et al., 2013; Paasonen et al., 2018). For this reason, we chose to use a low dose of ketamine/xylazine mix (Imalgene 500 mg/Rompun 2 %, Centravet, France) for functional acquisitions and progressively replaced this with a standard isoflurane anesthesia for morphological acquisitions to reduce motion artifacts during long scanning.

Scanning procedure. Sheep were placed on the MRI-compatible mechanical bed of a 3 Tesla VERIO Siemens system (Erlangen, Germany). They were gently restrained with a belt on the mechanical bed while their head was placed within a circular rigid coil (^{1}H, 24 channels, phased array, receiver only, 20/28 cm, P-H24LE-030, Siemens, Germany). During the functional resting state scanning procedure, sheep were ventilated continuously using an anesthesia system with an integrated ventilator (Aestiva MRI-compatible, GE Healthcare, Germany) delivering a 1:1 oxygen/air mix with a current volume of 500 mL for ewes and 650 mL for rams and the frequency rate set at 16 bpm. Heart rate and O_2 saturation were monitored continuously using an oximeter probe placed on the right hind paw (oxytip+ probe MRI-compatible, GE Healthcare, Germany) and maintained at 87.21 ± 1.002 bpm and 89.83 ± 8.84 % for ewes and 78.19 ± 9.28 bpm and 87.63 ± 6.18 % for rams, respectively (for details see **Figure S1**). After the functional resting state scanning procedure, the intravenous ketamine anesthesia regimen was progressively replaced by gas anesthesia using isoflurane added to the air mix at a

concentration of 2.8 ± 0.14 % in ewes and 3.07 ± 0.01 % in rams using the same ventilatory parameters (**Figure S1**).

MRI data acquisition.

Left-right orientation within the images was ensured by placing an α-tocopherol acetate capsule (Toco 500 mg, α-tocopherol acetate, Alkopharm, France) on the right side of the sheep's head. After positioning, a first localizer sequence was performed to align the brain on the anterior commissure-posterior commissure (AC-PC) axis within the field of view (FOV). Then, two successive gradient echoes (GRE) field maps were acquired using the same acquisition parameters: repetition time (TR) = 500 ms, echo time (TE) = 4.92 ms and 7.38 ms, number of excitations (NEX) = 1, flip angle (FA) = 55 degree, field of view = 166x166x166 mm^3 within a 64x64x64 matrix for a final voxel size = 2.6x2.6x2.6 mm^3. Both GRE field maps were acquired within the axial acquisition plane, but a left-right encoding direction was used on the first acquisition (LR-GRE); then, a right-left encoding direction was used on the second acquisition (RL-GRE). Both LR- and RL-GRE images were acquired to calculate inhomogeneity correction maps that were used within the functional analysis processing. Then, a spin-echo echo-planar imaging (SE-EPI) sequence of 8.5 min was acquired in the axial plane using the following parameters: TR=3260 ms, TE = 24 ms, NEX = 1, FOV = 170x170x45 mm^3 within a 110x110x90 matrix for a final voxel size = 1.5x1.5x2 mm^3. This sequence generated 150 volumes that were used for resting-state fMRI analysis. Finally, a T1-weighted 3D magnetization-prepared rapid acquisition of gradient echo (MPRAGE) sequence was acquired using the following parameters: TR = 2500 ms, TE = 3.18 ms, FA =12 degrees, NEX = 2, FOV = 190x190x190 mm within a 384x384x384 matrix for a final voxel size 0.5x0.5x0.5 mm^3. T1-weighted images were used for voxel-based morphometry analysis. Four rams were excluded from the analysis because of excessive motion during imaging acquisition, ($n_{(final)}$ = 8 males

198 and 12 females). The final translations were less than 0.4 mm, and rotations did not exceed
199 0.006 radians (0.3 degrees) in our acquisitions (**Figure S2**).
200
201 **Functional MRI (fMRI) data preprocessing.** Resting-state fMRI data were preprocessed in
202 MATLAB (R2017b, MathWorks) with SPM8 (http://www.fil.ion.ucl.ac.uk/spm) using the
203 SPMMouse Toolbox (Sawiak et al., 2014, 2009) and FSL5.1 (https://fsl.fmrib.ox.ac.uk). In the
204 first step of preprocessing, the EPI images were time corrected, realigned and resliced to the
205 first volume, corrected for inhomogeneity using the GRE field maps and coregistered with their
206 corresponding T1 anatomical images using SPM8. Thereafter, T1 anatomical images were
207 segmented using our previously published tissue priors (Ella et al., 2017), first to create specific
208 brain masks for each T1 image (gray matter (GM)+white matter (WM)+cerebrospinal fluid
209 (CSF) = Brain Mask) and second to normalize both T1 and EPI images onto our brain template
210 (Ella et al., 2017) using the affine matrix calculated by SPM8 during the segmentation step.
211 Finally, normalized images were masked to remove soft tissue using the brain masks generated
212 previously and spatially smoothed with a Gaussian kernel of 8 mm full-width at half-maximum
213 (FWHM). In the second step of preprocessing, EPI images were processed using FSL. The
214 effect of the six previously calculated motion parameters, including translations and rotations
215 and out brain signals, was removed from the data through linear regression using the FEAT
216 toolbox (https://fsl.fmrib.ox.ac.uk/fsl/fslwiki/FEAT). Then, acquisition artifacts (ghosting)
217 were identified using the *melodic* function. Briefly, *melodic* decomposes the signal of the 4D
218 smoothed images into independent spatial components. These components were thresholded
219 ($p<0.01$) and visually inspected for artifacts, which were removed using the *regfilt* function of
220 FSL (Kelly et al., 2010). Finally, a bandpass filtering (0.1 Hz-0.005 Hz) was applied to the time
221 series (**Figure 1B**).
222

Construction of resting-state functional networks. Pre- and post-gonadectomy, processed functional images of each animal (40 data sets) were segmented into 86 anatomical regions of interest (ROIs) (43 regions in each hemisphere) using the GM areas of our sheep atlas (Ella et al., 2017) and the REX function of the CONN toolbox (https://www.nitrc.org/projects/conn; **Figure 1B**). For each sheep, functional correlation coefficients (r values) were computed between the time courses of each pair of ROIs and then transformed to z-scores using Fisher's z transformation, resulting in an 86x86 matrix of normalized correlation coefficients for each animal. Networks of altered connectivity were computed, extracted and plotted using Network-Based Statistics (NBS, http://brain-connectivity-toolbox.net/comparison/nbs; Zalesky et al., 2010), the Brain Connectivity Toolbox (http://brain-connectivity-toolbox.net; Rubinov and Sporns, 2010), the BrainNet Viewer toolbox (https://www.nitrc.org/projects/bnv/; Xia et al., 2013) and in-house developed MATLAB scripts. As the sample size was unbalanced between both sexes (8 males *versus* 12 females), we estimated the type 2 error (β value = 0.898) to assess the number of permutations necessary to reach a β value = 0.95 (n = 1500). Statistical comparisons between groups were made at the global network level (*i.e.*, conjunction of all ROIs). The NBS methodology works in two steps: first, the statistical hypothesis is tested at each connection, and its statistical significance is determined; second, the connections are thresholded by a user-defined significance ($p < 0.05$, < 0.01 and < 0.001); the subnetwork components (groups of nodes and edges such that a path can be found between any pair of network members) were found; and their size (number of surviving connections) was determined. The component significance was determined through permutation testing (n = 5000), where the test subjects are randomly permutated between groups and the chance of randomly finding networks of similar size determined, outputting a family-wise error rate-corrected significance (α_{FWE}, 0.05). Differences between gonad-intact males and females and the effect of gonadectomy on males and females were determined using analysis of variance

(ANOVA) with group or time as a factor. A p value < 0.05 after correction was considered statistically significant. Considering the individual variability and as a control to test our statistical power, we compared two random groups balanced for sex (4 males and 6 females in each group; **Figure S3**). At the baseline, male and female z scores described a Gaussian distribution ($K2_{(Males)}$ = 11.96; p = 0.0025 and $K2_{(Females)}$ = 13.93; p = 0.0009; D'Agostino & Pearson normality test) that was significantly different ($p < 0.0001$; t = 4.995; df = 354, paired t-test) with a shift of female values to the right. After gonadectomy, z scores also followed Gaussian distributions ($K2_{(Males)}$ = 20.41; $p < 0.0001$ and $K2_{(Females)}$ = 22.93; $p < 0.0001$) and were significantly different between the sexes ($p < 0.0001$; t = 9.848; df = 354), again with a shift of the female values to the right. When baseline z scores for males and females were mixed, the Gaussian distributions were conserved ($K2_{(Males)}$ = 14.77; p = 0.0006 and $K2_{(Females)}$ = 18.58; $p < 0.0001$), but the curves were superimposed and not significantly different (p = 0.4382; t = 0.7758; df = 708). The same effect was observed after gonadectomy ($K2_{(Males)}$ = 20.53; $p < 0.0001$ and $K2_{(Females)}$ = 21.5; $p < 0.0001$; z score comparison: p = 0.8802, t = 0.1507; df = 708).

Voxel-Based Morphometry (VBM) data preprocessing. VBM data were preprocessed with SPM8 and SPMMouse 1.1 Toolbox. First, each T1 anatomical image was aligned to the stereotaxic space by registering each image to our anatomical template image (Ella et al., 2017) using SPMMouse. Then, each image was bias corrected and segmented into probability maps of GM, WM, and CSF using the default settings in the SPM8 toolbox and our GM, WM, CSF probability maps (Ella et al., 2017). The transformation matrices obtained were used to normalize and resample (0.5x0.5x0.5 mm^3) the GM, WM and CSF probability maps. To produce a more accurate registration within each sheep as well as across all sheep, the

Diffeomorphic Anatomical Registration Through Exponentiated Lie Algebra (DARTEL) algorithm, which is an automated, unbiased, and nonlinear template building program (Ashburner, 2007), was applied using the strategy described by (Asami et al., 2012). First, a subject-specific template was created by the DARTEL algorithm using the previous tissue class images (GM, WM, and CSF maps) obtained from each sheep at both time points (before and after gonadectomy). The DARTEL procedure releases individual-specific flow field maps, permitting the application of diffeomorphic normalization on each tissue class of images to spatially normalize each time point on a subject-specific template space. Each normalized tissue class of images was modulated by the determinant of the Jacobian to account for the expansion and/or contraction of brain regions over time. Then, a population-specific template was created by the DARTEL algorithm using all of the subject-specific templates of the tissue class of images. Here, the DARTEL procedure releases population-specific flow field maps, permitting the application of diffeomorphic normalization from each animal onto each tissue class of images. Finally, each tissue class image was modulated by the determinant of the Jacobian, and the final modulated GM images were spatially smoothed by convolving with a 4 mm full-width at half-maximum (FWHM) isotropic Gaussian kernel to create GMC maps (**Figure 1B**) (Sumiyoshi et al., 2017).

Voxel-Based Morphometry, statistics and analysis. Statistical Parametric Mapping (SPM8) was used to reveal the temporal and regional changes in gray matter occurring in GMC maps. Second level analysis from SPM, a flexible factorial model that is equivalent to a 2×2 mixed-model ANOVA, was used first to compare male *versus* female and then pregonadectomy *versus* postgonadectomy groups. Brain volume was used as a covariate (**Figure S4A**) with between-subject factor group and within-subject factor condition. The factors included in the analysis were subjects, group (male, female), and time (pregonadectomy, postgonadectomy). A brain

mask was used to constrain the analysis. For each cluster, the significance of the peak voxel was set as $p < 0.005$ (β value = 0.990, $t_{(35)} = 2.7238$), and the minimum cluster extent was set to 300 voxels. The results are presented on an axial brain slice series generated by the xjView plugin (http://www.alivelearn.net/xjview/) of SPM, and the corresponding surfacing results were assembled with a BrainNet viewer, which allows the generation of both brain mesh and brain plots for visualizing data. To assess the effect of individual variability and as a control test for statistical power, we compared two random groups balanced for sex (4 males and 6 females in each group (**Figure S4**). At baseline, the comparison shows only a small significant unilateral cluster on slices 14 and 12 corresponding to the left lateral *gyrus,* which was not observed previously (p= 0.005, β value = 0.990, $t_{(35)}$ =2.7238, voxel threshold = 300), while the comparison performed after the gonadectomy reveals no significant differences between the groups.

Postprocessing statistical analysis. VBM cluster peaks revealed by flexible factorial analysis data were identified using our atlas and a personal procedure developed in MATLAB. For each comparison, ROI masks from Ella's atlas were used to extract GMC values of corresponding regions within the GMC map using REX plugging. Endocrine, physiological, functional connectivity and GMC data were compiled and analyzed using Prism 6.02 software GraphPad Software, San Diego, CA) and were compared using two-way ANOVA with repeated measures followed by the two-stage setup method of Benjamini, Kriegger and Yekutieli as recommended by the software. Statistical significance was defined as $p < 0.05$ for these analyses.

Results

Morphological and functional sexual dimorphism in the adult sheep brain.

VBM analysis

Using a voxel-based morphometry (VBM) approach, we found 37 brain regions that were sexually dimorphic in intact sheep (see **Table S1 and S2** for detailed statistics). Specifically, our VBM analysis found that the gray matter concentration (GMC) within the left and right *gyrus ectolateralis*, left and right hippocampus, pituitary gland and right amygdala were significantly higher in intact females than in intact males (red clusters, **Figure 2A**). In contrast, GMC values in the hypothalamus and both posterior gyri sigmoideus were significantly higher in intact males *versus* luteal phase females (blue clusters, **Figure 2A**). Comparison between the same animals before and after gonadectomy reveals that only 22 brain regions were still dimorphic. Among them, four bilateral cortical regions of the gyri ectolateralis, both entolateral and lateral gyri, and the occipital lobe, still exhibited higher GMC values in gonadectomized females than in gonadectomized males (red clusters, **Figure 2B**). GMC values in the posterior gyri sigmoideus were still higher in gonadectomized males than in gonadectomized females (blue, clusters, **Figure 2B**). The volumes of several dimorphic subcortical structures, such as the right amygdala and the hypothalamus, decreased after gonadectomy and were no longer different between males and females. Moreover, we observed a large regression of the volume of the hippocampal cluster (120 mm^3 within the intact male/intact female comparison *versus* 15 mm^3 within the gonadectomized male/gonadectomized female comparison) and a large increase (10 times) of the volume of the pituitary cluster (28 mm^3 within the intact male/intact female comparison *versus* 280 mm^3 within the gonadectomized male/gonadectomized female comparison).

Using our anatomical atlas (Ella et al., 2017), we collected GMC values within the bilateral hippocampus, hypothalamus, pituitary gland and gyri ectolateralis to evaluate the effect of

gonadectomy on these structures. Within the hippocampus (**Figure 3A**), we observed a left-right asymmetry in both males and females as previously reported (Sadeghi et al., 2017; Samara et al., 2011), which was preserved after gonadectomy. In addition, we observed bilateral sexual dimorphism in the hippocampus with higher GMC values in luteal phase females than in intact males. This hippocampal sexual dimorphism was lost after gonadectomy. Within the hypothalamus (**Figure 3B**), no left-right asymmetry was observed, but significantly higher GMC values were found in intact males compared to luteal phase females. The sexual dimorphism in the hypothalamus was also eliminated after gonadectomy. No side asymmetry was observed within the pituitary gland (**Figure 3C**), but significantly higher GMC values were observed in luteal phase females compared to intact males. GMC concentration in the pituitary increased significantly in both sexes after gonadectomy, but sexual dimorphism was preserved. Finally, analysis of GMC within the gyri ectolateralis (**Figure 3D**) revealed no left-right asymmetry, but GMC values were significantly higher in luteal phase females when compared to gonad-intact males.

Resting-state fMRI analysis

The analysis of the functional connectome between intact males and females revealed a sexually dimorphic brain network composed of 332 functional connections shared between 77 functional nodes (**Figure 4A**, all statistics are available in **Table S3**). Intact luteal phase females displayed higher functional connectivity than intact males (**Figure 4B**). Three internal subnetworks involving the frontal region (red nodes), the occipitoparietal region (orange nodes) and the diencephalic region (yellow nodes) compose this dimorphic network. When we focused on the sexually dimorphic brain regions highlighted by our previous VBM analysis, we observed that both the left and right hippocampus, hypothalamus pineal gland and gyrus ectolateralis display higher functional connectivity in luteal phase females when compared to

intact males (**Table S3**). Notably, the hippocampus displayed stronger bilateral connections in luteal phase females than in intact males within the geniculate nucleus, the parahippocampal cortex, the periaqueductal gray substance (PAG), the suprasylvian *gyrus*, the cingulate cortex, the pineal gland, the temporal lobe and the thalamus. The hypothalamus displayed stronger bilateral connections in luteal phase females than in intact males within the lateral septal nucleus, the preoptic hypothalamic area, the subfornical organ and the substantia nigra. Importantly, the connectivity between the hypothalamus and the pituitary gland was also significantly higher in luteal phase females than in intact males. Finally, the gyrus ectolateralis displayed stronger bilateral connections in luteal phase females than in intact males within the gyri entolateralis and the lateral gyri.

Surprisingly, the analysis of the functional connectome between gonadectomized males and females revealed a similar brain network also composed of 332 functional connections shared between 80 functional nodes (**Figure 4C**, all statistics are available in **Table S4**). This functional network is characterized by higher functional connectivity in gonadectomized females when compared to gonadectomized males (**Figure 4D**) and displayed the same internal frontal, occipitoparietal and diencephalic subnetworks. Although it was statistically marginal, some changes in resting-state functional connectivity were also detected within the hippocampus, hypothalamus, and gyrus ectolateralis. Similar temporal correlations were observed within the previously described structures. Additional bilateral connections were observed within the gyrus ectolateralis, midbrain, left lateral *gyrus* and right nucleus of the horizontal limb of the diagonal band (NHLDB) of gonadectomized females compared to gonadectomized males. Within the hypothalamus, similar functional connectivity was observed to that described in intact animals. Additional functional connectivity was observed with the lateral septal nucleus bilaterally in gonadectomized females when compared to gonadectomized males and with the right bed nucleus of the stria terminalis (BNST), the left globus pallidum

and the left NHLDB. Finally, the gyrus ectolateralis also displayed similar higher functional connections with previously described structures and additional bilateral functional connectivity with the cingulate cortex, the occipital lobe, the suprasylvian gyrus and the hippocampus. Functional connections were also observed with the right parahippocampal cortex, the right posterior sylvian *gyrus* and the right temporal lobe in gonadectomized females when compared to gonadectomized males.

Effect of gonadal secretion on brain morphology and functional connectivity in both male and female adult sheep brains.

VBM analysis

To evaluate the sex-specific effects of gonadectomy, we evaluated both brain morphology and functional connectome modifications before and after gonadectomy in males and females. In males, VBM analysis revealed 29 regions with significant GMC modifications induced by gonadectomy (see **Table S5** for detailed statistics). We found significantly higher GMC values within the bilateral amygdala and the pituitary gland after gonadectomy (red clusters, **Figure 5A**). On the other hand, the GMC values were significantly decreased after gonadectomy within the medial mamillary nucleus, the periaqueductal gray substance (PAG), the pons and the medial preoptic hypothalamic area (blue clusters, **Figure 5A**). In females, VBM analysis revealed 22 regions with significant GMC modifications induced by gonadectomy (see **Table S6** for detailed statistics). We found significantly higher GMC values only within the pituitary gland (red clusters, **Figure 5B**). By contrast, GMC values were significantly decreased within the medial mamillary nucleus, *medulla oblongata* (MO), pons and preoptic hypothalamic area (blue clusters, **Figure 5B**). Interestingly, after gonadectomy, GMC values were also reduced within both gyri ectolateralis but only within the right hemisphere (**Figure 5B**).

Using our anatomical atlas, we collected GMC values within the bilateral amygdala and PAG in males and within the subfornical organ and NHLDB in females, which display sex-specific modifications after gonadectomy. In males, GMC was significantly increased after gonadectomy within the amygdala (**Figure 6A left panel**). On the other hand, the GMC values within the PAG were significantly decreased after gonadectomy (**Figure 6A, right panel**). In females, GMC values were significantly decreased after gonadectomy within the subfornical organ (**Figure 6B left panel**). GMC values within the NHLDB were also significantly decreased after gonadectomy (**Figure 6B, right panel**).

Resting-state fMRI analysis

The analysis of the functional connectome between intact and gonadectomized males revealed a brain network sensitive to gonadal hormones composed of 66 functional connections shared between 52 functional nodes (**Figure 7A**, all statistics are available in **Table S7**). This functional network was significantly higher in gonadectomized males (**Figure 7A, Right panel**) and was characterized by modifications of rostrocaudal functional connectivity and by intense modifications of functional connectivity within the diencephalon. Importantly, the pituitary gland, which is a critical structure in reproductive function and shows significant variations of GMC after gonadectomy, displayed increased functional connectivity together with the preoptic hypothalamic area, the BNST and the subfornical organ. By contrast, the analysis of the functional connectome between intact and gonadectomized females revealed a brain network sensitive to gonadal hormones composed of 94 functional connections shared between 65 functional nodes (**Figure 7B**, all statistics are available in **Table S8**). This functional network was also significantly higher in gonadectomized females (**Figure 7B, Right panel**) and was characterized by an interhemispheric modification of functional connectivity and, as previously described in males, by intense modifications of functional connectivity

444 within the diencephalon. As observed in males, the pituitary gland also displayed an increase
445 in GMC after gonadectomy in females along with an increase in the functional connectivity
446 within the medial septal nucleus, the BNST, the septum, the NHLBD, the preoptic
447 hypothalamic area and the subfornical organ.

Discussion

Our study is the first to report a detailed VBM analysis in sheep and to establish resting-state fMRI in this species. Thanks to these methodological developments, we were able to highlight brain sexually dimorphic territories and networks of functional connectivity differing between males and females, mainly in the hypothalamus and pituitary. We also showed that these differences are partly due to adult circulating levels of gonadal hormones, as some of these differences vanished following gonadectomy, suggesting that the differences observed are due to the activational effects of circulating gonadal hormones. These data add a high degree of neuroanatomical precision compared to the previous MRI report of differences between the sexes in sheep (Nuruddin et al., 2013) and were made possible through the construction of an adapted brain template and atlas of the ovine brain (Ella et al., 2017; Ella and Keller, 2015).

Sex differences in intact animals.

VBM analysis

First, our VBM analysis revealed clear differences in GMC between intact males and females in five main areas: the hippocampus, the hypothalamus—especially the arcuate region—the pituitary, the amygdala and the gyrus ectolateralis. For all these regions, with the exception of the hypothalamus, GMC was higher in males than in females. On the whole, the differences measured in the hypothalamus and pituitary, which are key components of the gonadotropic axis, are not very surprising because the axis is known to be highly sexually dimorphic. Indeed, sexual differences have been previously reported in other species or by other approaches in these areas. For example, similar to our results, MRI studies in humans have reported that the volume of the hypothalamus is larger in men than women (Goldstein et al., 2001; Makris et al., 2013). The hypothalamic cluster differing significantly between males and females appears to

include the region of the arcuate nucleus, a structure where the numbers of neurons expressing kisspeptin, neurokinin B and dynorphin (KNDy neurons) as well as progesterone receptors are higher in female than in male sheep (Cheng et al., 2010). This difference is linked to the fact that KNDy neurons mediate the negative feedback of progesterone on GnRH secretion in females. In the hypothalamic cluster, other regions, such as the ventromedial nucleus, are also known to be sexually dimorphic, being larger in males than females (Flanagan-Cato, 2011). Finally, it is important to note that a limitation of our study is the level of resolution that is achievable using our MRI conditions (500 µm isovoxel resolution). This level of resolution prevents visualization of very small neuron clusters, such as the sexually dimorphic nucleus of the medial preoptic area, which has been consistently shown to be larger in males than females, including in sheep (Roselli and Stormshak, 2010). In the pituitary, we found that females have a higher concentration of gray matter than males. A recent human MRI study demonstrated that the pituitary fossa, which grossly reflects the volume of the pituitary, is larger in women than men (Pecina et al., 2017), thus corroborating our observations.

In the amygdala, we confirmed the sexual dimorphism previously reported in sheep (Nuruddin et al., 2013) and recently in humans (Lotze et al., 2019). At the cellular level, it has been shown that the size of neurons in the amygdala, as well as the content in estradiol receptors, is higher in male than female sheep (Alexander et al., 2001; Perkins et al., 1995). In other animal models, for example, in the rat, the volume of the medial amygdala is also higher in males than females (Cooke et al., 1999). The hippocampus is another brain region that appears to be sexually dimorphic in our study. As the hippocampus is a primary site for the regulation of cognitive processes such as stress responses or spatial memory, which are also influenced by gonadal hormones, such a difference is not surprising (Juraska, 1991; McCarthy and Konkle, 2005). In addition, our results showing that part of the anterior hippocampus is larger in females than males is congruent with a recent MRI study in mice (Meyer et al., 2017). Finally, the difference

measured in the gyrus ectolateralis is more surprising because it is not known as a traditional region related to sex differences. Given the lack of anatomical and functional data regarding this region in sheep, it is difficult to interpret this result. It has been shown that the gyrus ectolateralis is part of the visual cortex (Clarke and Whitteridge, 1976), but further studies will be needed to assess the nature and role of this dimorphism.

We performed the same VBM comparison one month following gonadectomy to assess whether the differences observed are due to adult circulating levels of gonadal hormones. It is striking to note that most of the observed differences diminished significantly after gonadectomy, particularly in the hypothalamus and amygdala. Interestingly, adult castration of male rats induces a reduction of the volume of the medial amygdala to a level comparable to that observed in females, demonstrating that adult hormone manipulation can completely reverse the sexual dimorphism observed in intact animals. Interestingly, this region is also rich in aromatase and steroid receptors in adult sheep (Lehman et al., 1993; Roselli et al., 1998).

Resting-state fMRI

In addition to VBM analysis, our study is the first to report that the resting state connectome differs between male and female sheep. This analysis revealed a sexually dimorphic brain network composed of 332 functional connections shared between 77 functional nodes that displays increased functional connectivity in intact luteal phase females when compared to intact males. Three internal subnetworks involving the frontal region, the occipitoparietal region and the diencephalic region compose this dimorphic network, with the diencephalic region being by far the most sexually dimorphic. Interestingly, the functional connectivity within the diencephalic region and especially in the hypothalamic regions showed the highest degree of sexual dimorphism. Finally, these sexual differences were not significantly influenced

by adult circulating gonadal hormones, as the network differing between the sexes was not influenced by gonadectomy.

Sex differences in gonadectomized animals.

VBM analysis

When considering the effect of gonadectomy within each sex in the VBM analysis, it is striking to observe that gonadectomy induced very similar changes in GMC at the level of the hypothalamus and pituitary in both males and females. The fact that gonadectomy abolishes negative feedback (of testosterone for the males and progesterone for the females) is in line with a similar response of the hypothalamic-pituitary axis in both sexes. However, it is notable that in terms of GMC variations, the responses of the hypothalamus and pituitary were opposite. While an increase of GMC was observed in the pituitary following gonadectomy, a clear reduction was measured in the whole hypothalamus. The increase in GMC observed in the pituitary is in line with previous data showing that ovariectomy induces a strong increase in the number and size (2- to 3-fold hypertrophy) of the LH cell population in ewes (Polkowska et al., 1980).

By contrast, the medial preoptic area of the hypothalamus is long known to be highly sexually dimorphic in many species, including humans (Swaab et al., 1992). The size of the ovine sexually dimorphic nucleus, measured either by Nissl staining or the expression of aromatase, is significantly larger in adult rams than in ewes and is not affected by gonadectomy (Roselli et al., 2004, 2000). In contrast, gonadectomy induced a significant reduction in GMC in the hypothalamus in both sexes. This pattern of response remains to be explained in terms of cellular mechanisms.

Resting-state fMRI

When analyzing the effect of gonadectomy within each sex for resting-state fMRI, it is striking to first notice that within each sex, gonadectomy induced an increase in functional connectivity. The pituitary gland, which displayed an increase in GMC after gonadectomy, also expressed an increase in functional connectivity within the preoptic hypothalamic area and the BNST. However, intense modifications of functional connectivity within the diencephalon diverged according to sex. Indeed, while changes in males were characterized by rostrocaudal modifications of functional connectivity, changes were mostly interhemisphepric in females. The meaning of such differences remains to be explored in the future.

General considerations

As already mentioned, differences between sexes or between intact and gonadectomized animals are mainly located at the level of the hypothalamus and pituitary, reflecting differences in the regulation of the gonadotropic axis. To fully validate the role of adult circulating sex steroids, especially testosterone and progesterone, in the maintenance of these sexual differences and determine which of these hormones is involved, it will be necessary in a future study to supplement gonadectomized animals with adult levels of circulating steroids and see whether we are able to restore the initial pattern of differences observed in intact animals.

Finally, it is important to consider several limitations that arise from the segmentation of our brain atlas and the use of anesthetics in preclinical fMRI investigation. First, the current level of anatomical/functional mapping of sheep brain neuroanatomy is far less precise than those in other species such as rodents. Even if more than 80 brain structures have been segmented so far, it should be remembered that MRI segmentation is dependent upon the contrasts on MRI images that can differ from histological observations. Consequently, each label includes many brain structures, and thus labeling would differ from the expectation of the reader. Second, in our analysis, we failed to find any functional connectivity that was higher in males than in

571 females. Indeed, sex differences in ketamine sensitivity have been reported to affect the depth,
572 duration and efficacy of anesthesia (Molina et al., 2016). Thus, even though measures of heart
573 rate and O_2 saturation during functional acquisitions are similar between sexes (Figure S1), a
574 differential effect of ketamine on the resting-state network cannot be excluded. Moreover, the
575 greater sensitivity to ketamine displayed by males could obscure differences physiologically
576 present in males rather than in females, explaining the lack of higher functional connectivity in
577 males compared to females. Finally, our analysis was performed using Ella's Sheep brain
578 template and its associated probabilistic tissue maps, which were created from 18 ewes. Recent
579 studies have proposed using a more specific template to improve the segmentation step
580 (Fillmore et al., 2015; Huang et al., 2010). Hence, the development of a mixed brain template
581 (including males and females) with a higher number of animals (n = 100, sex ratio 1:1) will be
582 mandatory to improve the segmentation step and further develop future MRI studies using
583 sheep.
584 In conclusion, we demonstrated that MRI is a suitable method to study neuroendocrine
585 mechanisms that sustain sexual differences in the sheep brain and by inference in other large
586 animal models. In this context, sheep offer a unique mammalian model in which to study
587 neuroendocrine sexual differentiation and same-sex sexual partner preferences. Indeed, males
588 showing spontaneous preference for other rams (male-oriented) represent as many as 8 % of
589 the ram population (Roselli et al., 2011; Charles E. Roselli and Stormshak, 2009; Roselli and
590 Stormshak, 2010). The understanding of the biological determinants and underlying neural
591 networks mediating sexual attraction and mate selection are still quite incomplete in these
592 animals. Thus far, evidence supports the idea of an organization of neural substrates by
593 testosterone during prenatal development (C. E. Roselli and Stormshak, 2009). While much
594 attention has been given to the sexually dimorphic nucleus of the hypothalamus, a structure that

595 cannot be observed in MRI due to the limits of resolution, MRI could provide new insights on
596 whether the anatomy of other brain structures differ in male-oriented sheep.

Acknowledgment

We thank Didier Chesneau and Chantal Porte for their valuable help at different stages of this project. We thank all the shepherds, especially Damien Capo, Olivier Lasserre and Didier Dubreuil, from the experimental unit (UEPAO) for the care provided to the animals. We are also grateful to Anne-Lyse Lainé, Corinne Laclie and Dominique Gennetay from the laboratoire de Phénotypage-Endocrinologie for hormonal assays. We thank all the staff from the CIRE platform for their help during surgeries and imaging sessions, especially Gilles Gomot, Christian Moussu and Frédéric Elleboudt. Finally, we thank Julie Bakker, Charlotte Cornil and Jacques Balthazart for helpful feedback on this manuscript. This project was funded by grants from the French Agence Nationale de la Recherche (ANR) and the regional council Centre-Val-de-Loire (Pherobouc project).

References

Alexander, B.M., Rose, J.D., Stellflug, J.N., Fitzgerald, J.A., Moss, G.E., 2001. Low-sexually performing rams but not male-oriented rams can be discriminated by cell size in the amygdala and preoptic area: a morphometric study. Behav. Brain Res. 119, 15–21. https://doi.org/10.1016/S0166-4328(00)00335-1

Alexander, B.M., Skinner, D.C., Roselli, C.E., 2011. Wired on steroids: sexual differentiation of the brain and its role in the expression of sexual partner preferences. Front. Endocrinol. 2, 42. https://doi.org/10.3389/fendo.2011.00042

Arnold, A.P., 2009. The organizational-activational hypothesis as the foundation for a unified theory of sexual differentiation of all mammalian tissues. Horm. Behav. 55, 570–578. https://doi.org/10.1016/j.yhbeh.2009.03.011

Asami, T., Bouix, S., Whitford, T.J., Shenton, M.E., Salisbury, D.F., McCarley, R.W., 2012. Longitudinal loss of gray matter volume in patients with first-episode schizophrenia: DARTEL automated analysis and ROI validation. NeuroImage 59, 986–996. https://doi.org/10.1016/j.neuroimage.2011.08.066

Ashburner, J., 2007. A fast diffeomorphic image registration algorithm. NeuroImage 38, 95–113. https://doi.org/10.1016/j.neuroimage.2007.07.007

Bakker, J., Baum, M.J., 2008. Role for estradiol in female-typical brain and behavioral sexual differentiation. Front. Neuroendocrinol. 29, 1–16. https://doi.org/10.1016/j.yfrne.2007.06.001

Burke, S.M., Kreukels, B.P.C., Cohen-Kettenis, P.T., Veltman, D.J., Klink, D.T., Bakker, J., 2016. Male-typical visuospatial functioning in gynephilic girls with gender dysphoria - organizational and activational effects of testosterone. J. Psychiatry Neurosci. JPN 41, 395–404. https://doi.org/10.1503/jpn.150147

Burke, S.M., Veltman, D.J., Gerber, J., Hummel, T., Bakker, J., 2012. Heterosexual men and women both show a hypothalamic response to the chemo-signal androstadienone. PloS One 7, e40993. https://doi.org/10.1371/journal.pone.0040993

Chasles, M., Chesneau, D., Moussu, C., Delgadillo, J.A., Chemineau, P., Keller, M., 2016. Sexually active bucks are efficient to stimulate female ovulatory activity during the anestrous season also under temperate latitudes. Anim. Reprod. Sci. 168, 86–91. https://doi.org/10.1016/j.anireprosci.2016.02.030

Cheng, G., Coolen, L.M., Padmanabhan, V., Goodman, R.L., Lehman, M.N., 2010. The kisspeptin/neurokinin B/dynorphin (KNDy) cell population of the arcuate nucleus: sex differences and effects of prenatal testosterone in sheep. Endocrinology 151, 301–311. https://doi.org/10.1210/en.2009-0541

Clarke, I.J., Cummins, J.T., 1982. The temporal relationship between gonadotropin releasing hormone (GnRH) and luteinizing hormone (LH) secretion in ovariectomized ewes. Endocrinology 111, 1737–1739. https://doi.org/10.1210/endo-111-5-1737

Clarke, P.G., Whitteridge, D., 1976. The cortical visual areas of the sheep. J. Physiol. 256, 497–508. https://doi.org/10.113/jphysiol.1976.sp011335

Cooke, B.M., Tabibnia, G., Breedlove, S.M., 1999. A brain sexual dimorphism controlled by adult circulating androgens. Proc. Natl. Acad. Sci. U. S. A. 96, 7538–7540. https://doi.org/101073/pnas.96.13.7538

Ella, A., Delgadillo, J.A., Chemineau, P., Keller, M., 2017. Computation of a high-resolution MRI 3D stereotaxic atlas of the sheep brain. J. Comp. Neurol. 525, 676–692. https://doi.org/10.1002/cne.24079

Ella, A., Keller, M., 2015. Construction of an MRI 3D high resolution sheep brain template. Magn. Reson. Imaging 33, 1329–1337. https://doi.org/10.1016/j.mri.2015.09.001

Fillmore, P.T., Phillips-Meek, M.C., Richards, J.E., 2015. Age-specific MRI brain and head templates for healthy adults from 20 through 89 years of age. Front. Aging Neurosci. 7. https://doi.org/10.3389/fnagi.2015.00044

Flanagan-Cato, 2011. Sex differences in the neural circuit that mediates female sexual receptivity. Front. Neuroendocrinol. 32, 124–136. https://doi.org/10.1016/j.yfrne.2011.02.008

Foster, D.L., Padmanabhan, V., Wood, R.I., Robinson, J.E., 2002. Sexual differentiation of the neuroendocrine control of gonadotrophin secretion: concepts derived from sheep models. Reprod. Camb. Engl. Suppl. 59, 83–99.

Goldstein, J.M., Seidman, L.J., Horton, N.J., Makris, N., Kennedy, D.N., Caviness, V.S., Faraone, S.V., Tsuang, M.T., 2001. Normal sexual dimorphism of the adult human brain assessed by in vivo magnetic resonance imaging. Cereb. Cortex N. Y. N 1991 11, 490–497. https://doi.org/10.1093/cercor/11.6.490

Hochereau-de Reviers, M.T., Perreau, C., Pisselet, C., Fontaine, I., Monet-Kuntz, C., 1990. Comparisons of endocrinological and testis parameters in 18-month-old Ile de France and Romanov rams. Domest. Anim. Endocrinol. 7, 63–73. https://doi.org/10.1016/0739-7240(90)90055-5

Huang, C.-M., Lee, S.-H., Hsiao, I.-T., Kuan, W.-C., Wai, Y.-Y., Ko, H.-J., Wan, Y.-L., Hsu, Y.-Y., Liu, H.-L., 2010. Study-specific EPI template improves group analysis in functional MRI of young and older adults. J. Neurosci. Methods 189, 257–266. https://doi.org/10.1016/j.jneumeth.2010.03.021

Juraska, J.M., 1991. Sex differences in "cognitive" regions of the rat brain. Psychoneuroendocrinology 16, 105–109. https://doi.org/10.1016/0306-4530(91)90073-3

Kalthoff, D., Po, C., Wiedermann, D., Hoehn, M., 2013. Reliability and spatial specificity of rat brain sensorimotor functional connectivity networks are superior under sedation compared with general anesthesia. NMR Biomed. 26, 638–650. https://doi.org/10.1002/nbm.2908

Kelly, R.E., Alexopoulos, G.S., Wang, Z., Gunning, F.M., Murphy, C.F., Morimoto, S.S., Kanellopoulos, D., Jia, Z., Lim, K.O., Hoptman, M.J., 2010. Visual inspection of independent components: defining a procedure for artifact removal from fMRI data. J. Neurosci. Methods 189, 233–245. https://doi.org/10.1016/j.jneumeth.2010.03.028

Lehman, M.N., Ebling, F.J., Moenter, S.M., Karsch, F.J., 1993. Distribution of estrogen receptor-immunoreactive cells in the sheep brain. Endocrinology 133, 876–886. https://doi.org/10.1210/endo.133.2.8344223

Liu, X., Zhu, X.-H., Zhang, Y., Chen, W., 2013. The Change of Functional Connectivity Specificity in Rats Under Various Anesthesia Levels and its Neural Origin. Brain Topogr. 26, 363–377. https://doi.org/10.1007/s10548-012-0267-5

Lotze, M., Domin, M., Gerlach, F.H., Gaser, C., Lueders, E., Schmidt, C.O., Neumann, N., 2019. Novel findings from 2,838 Adult Brains on Sex Differences in Gray Matter Brain Volume. Sci. Rep. 9, 1671. https://doi.org/10.1038/s41598-018-38239-2

Makris, N., Swaab, D.F., van der Kouwe, A., Abbs, B., Boriel, D., Handa, R.J., Tobet, S., Goldstein, J.M., 2013. Volumetric parcellation methodology of the human hypothalamus in neuroimaging: normative data and sex differences. NeuroImage 69, 1–10. https://doi.org/10.1016/j.neuroimage.2012.12.008

McCarthy, M.M., Konkle, A.T.M., 2005. When is a sex difference not a sex difference? Front. Neuroendocrinol. 26, 85–102. https://doi.org/10.1016/j.yfrne.2005.06.001

McCarthy, M.M., Pickett, L.A., VanRyzin, J.W., Kight, K.E., 2015. Surprising origins of sex differences in the brain. Horm. Behav. 76, 3–10. https://doi.org/10.1016/j.yhbeh.2015.04.013

Meyer, C.E., Kurth, F., Lepore, S., Gao, J.L., Johnsonbaugh, H., Oberoi, M.R., Sawiak, S.J., MacKenzie-Graham, A., 2017. In vivo magnetic resonance images reveal neuroanatomical sex differences through the application of voxel-based morphometry in C57BL/6 mice. NeuroImage 163, 197–205. https://doi.org/10.1016/j.neuroimage.2017.09.027

Miller, L.R., Marks, C., Becker, J.B., Hurn, P.D., Chen, W.-J., Woodruff, T., McCarthy, M.M., Sohrabji, F., Schiebinger, L., Wetherington, C.L., Makris, S., Arnold, A.P., Einstein, G., Miller, V.M., Sandberg, K., Maier, S., Cornelison, T.L., Clayton, J.A., 2017. Considering sex as a biological variable in preclinical research. FASEB J. Off. Publ. Fed. Am. Soc. Exp. Biol. 31, 29–34. https://doi.org/10.1096/fj.201600781R

Molina, A., Moyano, M., Serrano-Rodriguez, J., Ayala, N., Lora, A., Serrano-Caballero, J., 2016. Analyses of anaesthesia with ketamine combined with different sedatives in rats. Veterinární Medicína 60, 368–375. https://doi.org/10.17221/8384-VETMED

Nuruddin, S., Bruchhage, M., Ropstad, E., Krogenæs, A., Evans, N.P., Robinson, J.E., Endestad, T., Westlye, L.T., Madison, C., Haraldsen, I.R.H., 2013. Effects of peripubertal gonadotropin-releasing hormone agonist on brain development in sheep--a magnetic resonance imaging study. Psychoneuroendocrinology 38, 1994–2002. https://doi.org/10.1016/j.psyneuen.2013.03.009

Paasonen, J., Stenroos, P., Salo, R.A., Kiviniemi, V., Gröhn, O., 2018. Functional connectivity under six anesthesia protocols and the awake condition in rat brain. NeuroImage 172, 9–20. https://doi.org/10.1016/j.neuroimage.2018.01.014

Pecina, H.I., Pecina, T.C., Vyroubal, V., Kruljac, I., Slaus, M., 2017. Age and sex related differences in normal pituitary gland and fossa volumes. Front. Biosci. Elite Ed. 9, 204–213.

Perkins, A., Fitzgerald, J.A., Moss, G.E., 1995. A comparison of LH secretion and brain estradiol receptors in heterosexual and homosexual rams and female sheep. Horm. Behav. 29, 31–41. https://doi.org/10.1006/hbeh.1995.1003

Perkins, A., Roselli, C.E., 2007. The ram as a model for behavioral neuroendocrinology. Horm. Behav. 52, 70–77. https://doi.org/10.1016/j.yhbeh.2007.03.016

713 Polkowska, J., Dubois, M.P., Domański, E., 1980. Immunocytochemistry of luteinizing hormone releasing
714 hormone (LHRH) in the sheep hypothalamus during variuos reproductive stages: correlation with the gonadotropic
715 hormones of the pituitary. Cell Tissue Res. 208, 327–341. https://doi.org/10.1007/BF00234880

716 Robinson, J.E., Forsdike, R.A., Taylor, J.A., 1999. In utero exposure of female lambs to testosterone reduces the
717 sensitivity of the gonadotropin-releasing hormone neuronal network to inhibition by progesterone. Endocrinology
718 140, 5797–5805. https://doi.org/10.1210/endo.140.12.7205

719 Roselli, C.E., Larkin, K., Resko, J.A., Stellflug, J.N., Stormshak, F., 2004. The volume of a sexually dimorphic
720 nucleus in the ovine medial preoptic area/anterior hypothalamus varies with sexual partner preference.
721 Endocrinology 145, 478–483. https://doi.org/10.1210/en.2003-1098.

722 Roselli, C.E., Reddy, R.C., Kaufman, K.R., 2011. The development of male-oriented behavior in rams. Front.
723 Neuroendocrinol. 32, 164–169. https://doi.org/10.1016/j.yfrne.2010.12.007

724 Roselli, C.E., Stormshak, F., 2010. The ovine sexually dimorphic nucleus, aromatase, and sexual partner
725 preferences in sheep. J. Steroid Biochem. Mol. Biol. 118, 252–256. https://doi.org/10.1016/j.jsbmb.2009.10.009

726 Roselli, Charles E., Stormshak, F., 2009. The neurobiology of sexual partner preferences in rams. Horm. Behav.
727 55, 611–620. https://doi.org/10.1016/j.yhbeh.2009.03.013

728 Roselli, C. E., Stormshak, F., 2009. Prenatal programming of sexual partner preference: the ram model. J.
729 Neuroendocrinol. 21, 359–364. https://doi.org/10.1111/j.1365-2826.2009.01828.x

730 Roselli, C.E., Stormshak, F., Resko, J.A., 2000. Distribution of aromatase mRNA in the ram hypothalamus: an in
731 situ hybridization study. J. Neuroendocrinol. 12, 656–664. https://doi.org/10.1046/j.1365-2826.2000.00496.x

732 Roselli, C.E., Stormshak, F., Resko, J.A., 1998. Distribution and regulation of aromatase activity in the ram
733 hypothalamus and amygdala. Brain Res. 811, 105–110. https://doi.org/10.1016/S0006-8993(98)00995-0

734 Rubinov, M., Sporns, O., 2010. Complex network measures of brain connectivity: Uses and interpretations.
735 NeuroImage, Computational Models of the Brain 52, 1059–1069.
736 https://doi.org/10.1016/j.neuroimage.2009.10.003

737 Sadeghi, L., Rizvanov, A.A., Salafutdinov, I.I., Dabirmanesh, B., Sayyah, M., Fathollahi, Y., Khajeh, K., 2017.
738 Hippocampal asymmetry: differences in the left and right hippocampus proteome in the rat model of temporal lobe
739 epilepsy. J. Proteomics 154, 22–29. https://doi.org/10.1016/j.jprot.2016.11.023

740 Samara, A., Vougas, K., Papadopoulou, A., Anastasiadou, E., Baloyanni, N., Chrousos G.P., Tsangaris, G.T.,
741 2011. Proteomics reveal rat hippocampal lateral asymmetry. Hippocampus 21, 108–119.
742 https://doi.org/10.1002/hipo.20727

743 Sawiak, S.J., Picq, J.-L., Dhenain, M., 2014. Voxel-based morphometry analyses of in vivo MRI in the aging
744 mouse lemur primate. Front. Aging Neurosci. 6. https://doi.org/10.3389/fnagi.2014.00082

745 Sawiak, S.J., Wood, N.I., Williams, G.B., Morton, A.J., Carpenter, T.A., 2009. SPMMouse: A new toolbox for
746 SPM in the animal brain. Presented at the ISMRM 17th Scientific Meeting & Exhibition, April, pp. 18–24.

747 Sumiyoshi, A., Nonaka, H., Kawashima, R., 2017. Sexual differentiation of the adolescent rat brain: A longitudinal
748 voxel-based morphometry study. Neurosci. Lett. 642, 168–173. https://doi.org/10.1016/j.neulet.2016.12.023

749 Swaab, D.F., Gooren, L.J., Hofman, M.A., 1992. The human hypothalamus in relation to gender and sexual
750 orientation. Prog. Brain Res. 93, 205–217; discussion 217-219. https://doi.org/10.1016/S0079-6123(08)64573-2

751 Xia, M., Wang, J., He, Y., 2013. BrainNet Viewer: a network visualization tool for human brain connectomics.
752 PloS One 8, e68910. https://doi.org/10.1371/journal.pone.0068910

753 Zalesky, A., Fornito, A., Bullmore, E.T., 2010. Network-based statistic: Identifying differences in brain networks.
754 NeuroImage 53, 1197–1207. https://doi.org/10.1016/j.neuroimage.2010.06.041

755

Figures

Fig 1. Overview of the experiment. **A.** Experimental design and concentrations of testosterone and progesterone before and after gonadectomy in both males and females. **B.** Processing workflow for functional connectivity and voxel-based morphometry (VBM) analysis. Both functional and anatomical images are coregistrated onto the Ella' sheep brain template and then processed using a dedicated processing developed from SPM and FSL toolbox. **C.** 3D rendering of the Ella' sheep brain template and atlas. Sheep brain atlas is composed by a mosaic of 86 anatomical region of interest (ROI) which were used to create the functional connectivity matrix and functional networks analysis to identify brain territories revealed by the VBM analysis (for further information, see Material & Method section).

Data are compared using a two-way ANOVA followed by Holm-Sidak multiple comparisons test and expressed as mean ± SEM; *** $p < 0.001$.

768 **Fig 2.** Morphological brain sexual dimorphisms in intact and gonadectomized animals. Male
769 *versus* female VBM comparison before and after the gonadectomy procedure. **A. left panel**:
770 brain plots representing the surface map of regional grey matter concentration (GMC)
771 differences between gonad-intact male *versus* luteal phase female sheep. **A. right panel**: brain
772 slices showing GMC differences between intact male *versus* intact female sheep. **B. left panel**:
773 brain plots representing the surface map of GMC differences between gonadectomized male
774 *versus* gonadectomized female sheep. **B. right panel**: brain slices showing GMC differences
775 between gonadectomized male *versus* gonadectomized female sheep.
776 Ecto = ectolateralis gyrus ; Hippo = hippocampus ; Pit = pituitary gland ; Hypo = hypothalamus.
777 Data are the results of interaction analysis (**A**) males versus females at the baseline (**B**) males
778 *versus* females after gonadectomy using a p value < 0.005 (β value = 0.990) corresponding to
779 $t_{(35)} = 2.7238$ and a cluster threshold set at 300 voxels. N = 20 animals (8 males and 12 females).

780 **Fig 3.** Effect of gonadectomy on sexually dimorphic structures. The mean values of Grey Matter
781 Concentration (GMC) were evaluated bilaterally in **A.** hippocampus, **B.** hypothalamus, **C.**
782 pituitary gland and **D.** ectolateralis gyrus for both male and female sheep before and after
783 gonadectomy.
784 Data were compared using a two-way ANOVA followed by Holm-Sidak multiple comparisons
785 test and expressed as mean ± SEM; *$p < 0.05$; ** $p < 0.01$ and *** $p < 0.001$. N = 20 animals
786 (8 males and 12 females).

Fig 4. Functional brain sexual dimorphisms in intact and gonadectomized sheep. **A.** Sagittal and dorsal view of the sexually dimorphic brain functional network between entire males *versus* entire females. **B.** Mean connectivity values within the previous network between entire males and entire females. **C.** sagittal and dorsal view of the sexually dimorphic brain functional network between gonadectomized males *versus* gonadectomized females. **D.** Mean connectivity values within the previous network between gonadectomized males and gonadectomized females.

The sexually dimorphic functional network are the results of interaction analysis between (**A**) males *versus* females at the baseline and between (**C**) males *versus* females after gonadectomy using network-based statistics (NBS; connection-level threshold *p*-uncorrected < 0.001, networks were significant at $p < 0.05$ family-wise error (FWE) corrected), nodes and edges colour coded according to statistical strength (*t*-value). Both comparison of the mean values of the networks were evaluated using a two-tailed Student t-test and expressed as mean ± SEM; $*p < 0.05$. N = 20 animals (8 males and 12 females).

Fig 5. Effect of the gonadectomy procedure in both males and females on brain morphology. **A. left panel**: brain plots representing the surface map of regional grey matter concentration (GMC) differences between entire male *versus* gonadectomized male. **A. right panel**: brain slices showing GMC differences between entire male *versus* gonadectomized male. **B. left panel**: brain plots representing the surface map of GMC differences between entire female *versus* gonadectomized female. **B. right panel:** brain slices showing GMC differences between entire female *versus* gonadectomized female.

PAG : periaqueductal grey ; Amyg = amygdala ; Pit = pituitary gland ; Hypo = hypothalamus ; MPOA = medial preoptic area. Data are the results of interaction analysis between (**A**) baseline *versus* gonadectomy in males and between (**B**) baseline versus gonnadectomy in female using a p value < 0.005 (β value = 0.990) corresponding to $t_{(35)} = 2.7238$ and a cluster threshold set at 300 voxels. N = 8 in male group and n = 12 in female group.

Fig 6. Effect of the gonadectomy procedure on non-sexually dimorphic structures in both male and female sheep. In males, the mean grey matter concentration (GMC) values were evaluated bilaterally within **A.** the amygdala (Left), and the periaqueductal grey substance (PAG, Right). In females, the mean GMC values were evaluated bilaterally within **B.** the subfornical organ (Left), and the nucleus of the horizontal limb of the diagonal band (NHLDB, Right).

Data were compared using a two-way ANOVA followed by Holm-Sidak multiple comparisons test and expressed as mean ± SEM; *$p < 0.05$ and *** $p < 0.001$. N = 8 in male group and n = 12 in female group.

Fig 7. Effect of the gonadectomy procedure on brain functional connectivity in male and female sheep. **A.** Sagittal and dorsal view of the altered functional network induced by gonadectomy in males. **B.** Mean connectivity values within the previous network between entire *versus* gonadectomized males. **C.** Sagittal and dorsal view of the altered functional network induced by gonadectomy in females **D.** right panel: Mean connectivity values within the previous network between gonad-intact or luteal phase females versus gonadectomized females.

The sexually dimorphic functional network are the results of interaction analysis between (**A**) baseline *versus* gonadectomy in male group and between (**B**) Baseline versus gonadectomy in female group using network-based statistics (NBS; connection-level threshold *p*-uncorrected < 0.05, networks were significant at $p < 0.05$ family-wise error (FWE) corrected), nodes and edges colour coded according to statistical strength (*t*-value). Both comparison of the mean values of the networks were evaluated using a two-tailed Student t-test and expressed as mean ± SEM; *$p < 0.05$ and ** $p < 0.01$. N = 8 in male group and n = 12 in female group.

Supplementary Figures

Fig S1. Physiological parameters recorded during the acquisition of functional scanning in males and females, before and after the gonadectomy procedure. (**A**) animal weight, (**B**) Heart rate, (**C**) O_2 saturation, (**D**) isoflurane concentration.

Data are compared using a two-way ANOVA followed by Holm-Sidak multiple comparisons test and expressed as mean ± SEM; *** $p < 0.001$.

Fig S2. Motions parameters recorded during the acquisitions. (**A**) Translations, (**B**) rotations, (**C**) estimation of the breath during the acquisition, (**D**) a significant correlation is observed between the Y-translation motion (Up-down motions) and breathing.

Data are expressed as mean ± SD; Correlation was estimated using a two-tailed parametric Pearson test ** $p < 0.001$.

Fig S3. Control testing of individual variability in functional data. Here, we compared two group of sheep after randomly grouped (4 males and 6 females in each group) to insure our statistical power. (**A**) Distribution of Z score in intact males (shaded blue) and intact females (shaded red) is associated with a significant network in females. (**B**) Distribution of Z score in mix 1 (shaded blue) and mix 2 (shaded red) is not associated with a significant network in intact animals. (**C**) Distribution of Z score in gonadectomized males (shaded blue) and gonadectomized females (shaded red) is associated with a significant network in females. (**B**) Distribution of Z score in mix 1 (shaded blue) and mix 2 (shaded red) is not associated with a significant network in gonadectomized animals. The sexually dimorphic functional network are the results of interaction analysis entire male x luteal females at the baseline (A) and male x females after gonadectomy using network-based statistics (NBS; connection-level threshold p-

uncorrected < 0.001, networks were significant at p < 0.005 family-wise error (FWE) corrected), nodes and edges colour coded according to statistical strength (t-value).

Fig S4. Control testing of individual variability in morphological data. Here, we compared two group of sheep after randomly grouped (4 males and 6 females in each group) to insure our statistical power. (**A**) Statistical analytical design showing the flexible factorial design used in the study. The last colum correspond to the brains volumes wich are used as covariate. (**B**) Comparisons of GMC between the mix 1 and the mix 2 at the baseline. A significant cluster within the left lateral *gyrus* is observable. (**C**) Comparisons of GMC between the mix 1 and the mix 2 after gonadectomy. No significant cluster observable.

Data are the results of interaction analysis Mix 1 *x* Mix 2 at baseline (**B**) and Mix 1 *x* Mix 2 at gonadectomy (**C**) using a *p* value = 0.005 (β value = 0.990) corresponding to $t_{(35)}$ =2.7238 and a cluster threshold set at 5 voxels.

Supplementary Tables

Table S1. Sexually dimorphic brain regions sensitive to the gonadectomy procedure. Data are compared using a two-way ANOVA followed by Holm-Sidak multiple comparisons test and expressed as mean ± SEM; *$p < 0.05$; ** $p < 0.01$ and *** $p < 0.001$.

Table S2. Sexually dimorphism brain region unsensitive to the gonadectomy procedure. Data are compared using a two-way ANOVA followed by Holm-Sidak multiple comparisons test and expressed as mean ± SEM; *$p < 0.05$; ** $p < 0.01$ and *** $p < 0.001$.

Table S3. Sexually dimorphic brain functional connections. The sexually dimorphic functional network between entire males *versus* entire females has been calculated in network-based statistics (NBS; connection-level threshold *p*-uncorrected < 0.001, networks were significant at $p < 0.05$ family-wise error (FWE) corrected), nodes and edges colour coded according to statistical strength (*t*-value).

Table S4. Sexually dimorphic brain functional connections. The sexually dimorphic functional network between gonadectomized males *versus* gonadectomized females has been calculated in network-based statistics (NBS; connection-level threshold *p*-uncorrected < 0.001, networks were significant at $p < 0.05$ family-wise error (FWE) corrected), nodes and edges colour coded according to statistical strength (*t*-value).

Table S5. Effect of the gonadectomy procedure on brain morphology in males. Data are compared using a two-way ANOVA followed by Holm-Sidak multiple comparisons test and expressed as mean ± SEM; *$p < 0.05$; ** $p < 0.01$ and *** $p < 0.001$.

Table S6. Effect of the gonadectomy procedure on brain morphology in females. Data are compared using a two-way ANOVA followed by Holm-Sidak multiple comparisons test and expressed as mean ± SEM; *$p < 0.05$; ** $p < 0.01$ and *** $p < 0.001$.

Table S7. Effect of the gonadectomy procedure on resting state functional connectivity in males. The network has been calculated in network-based statistics (NBS; connection-level threshold p-uncorrected < 0.05, networks were significant at $p < 0.05$ family-wise error (FWE) corrected), nodes and edges colour coded according to statistical strength (t-value).

Table S8. Effect of the gonadectomy procedure on resting state functional connectivity in females. The network has been calculated in network-based statistics (NBS; connection-level threshold p-uncorrected < 0.05, networks were significant at $p < 0.05$ family-wise error (FWE) corrected), nodes and edges colour coded according to statistical strength (t-value).

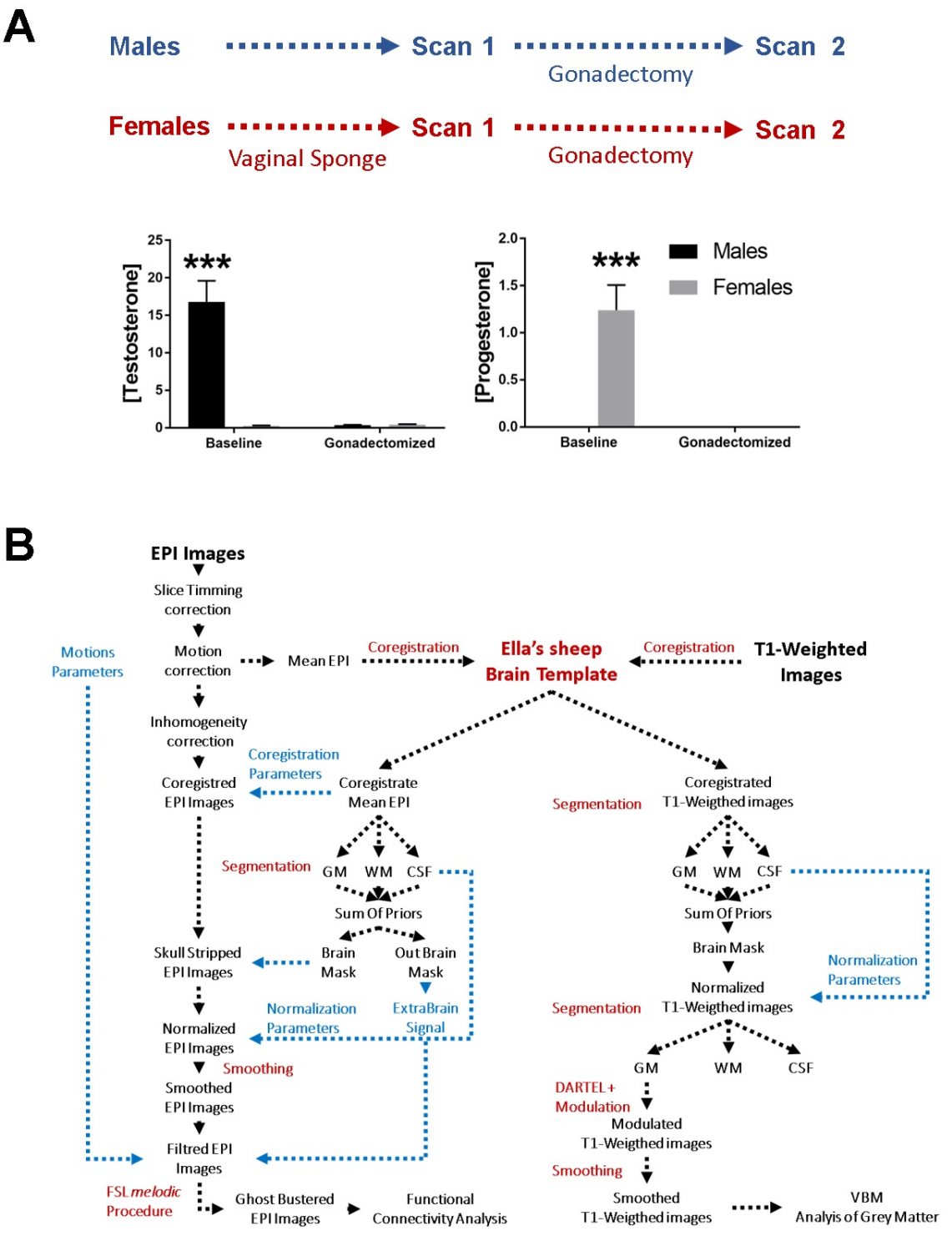
A
Males
Scan 1
Scan 2
Gonadectomy
Females
Scan 1
Scan 2
Vaginal Sponge
Gonadectomy
[Testosterone]
***
Baseline
Gonadectomized
[Progesterone]
***
Males
Females
Baseline
Gonadectomized
B
EPI Images
Slice Timming correction
Motion correction
Motions Parameters
Mean EPI
Coregistration
Ella's sheep Brain Template
Coregistration
T1-Weighted Images
Inhomogeneity correction
Coregistred EPI Images
Coregistration Parameters
Coregistrate Mean EPI
Segmentation
GM WM CSF
Sum Of Priors
Brain Mask
Out Brain Mask
Skull Stripped EPI Images
Normalization Parameters
ExtraBrain Signal
Normalized EPI Images
Smoothing
Smoothed EPI Images
Filtred EPI Images
FSL melodic Procedure
Ghost Bustered EPI Images
Functional Connectivity Analysis
Coregistrated T1-Weigthed images
Segmentation
GM WM CSF
Sum Of Priors
Brain Mask
Normalization Parameters
Normalized T1-Weigthed images
Segmentation
GM WM CSF
DARTEL+ Modulation
Modulated T1-Weigthed images
Smoothing
Smoothed T1-Weigthed images
VBM Analyis of Grey Matter
C

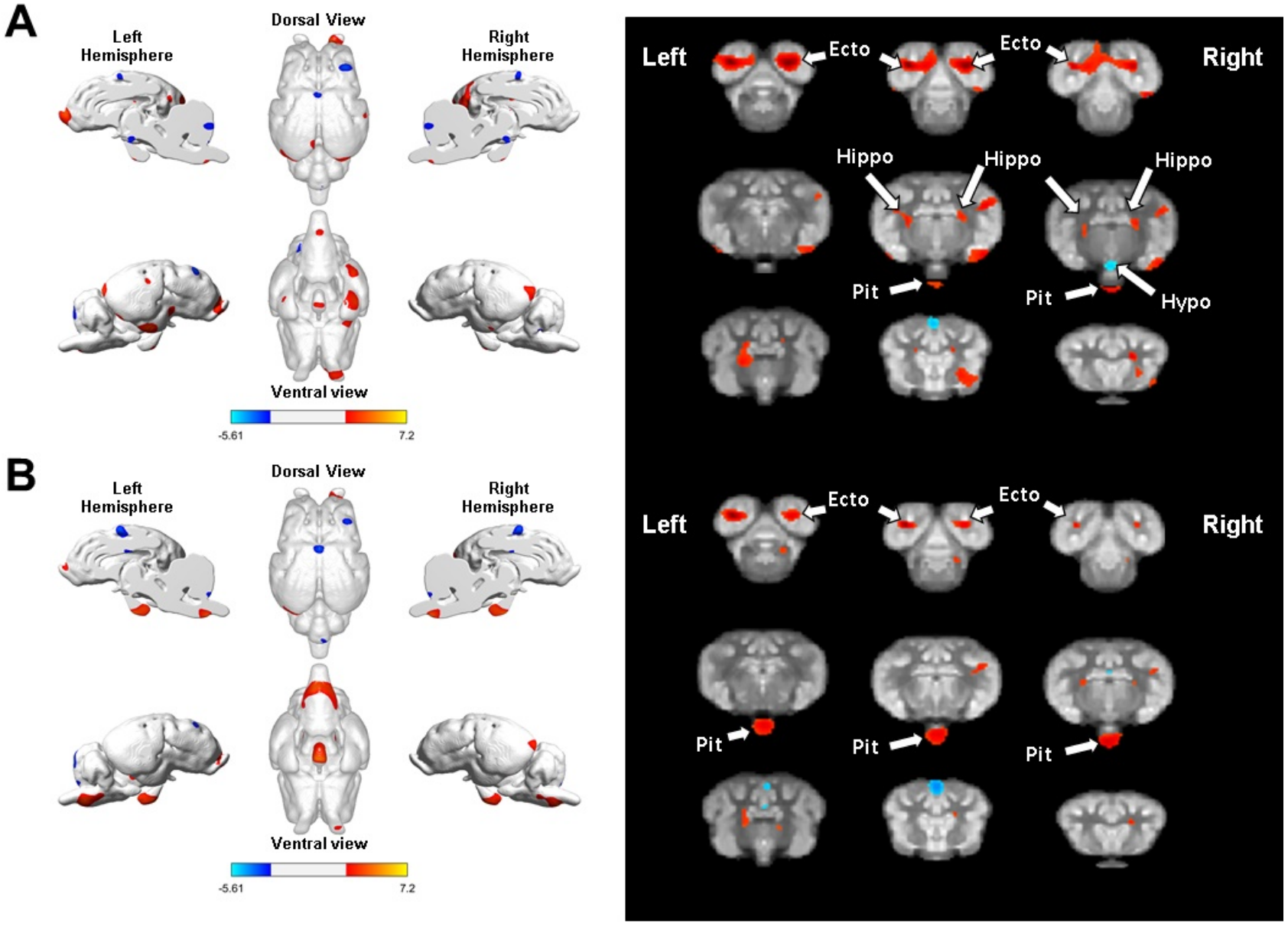
A
Left Hemisphere
Dorsal View
Right Hemisphere
Ventral view
-5.61
7.2
B
Left Hemisphere
Dorsal View
Right Hemisphere
Ventral view
-5.61
7.2
Left
Ecto
Ecto
Right
Hippo
Hippo
Hippo
Pit
Pit
Hypo
Left
Ecto
Ecto
Right
Pit
Pit
Pit

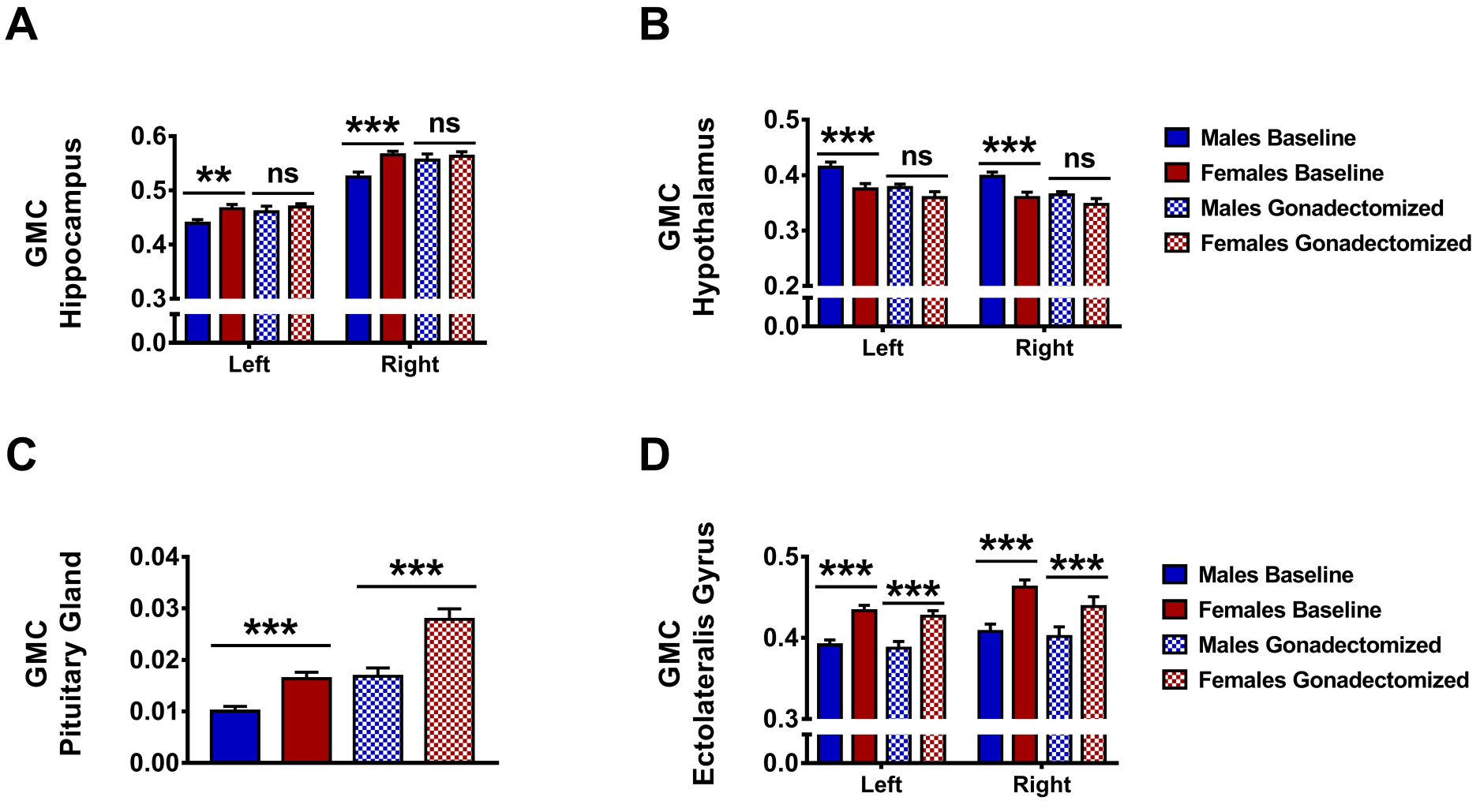
A
GMC
Hippocampus
0.6
0.5
0.4
0.3
0.0
**
ns
***
ns
Left
Right
B
GMC
Hypothalamus
0.5
0.4
0.3
0.2
0.0
***
ns
***
ns
Left
Right
Males Baseline
Females Baseline
Males Gonadectomized
Females Gonadectomized
C
GMC
Pituitary Gland
0.04
0.03
0.02
0.01
0.00
***
***
D
GMC
Ectolateralis Gyrus
0.5
0.4
0.3
0.0
***
***
***
***
Left
Right
Males Baseline
Females Baseline
Males Gonadectomized
Females Gonadectomized

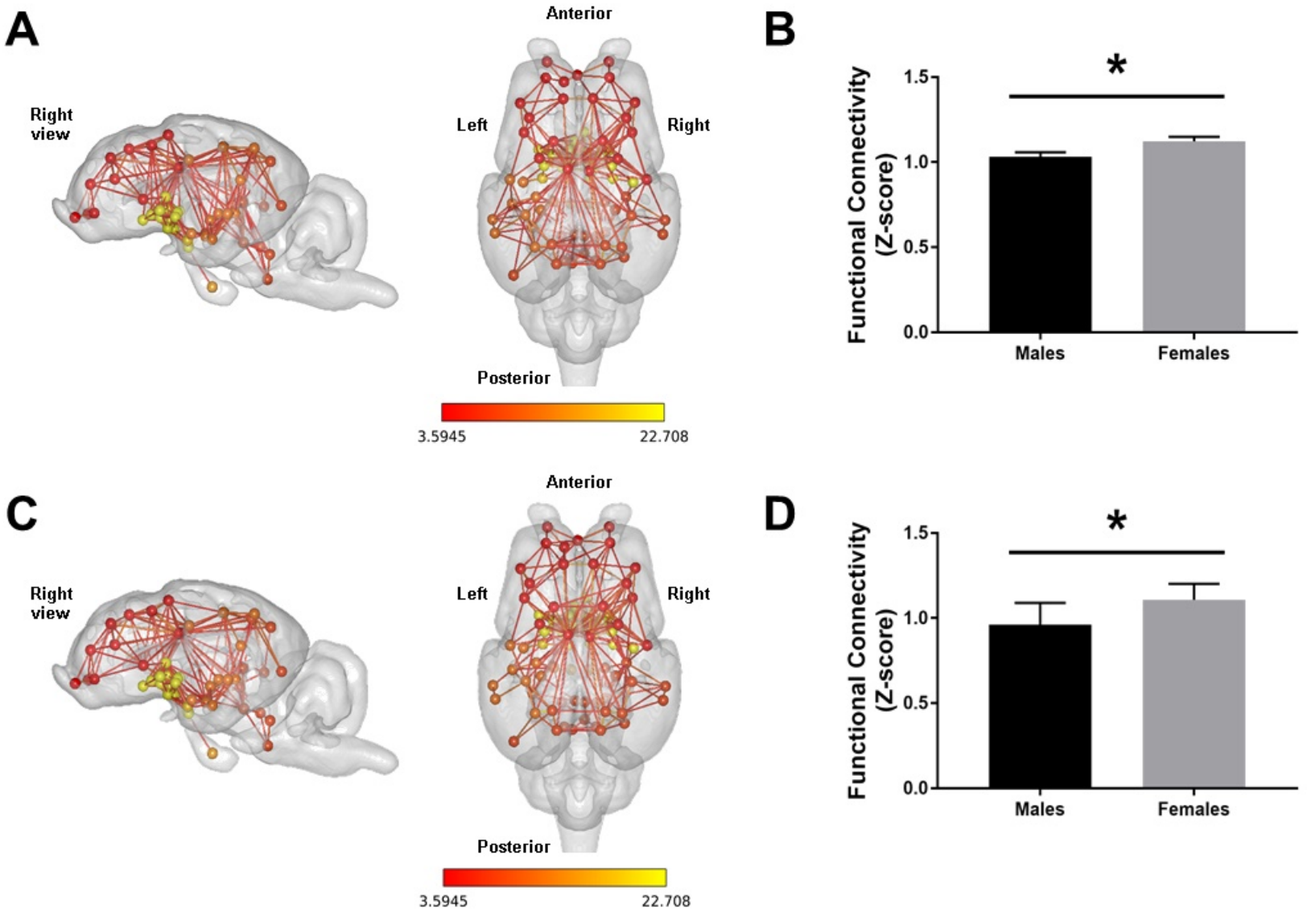
A
Right view
Anterior
Left
Right
Posterior
3.5945
22.708
B
Functional Connectivity (Z-score)
1.5
1.0
0.5
0.0
*
Males
Females
C
Right view
Anterior
Left
Right
Posterior
3.5945
22.708
D
Functional Connectivity (Z-score)
1.5
1.0
0.5
0.0
*
Males
Females

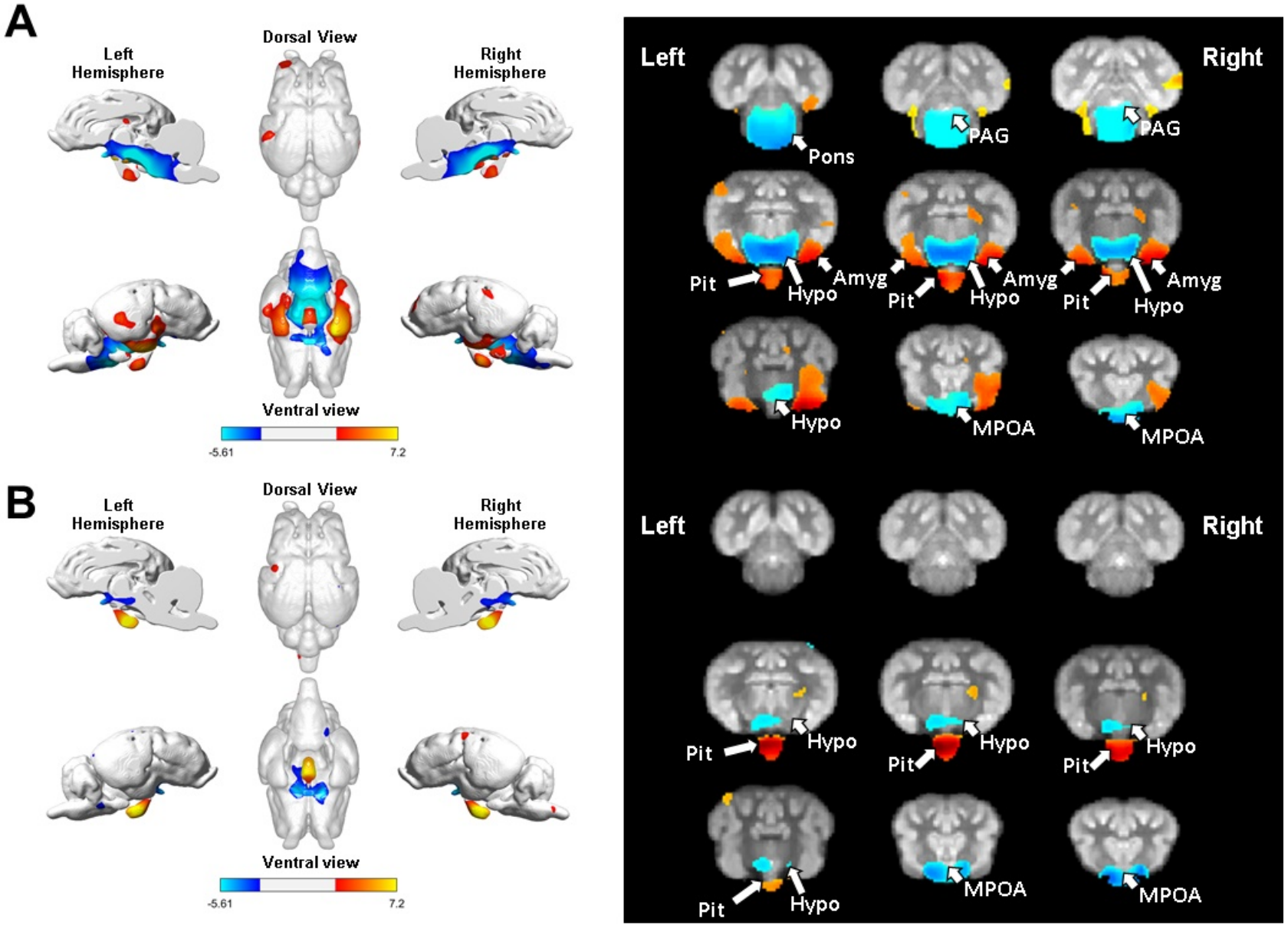
A
Left Hemisphere
Dorsal View
Right Hemisphere
Ventral view
-5.61
7.2
B
Left Hemisphere
Dorsal View
Right Hemisphere
Ventral view
-5.61
7.2
Left
Right
Pons
PAG
PAG
Pit
Hypo
Amyg
Pit
Hypo
Amyg
Pit
Hypo
Amyg
Hypo
MPOA
MPOA
Left
Right
Pit
Hypo
Pit
Hypo
Pit
Hypo
Pit
Hypo
MPOA
MPOA

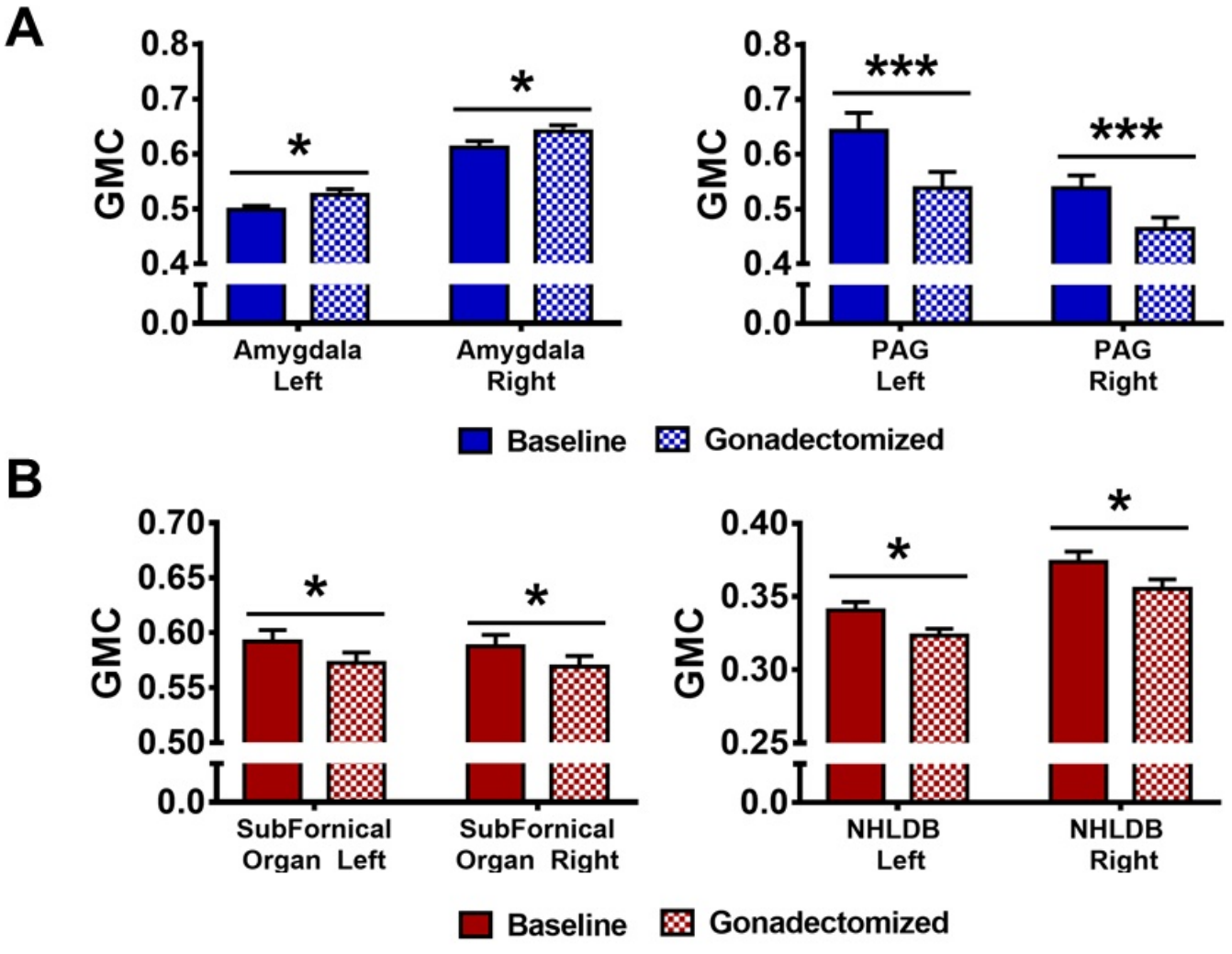
A
GMC
0.8
0.7
0.6
0.5
0.4
0.0
*
*
Amygdala Left
Amygdala Right
***
***
PAG Left
PAG Right
Baseline
Gonadectomized
B
GMC
0.70
0.65
0.60
0.55
0.50
0.0
*
*
SubFornical Organ Left
SubFornical Organ Right
0.40
0.35
0.30
0.25
0.0
*
*
NHLDB Left
NHLDB Right
Baseline
Gonadectomized

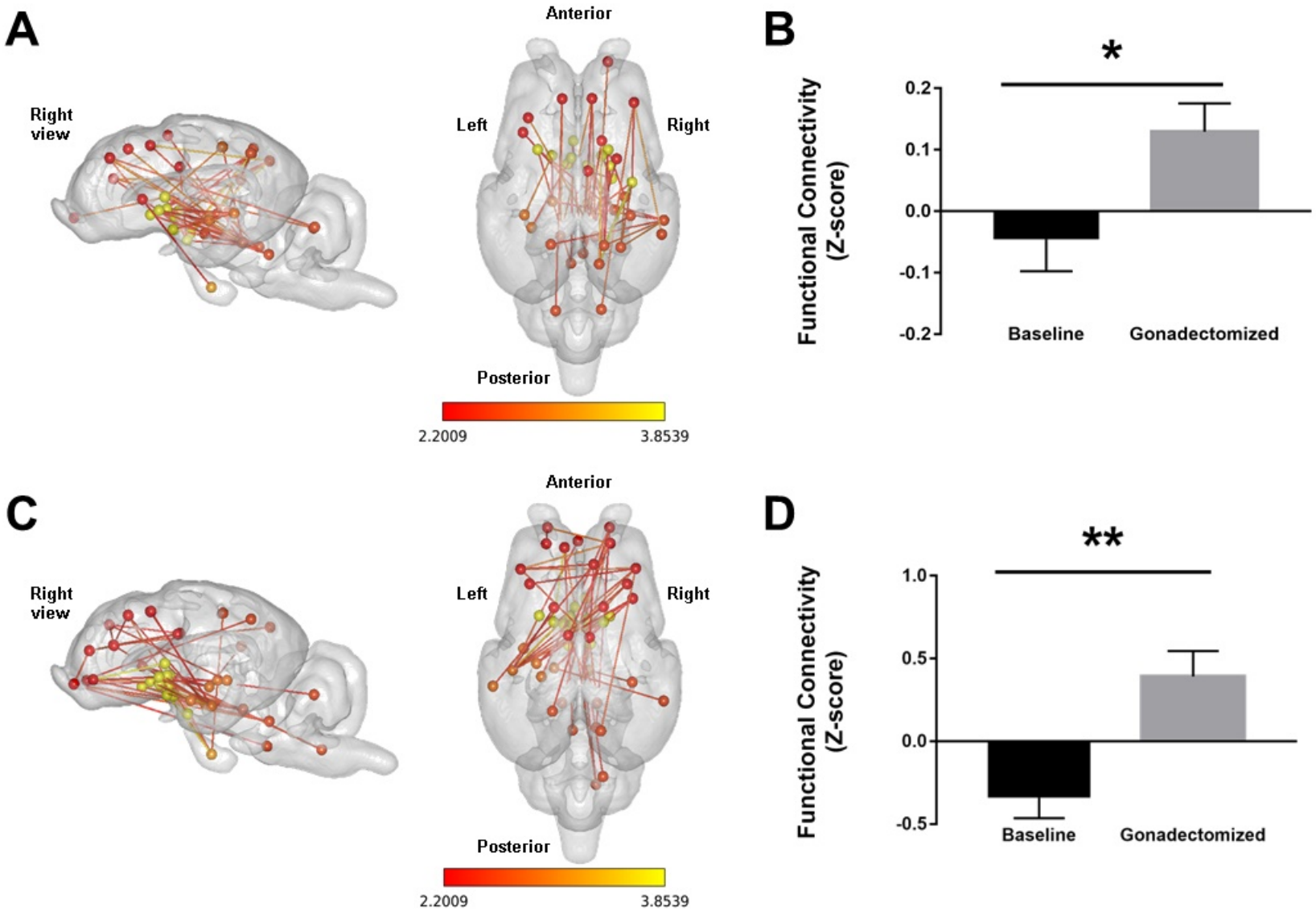
A
Right view
Anterior
Left
Right
Posterior
2.2009
3.8539
B
*
Functional Connectivity (Z-score)
0.2
0.1
0.0
-0.1
-0.2
Baseline
Gonadectomized
C
Right view
Anterior
Left
Right
Posterior
2.2009
3.8539
D
**
Functional Connectivity (Z-score)
1.0
0.5
0.0
-0.5
Baseline
Gonadectomized

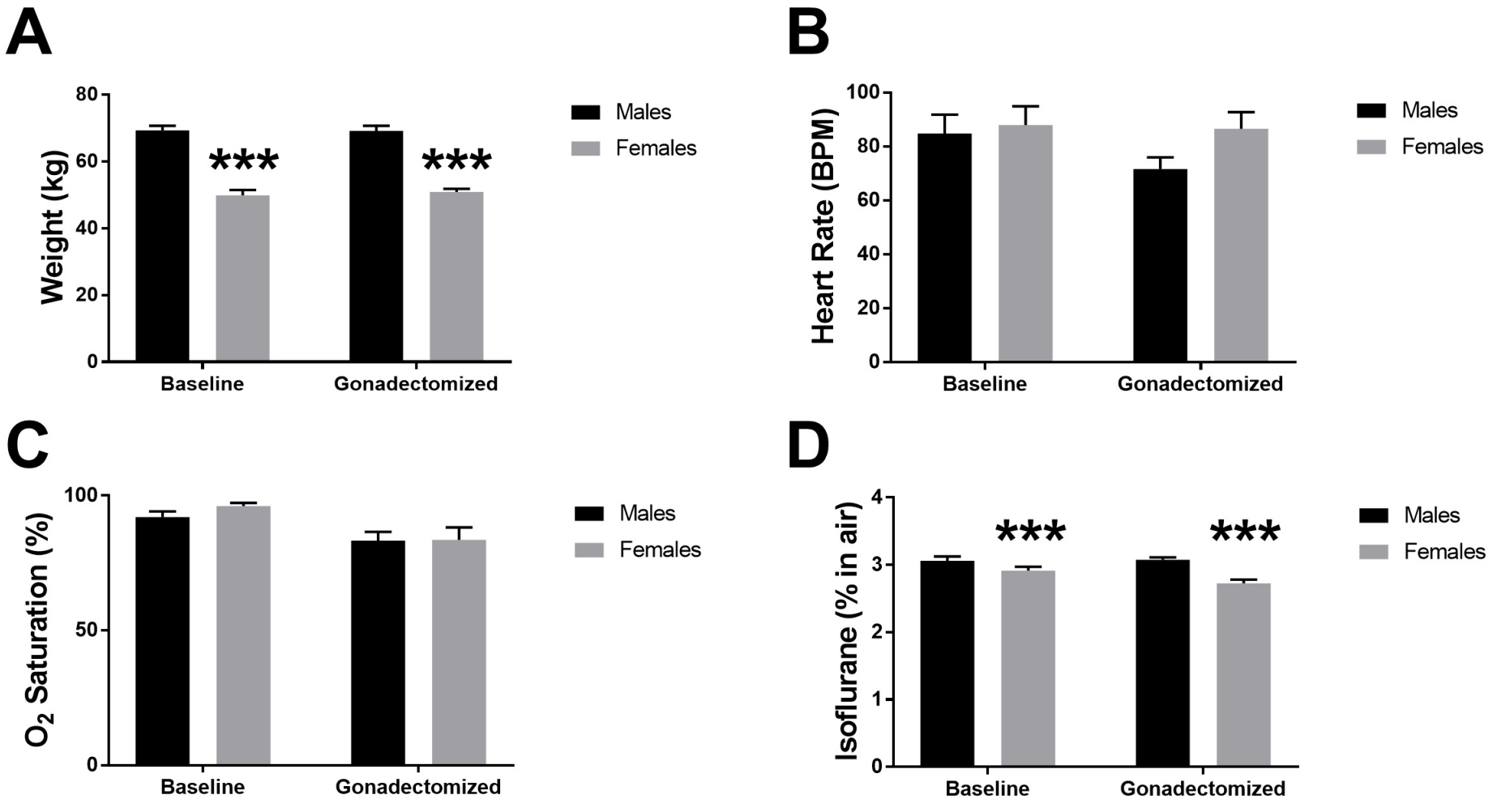
A
Weight (kg)
80
60
40
20
0
***
***
Baseline
Gonadectomized
Males
Females
B
Heart Rate (BPM)
100
80
60
40
20
0
Baseline
Gonadectomized
Males
Females
C
O2 Saturation (%)
100
50
0
Baseline
Gonadectomized
Males
Females
D
Isoflurane (% in air)
4
3
2
1
0
***
***
Baseline
Gonadectomized
Males
Females

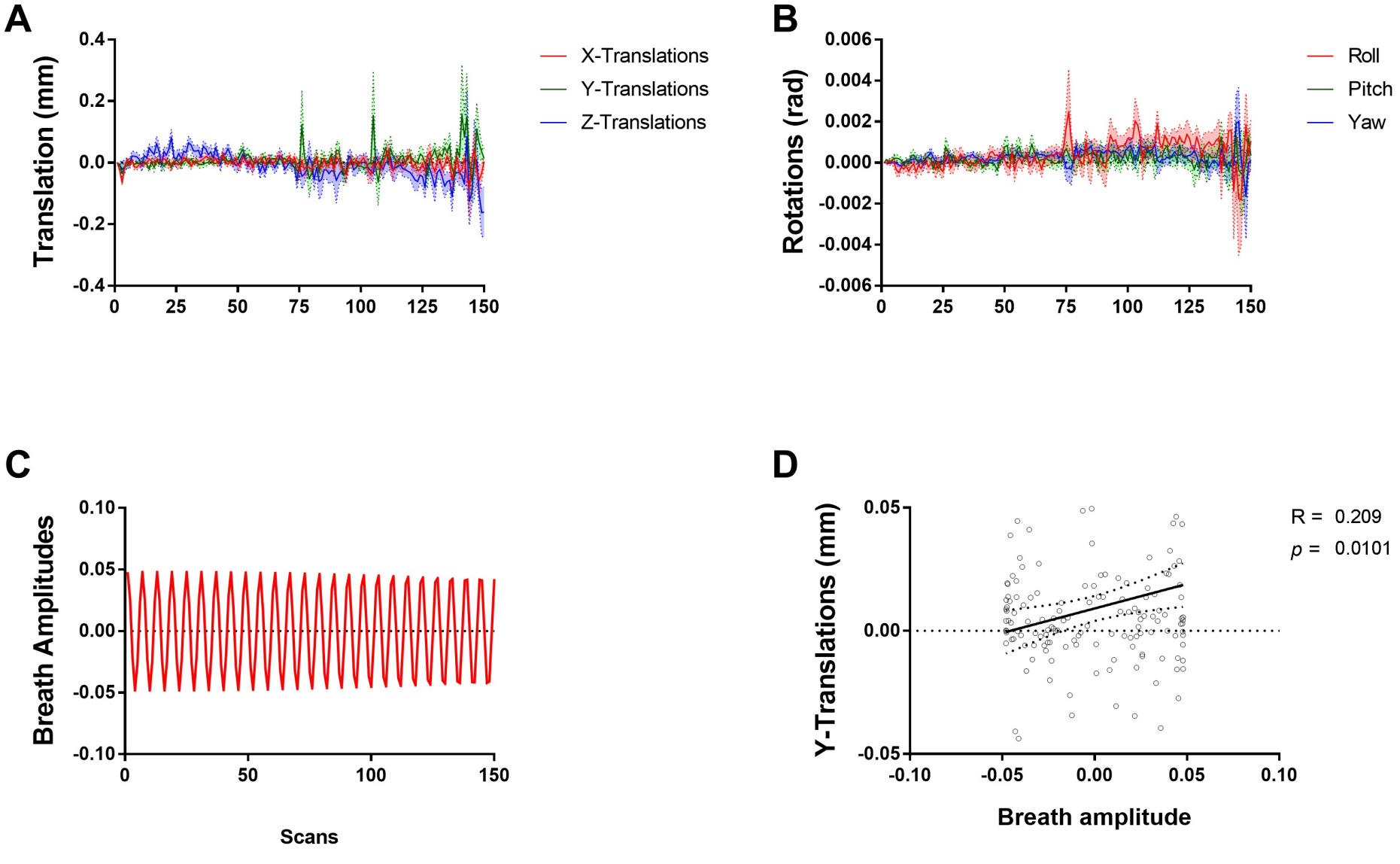
A
Translation (mm)
0.4
0.2
0.0
-0.2
-0.4
0
25
50
75
100
125
150
X-Translations
Y-Translations
Z-Translations
B
Rotations (rad)
0.006
0.004
0.002
0.000
-0.002
-0.004
-0.006
0
25
50
75
100
125
150
Roll
Pitch
Yaw
C
Breath Amplitudes
0.10
0.05
0.00
-0.05
-0.10
0
50
100
150
Scans
D
Y-Translations (mm)
0.05
0.00
-0.05
-0.10
-0.05
0.00
0.05
0.10
Breath amplitude
R = 0.209
p = 0.0101

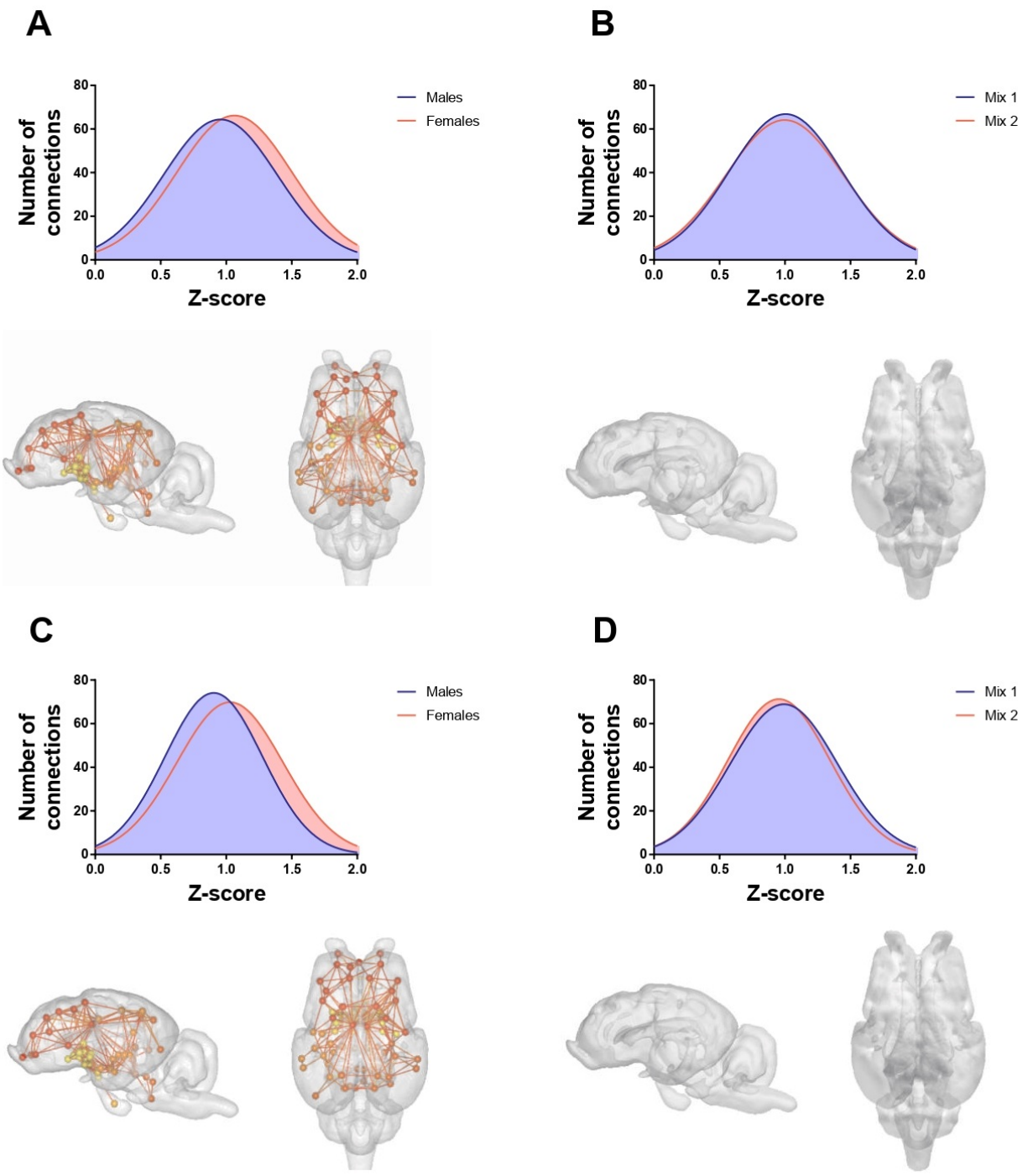
A
Number of connections
Z-score
Males
Females
B
Mix 1
Mix 2
C
D

A

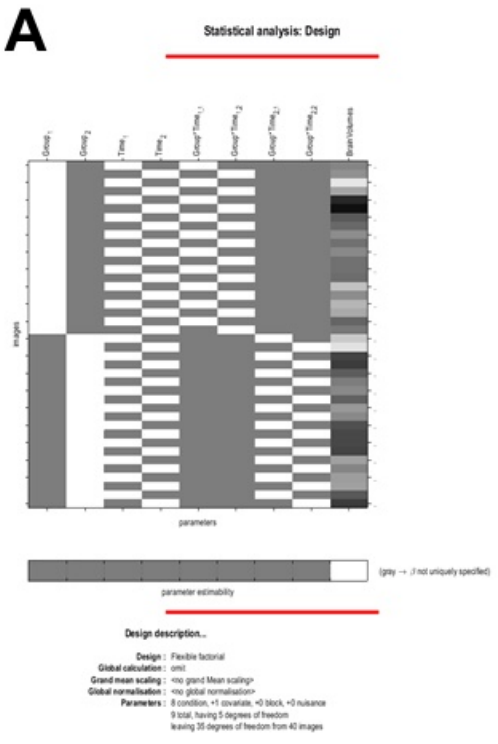

Design description..

Design : Flexible factorial
Global calculation : omit
Grand mean scaling : <no grand Mean scaling>
Global normalisation : <no global normalisation>
Parameters : 8 condition, +1 covariate, +0 block, +0 nuisance
9 total, having 5 degrees of freedom
leaving 35 degrees of freedom from 40 images

B

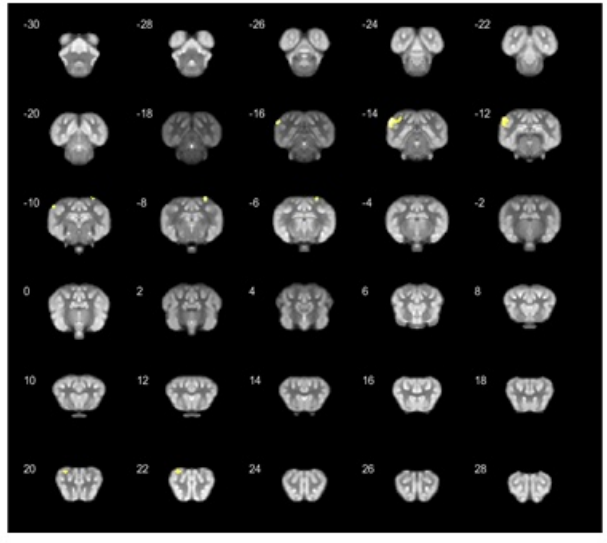

C

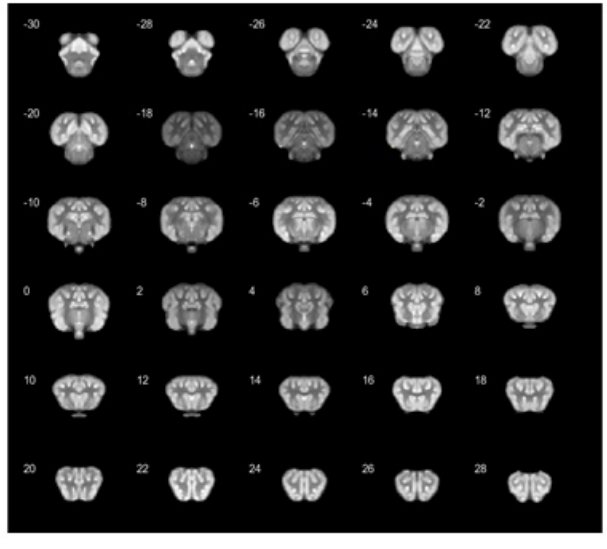

Comparison	Mean Males	Mean Females	Mean Diff	95,00% CI of diff	t	Individual P Value	Summary
Amygdala Right							
Males Baseline vs. Females Baseline	0,4821	0,5064	-0,02427	-0,04726 to -0,001285	2,071	0,0385	*
Males Gonadectomized vs. Females Gonadectomized	0,4952	0,501	-0,005836	-0,0279 to 0,01623	0,5188	0,6039	ns
Cingulate Cortex Left							
Males Baseline vs. Females Baseline	0,3795	0,4087	-0,02927	-0,05226 to -0,006284	2,497	0,0126	*
Males Gonadectomized vs. Females Gonadectomized	0,3748	0,394	-0,01917	-0,04124 to 0,002891	1,704	0,0885	ns
Hippocampus Left							
Males Baseline vs. Females Baseline	0,4393	0,4659	-0,02663	-0,04819 to -0,005069	2,422	0,0155	*
Males Gonadectomized vs. Females Gonadectomized	0,4602	0,4692	-0,008939	-0,0305 to 0,01262	0,813	0,4163	ns
Hippocampus Right							
Males Baseline vs. Females Baseline	0,5447	0,5915	-0,04677	-0,06976 to -0,02378	3,99	<0,0001	****
Males Gonadectomized vs. Females Gonadectomized	0,5856	0,588	-0,002384	-0,02445 to 0,01968	0,2119	0,8322	ns
Gyrus Rectus Right							
Males Baseline vs. Females Baseline	0,3713	0,3986	-0,0273	-0,05029 to -0,00431	2,329	0,02	*
Males Gonadectomized vs. Females Gonadectomized	0,3729	0,3903	-0,01737	-0,03944 to 0,004689	1,545	0,1226	ns
Medial Mamillary Nucleus Left							
Males Baseline vs. Females Baseline	0,4145	0,3754	0,03906	0,0175 to 0,06063	3,553	0,0004	***
Males Gonadectomized vs. Females Gonadectomized	0,3778	0,3596	0,0182	-0,003361 to 0,03976	1,655	0,098	ns
Medial Mamillary Nucleus Right							
Males Baseline vs. Females Baseline	0,3979	0,3599	0,03801	0,01644 to 0,05957	3,457	0,0006	***
Males Gonadectomized vs. Females Gonadectomized	0,3647	0,3474	0,01731	-0,004256 to 0,03887	1,574	0,1156	ns
Parahippocampal Cortex Left							
Males Baseline vs. Females Baseline	0,2995	0,3216	-0,02207	-0,04506 to 0,0009229	1,883	0,05	*
Males Gonadectomized vs. Females Gonadectomized	0,314	0,322	-0,008038	-0,0301 to 0,01403	0,7145	0,475	ns
Parahippocampal Cortex Right							
Males Baseline vs. Females Baseline	0,4254	0,4559	-0,03051	-0,0535 to -0,00752	2,603	0,0093	**
Males Gonadectomized vs. Females Gonadectomized	0,4503	0,4543	-0,004017	-0,02608 to 0,01805	0,3571	0,7211	ns
Pituitary Gland Left							
Males Baseline vs. Females Baseline	0,1744	0,1472	0,02718	0,005614 to 0,04874	2,657	0,015	*
Males Gonadectomized vs. Females Gonadectomized	0,1798	0,1653	0,01447	-0,007096 to 0,03603	1,236	0,1984	ns
Pituitary Gland Right							
Males Baseline vs. Females Baseline	0,1923	0,1631	0,02925	0,007684 to 0,05081	2,76	0,0069	**
Males Gonadectomized vs. Females Gonadectomized	0,1971	0,1832	0,0139	-0,007664 to 0,03546	1,64	0,1963	ns
Putamen Right							
Males Baseline vs. Females Baseline	0,3928	0,4173	-0,02443	-0,04741 to -0,001435	2,084	0,0373	*
Males Gonadectomized vs. Females Gonadectomized	0,4033	0,416	-0,01274	-0,0348 to 0,009325	1,132	0,2576	ns
Suprasylvian Gyrus Right							
Males Baseline vs. Females Baseline	0,415	0,4498	-0,03488	-0,05787 to -0,01189	2,976	0,003	**
Males Gonadectomized vs. Females Gonadectomized	0,4467	0,4477	-0,0009936	-0,02306 to 0,02107	0,08833	0,9296	ns
Medial Mamillary Nucleus Left							
Males Baseline vs. Females Baseline	0,4145	0,3754	0,03906	0,0175 to 0,06063	3,553	0,0004	***
Males Gonadectomized vs. Females Gonadectomized	0,3778	0,3596	0,0182	-0,003361 to 0,03976	1,655	0,098	ns
Medial Mamillary Nucleus Right							
Males Baseline vs. Females Baseline	0,3979	0,3599	0,03801	0,01644 to 0,05957	3,457	0,0006	***
Males Gonadectomized vs. Females Gonadectomized	0,3647	0,3474	0,01731	-0,004256 to 0,03887	1,574	0,1156	ns

Comparison	Mean Males	Mean Females	Mean Diff	95,00% CI of diff	t	Individual P Value	Summary
AnteriorSigmoideus Gyrus Right							
Males Baseline vs. Females Baseline	0,2171	0,1821	0,03498	0,01199 to 0,05797	2,984	0,0029	**
Males Gonadectomized vs. Females Gonadectomized	0,2073	0,1791	0,02817	0,006102 to 0,05023	2,504	0,0124	*
Cerebellum Left							
Males Baseline vs. Females Baseline	0,5363	0,5033	0,03296	0,009972 to 0,05595	2,812	0,005	**
Males Gonadectomized vs. Females Gonadectomized	0,5331	0,4969	0,03621	0,01415 to 0,05827	3,219	0,0013	**
Cerebellum Right							
Males Baseline vs. Females Baseline	0,452	0,4275	0,0245	0,00151 to 0,04749	2,09	0,0368	*
Males Gonadectomized vs. Females Gonadectomized	0,4499	0,4211	0,0288	0,006735 to 0,05086	2,56	0,0106	*
Ectolateralis Gyrus Left							
Males Baseline vs. Females Baseline	0,4044	0,4461	-0,04163	-0,06462 to -0,01864	3,552	0,0004	***
Males Gonadectomized vs. Females Gonadectomized	0,3992	0,4382	-0,03897	-0,06104 to -0,01691	3,465	0,0005	***
Ectolateralis Gyrus Right							
Males Baseline vs. Females Baseline	0,4137	0,4663	-0,05258	-0,07557 to -0,02959	4,486	<0,0001	****
Males Gonadectomized vs. Females Gonadectomized	0,4047	0,4428	-0,03806	-0,06013 to -0,016	3,384	0,0007	***
Entolateral Gyrus Left							
Males Baseline vs. Females Baseline	0,433	0,4709	-0,03788	-0,06087 to -0,01489	3,232	0,0013	**
Males Gonadectomized vs. Females Gonadectomized	0,4318	0,4572	-0,02542	-0,04748 to -0,003356	2,26	0,024	*
Entolateral Gyrus Right							
Males Baseline vs. Females Baseline	0,4938	0,5382	-0,04439	-0,06738 to -0,0214	3,787	0,0002	***
Males Gonadectomized vs. Females Gonadectomized	0,4909	0,5205	-0,02962	-0,05169 to -0,007559	2,633	0,0085	**
Insula Right							
Males Baseline vs. Females Baseline	0,4799	0,5232	-0,04335	-0,06634 to -0,02036	3,698	0,0002	***
Males Gonadectomized vs. Females Gonadectomized	0,4853	0,5159	-0,03066	-0,05272 to -0,008596	2,725	0,0065	**
Lateral Gyrus Left							
Males Baseline vs. Females Baseline	0,4826	0,5276	-0,045	-0,06799 to -0,02201	3,839	0,0001	***
Males Gonadectomized vs. Females Gonadectomized	0,4804	0,5171	-0,03669	-0,05876 to -0,01463	3,262	0,0011	**
Lateral Gyrus Right							
Males Baseline vs. Females Baseline	0,4761	0,5282	-0,05214	-0,07513 to -0,02915	4,448	<0,0001	****
Males Gonadectomized vs. Females Gonadectomized	0,4725	0,5081	-0,03556	-0,05763 to -0,0135	3,162	0,0016	**
Medial Mamillary Nucleus Left							
Males Baseline vs. Females Baseline	0,3947	0,3483	0,04637	0,02338 to 0,06936	3,956	<0,0001	****
Males Gonadectomized vs. Females Gonadectomized	0,3615	0,3369	0,02457	0,002504 to 0,04663	2,184	0,0291	*
Medial Mamillary Nucleus Right							
Males Baseline vs. Females Baseline	0,3758	0,3316	0,04415	0,02116 to 0,06714	3,767	0,0002	***
Males Gonadectomized vs. Females Gonadectomized	0,346	0,3228	0,02318	0,001121 to 0,04525	2,061	0,0395	*
Medial Septal Nucleus Left							
Males Baseline vs. Females Baseline	0,3558	0,3852	-0,02944	-0,05243 to -0,006455	2,512	0,0121	*
Males Gonadectomized vs. Females Gonadectomized	0,3612	0,385	-0,02386	-0,04592 to -0,001795	2,121	0,0341	*
Occipital Lobe Left							
Males Baseline vs. Females Baseline	0,4001	0,443	-0,04296	-0,06595 to -0,01997	3,665	0,0003	***
Males Gonadectomized vs. Females Gonadectomized	0,3982	0,4349	-0,03663	-0,0587 to -0,01457	3,257	0,0011	**
Occipital Lobe Right							
Males Baseline vs. Females Baseline	0,4175	0,4589	-0,04142	-0,06441 to -0,01844	3,534	0,0004	***
Males Gonadectomized vs. Females Gonadectomized	0,4182	0,4438	-0,0256	-0,04766 to -0,003535	2,276	0,023	*
Olfactory Bulb Right							
Males Baseline vs. Females Baseline	0,2664	0,3154	-0,04899	-0,07198 to -0,026	4,18	<0,0001	****
Males Gonadectomized vs. Females Gonadectomized	0,2749	0,3135	-0,03868	-0,06074 to -0,01661	3,438	0,0006	***
Orbital Gyrus Right							
Males Baseline vs. Females Baseline	0,4071	0,4407	-0,03356	-0,05655 to -0,01058	2,864	0,0042	**
Males Gonadectomized vs. Females Gonadectomized	0,4101	0,4337	-0,02368	-0,04574 to -0,001613	2,105	0,0355	*
PostCruciate Gyrus Left							
Males Baseline vs. Females Baseline	0,4971	0,4549	0,04219	0,0192 to 0,06518	3,6	0,0003	***
Males Gonadectomized vs. Females Gonadectomized	0,4891	0,4472	0,04187	0,01981 to 0,06393	3,722	0,0002	***
Posterior Sygmoideus Gyrus Left							
Males Baseline vs. Females Baseline	0,3077	0,2794	0,02831	0,005325 to 0,0513	2,416	0,0158	*
Males Gonadectomized vs. Females Gonadectomized	0,3027	0,274	0,02874	0,006673 to 0,0508	2,555	0,0107	*
Posterior Sygmoideus Gyrus Right							
Males Baseline vs. Females Baseline	0,3678	0,337	0,03078	0,007788 to 0,05377	2,626	0,0087	**
Males Gonadectomized vs. Females Gonadectomized	0,363	0,3274	0,03554	0,01347 to 0,0576	3,159	0,0016	**
Posterior Sylvian Gyrus Right							
Males Baseline vs. Females Baseline	0,4803	0,5318	-0,05155	-0,07454 to -0,02856	4,398	<0,0001	****
Males Gonadectomized vs. Females Gonadectomized	0,4782	0,515	-0,03686	-0,05892 to -0,0148	3,277	0,0011	**
Sylvian Gyrus Right							
Males Baseline vs. Females Baseline	0,4623	0,5024	-0,0402	-0,06318 to -0,01721	3,429	0,0006	***
Males Gonadectomized vs. Females Gonadectomized	0,4597	0,4886	-0,02888	-0,05094 to -0,006813	2,567	0,0103	*

Brain Region 1	Brain Region 2	Mean functionnal connectivity Male baseline (Z score)	Mean functionnal connectivity Female baseline (Z score)
Amygdala Left	Substantia Nigra Left	1,311	3,452
Amygdala Left	Globus Pallidum Left	2,148	1,805
Amygdala Right	Parahippocampal Cortex Right	1,223	1,021
Amygdala Right	Substantia Nigra Right	0,845	1,507
Amygdala Right	Globus Pallidum Right	0,732	-0,067
AnteriorSigmoideus Gyrus Left	Orbitofrontal Gyrus Left	1,446	1,935
AnteriorSigmoideus Gyrus Left	Precruciate Gyrus Left	0,622	1,501
AnteriorSigmoideus Gyrus Left	PostCruciate Gyrus Left	0,887	1,685
AnteriorSigmoideus Gyrus Left	Posterior Sygmoideus Gyrus Left	0,372	0,703
AnteriorSigmoideus Gyrus Right	Cingulate Cortex Right	1,019	0,960
AnteriorSigmoideus Gyrus Right	Orbital Gyrus Right	0,585	-0,354
AnteriorSigmoideus Gyrus Right	Orbitofrontal Gyrus Right	1,163	1,868
AnteriorSigmoideus Gyrus Right	Caudate Right	1,276	1,075
AnteriorSigmoideus Gyrus Right	Precruciate Gyrus Right	1,159	1,125
AnteriorSigmoideus Gyrus Right	Putamen Right	1,245	0,960
AnteriorSigmoideus Gyrus Right	Claustrocortex(Insula) Right	1,213	1,599
AnteriorSigmoideus Gyrus Right	PostCruciate Gyrus Right	1,360	1,512
AnteriorSigmoideus Gyrus Right	Posterior Sygmoideus Gyrus Right	1,141	0,650
AnteriorSigmoideus Gyrus Right	Sylvian Gyrus Right	1,070	0,855
Bed Nucleus of Stria Terminalis Left	Lateral Septal Nucleus Left	1,017	1,913
Bed Nucleus of Stria Terminalis Left	Medial Septal Nucleus Left	1,292	1,638
Bed Nucleus of Stria Terminalis Left	Septum Left	1,054	1,776
Bed Nucleus of Stria Terminalis Left	Preoptic Hypothalamic Area Left	2,034	2,103
Bed Nucleus of Stria Terminalis Left	Nucleus Of The Horizontal Limb Of The Diagonal Band Left	1,773	2,092
Bed Nucleus of Stria Terminalis Left	Caudate Left	0,523	1,668
Bed Nucleus of Stria Terminalis Left	Globus Pallidum Left	1,194	0,931
Bed Nucleus of Stria Terminalis Left	Putamen Left	0,329	0,977
Bed Nucleus of Stria Terminalis Left	PostCruciate Gyrus Left	0,265	1,088
Bed Nucleus of Stria Terminalis Left	SubFornical Organ Right	1,246	1,844
Bed Nucleus of Stria Terminalis Left	Bed Nucleus of Stria Terminalis Right	1,285	1,735
Bed Nucleus of Stria Terminalis Left	Lateral Septal Nucleus Right	0,629	1,532
Bed Nucleus of Stria Terminalis Left	Septum Right	0,525	1,376
Bed Nucleus of Stria Terminalis Left	Preoptic Hypothalamic Area Right	1,542	1,735
Bed Nucleus of Stria Terminalis Right	Lateral Septal Nucleus Right	1,154	1,660
Bed Nucleus of Stria Terminalis Right	Medial Septal Nucleus Right	1,414	1,780
Bed Nucleus of Stria Terminalis Right	Septum Right	0,319	1,519
Bed Nucleus of Stria Terminalis Right	Preoptic Hypothalamic Area Right	1,955	1,896
Bed Nucleus of Stria Terminalis Right	Caudate Right	-0,261	1,093
Bed Nucleus of Stria Terminalis Right	Globus Pallidum Right	0,327	1,601
Bed Nucleus of Stria Terminalis Right	Putamen Right	-0,336	1,525
Caudate Left	Globus Pallidum Left	1,302	0,969
Caudate Left	Putamen Left	1,533	2,379
Caudate Left	Claustrocortex(Insula) Left	1,290	0,011
Caudate Left	PostCruciate Gyrus Left	0,753	0,528
Caudate Left	SubFornical Organ Right	-0,954	0,930
Caudate Left	Bed Nucleus of Stria Terminalis Right	-0,289	0,981
Caudate Left	Septum Right	1,279	0,922
Caudate Left	Preoptic Hypothalamic Area Right	0,543	1,115
Caudate Left	Caudate Right	1,047	0,867
Caudate Right	Globus Pallidum Right	0,759	1,362
Caudate Right	Precruciate Gyrus Right	0,821	0,779
Caudate Right	Putamen Right	1,591	2,012
Caudate Right	Claustrocortex(Insula) Right	1,075	1,534
Caudate Right	PostCruciate Gyrus Right	1,159	1,515
Caudate Right	Posterior Sygmoideus Gyrus Right	0,868	1,505
Caudate Right	Suprasylvian Gyrus Right	0,306	0,854
Caudate Right	Sylvian Gyrus Right	0,759	1,408
Cingulate Cortex Left	Orbitofrontal Gyrus Left	1,292	0,549
Cingulate Cortex Left	Hippocampus Left	0,163	1,108
Cingulate Cortex Left	Caudate Left	1,008	1,235
Cingulate Cortex Left	Precruciate Gyrus Left	1,605	2,187
Cingulate Cortex Left	Putamen Left	0,853	1,227
Cingulate Cortex Left	Thalamus Left	0,705	0,804
Cingulate Cortex Left	Lateral Gyrus Left	0,225	1,482
Cingulate Cortex Left	PostCruciate Gyrus Left	1,231	1,063
Cingulate Cortex Left	Posterior Sygmoideus Gyrus Left	0,594	0,885
Cingulate Cortex Left	Suprasylvian Gyrus Left	0,763	0,684
Cingulate Cortex Left	Ectolateralis Gyrus Left	-0,157	1,349
Cingulate Cortex Left	Entolateral Gyrus Left	1,118	0,943
Cingulate Cortex Left	Bed Nucleus of Stria Terminalis Right	-0,209	0,266
Cingulate Cortex Left	Medial Septal Nucleus Right	-0,468	-0,210
Cingulate Cortex Left	Pineal Gland Right	0,595	0,551
Cingulate Cortex Left	Septum Right	1,042	1,050
Cingulate Cortex Left	Preoptic Hypothalamic Area Right	0,636	0,395
Cingulate Cortex Left	AnteriorSigmoideus Gyrus Right	1,054	0,830
Cingulate Cortex Left	Cingulate Cortex Right	1,249	2,113
Cingulate Cortex Left	Orbitofrontal Gyrus Right	1,107	1,375
Cingulate Cortex Left	Nucleus Of The Horizontal Limb Of The Diagonal Band Right	0,845	0,728
Cingulate Cortex Left	Caudate Right	1,055	1,130
Cingulate Cortex Left	Precruciate Gyrus Right	1,376	1,479
Cingulate Cortex Left	Putamen Right	0,917	0,268
Cingulate Cortex Left	Claustrocortex(Insula) Right	0,988	1,079
Cingulate Cortex Left	Lateral Gyrus Right	0,592	0,787
Cingulate Cortex Left	PostCruciate Gyrus Right	1,013	1,285
Cingulate Cortex Left	Suprasylvian Gyrus Right	0,754	0,628
Cingulate Cortex Right	Orbitofrontal Gyrus Right	1,230	1,517
Cingulate Cortex Right	Hippocampus Right	1,173	1,344
Cingulate Cortex Right	Caudate Right	1,049	1,066
Cingulate Cortex Right	Precruciate Gyrus Right	1,385	1,673
Cingulate Cortex Right	Putamen Right	0,949	0,301
Cingulate Cortex Right	Thalamus Right	0,810	0,863
Cingulate Cortex Right	Claustrocortex(Insula) Right	1,150	1,390
Cingulate Cortex Right	Lateral Gyrus Right	0,955	1,556
Cingulate Cortex Right	PostCruciate Gyrus Right	1,244	1,282
Cingulate Cortex Right	Posterior Sygmoideus Gyrus Right	1,112	1,288
Cingulate Cortex Right	Suprasylvian Gyrus Right	1,048	1,272
Cingulate Cortex Right	Sylvian Gyrus Right	1,048	1,015
Cingulate Cortex Right	Ectolateralis Gyrus Right	0,939	1,796

Claustrocortex(Insula) Left	Sylvian Gyrus Left	0,944	0,346
Claustrocortex(Insula) Right	Sylvian Gyrus Right	1,381	1,561
Ectolateralis Gyrus Left	Entolateral Gyrus Left	-0,267	1,271
Ectolateralis Gyrus Left	Occipital Lobe Left	2,657	1,682
Ectolateralis Gyrus Left	Lateral Gyrus Right	-0,085	0,948
Geniculate Nucleus Left	Thalamus Left	1,797	2,872
Geniculate Nucleus Left	Midbrain Left	0,203	1,025
Geniculate Nucleus Right	Thalamus Right	1,801	0,225
Globus Pallidum Left	Putamen Left	0,621	1,291
Globus Pallidum Right	Putamen Right	0,485	1,770
Gyrus Rectus Left	Olfactory Bulb Left	2,989	2,483
Gyrus Rectus Left	Gyrus Rectus Right	2,883	2,094
Gyrus Rectus Right	Olfactory Bulb Right	2,231	2,710
Hippocampus Left	Parahippocampal Cortex Left	-0,225	1,241
Hippocampus Left	Geniculate Nucleus Left	1,009	2,304
Hippocampus Left	Thalamus Left	0,455	2,052
Hippocampus Left	Lateral Gyrus Left	0,524	1,795
Hippocampus Left	Suprasylvian Gyrus Left	0,572	2,436
Hippocampus Left	Ectolateralis Gyrus Left	0,528	1,865
Hippocampus Left	Midbrain Left	-0,702	1,017
Hippocampus Left	Pineal Gland Right	-0,915	0,854
Hippocampus Left	Nucleus Of The Horizontal Limb Of The Diagonal Band Right	0,175	1,284
Hippocampus Left	Periaqueductal Grey Substance Right	-1,578	-0,655
Hippocampus Right	Parahippocampal Cortex Right	0,858	1,224
Hippocampus Right	Geniculate Nucleus Right	1,061	0,727
Hippocampus Right	Periaqueductal Grey Substance Right	1,602	0,235
Hippocampus Right	Thalamus Right	0,940	0,796
Hippocampus Right	Suprasylvian Gyrus Right	1,143	1,893
Lateral Gyrus Left	Suprasylvian Gyrus Left	0,877	1,772
Lateral Gyrus Left	Ectolateralis Gyrus Left	2,332	2,461
Lateral Gyrus Left	Entolateral Gyrus Left	0,144	2,306
Lateral Gyrus Left	Occipital Lobe Left	2,382	1,454
Lateral Gyrus Left	Pineal Gland Right	1,109	0,802
Lateral Gyrus Left	Lateral Gyrus Right	0,158	0,756
Lateral Gyrus Right	Suprasylvian Gyrus Right	1,306	1,849
Lateral Septal Nucleus Left	Medial Septal Nucleus Left	1,060	2,146
Lateral Septal Nucleus Left	Septum Left	-0,136	0,654
Lateral Septal Nucleus Left	Preoptic Hypothalamic Area Left	1,236	1,554
Lateral Septal Nucleus Left	Nucleus Of The Horizontal Limb Of The Diagonal Band Left	2,579	2,331
Lateral Septal Nucleus Left	Substantia Nigra Left	1,295	0,142
Lateral Septal Nucleus Left	Globus Pallidum Left	-0,012	1,548
Lateral Septal Nucleus Left	Medial Mamillary Nucleus Right	1,400	0,503
Lateral Septal Nucleus Left	SubFornical Organ Right	2,200	1,703
Lateral Septal Nucleus Left	Bed Nucleus of Stria Terminalis Right	1,220	1,082
Lateral Septal Nucleus Left	Lateral Septal Nucleus Right	2,345	1,966
Lateral Septal Nucleus Left	Preoptic Hypothalamic Area Right	0,751	0,933
Lateral Septal Nucleus Right	Medial Septal Nucleus Right	1,650	1,786
Lateral Septal Nucleus Right	Preoptic Hypothalamic Area Right	0,654	1,188
Lateral Septal Nucleus Right	Nucleus Of The Horizontal Limb Of The Diagonal Band Right	-0,590	-0,473
Lateral Septal Nucleus Right	Substantia Nigra Right	0,394	1,001
Lateral Septal Nucleus Right	Globus Pallidum Right	-0,520	0,729
Medial Mamillary Nucleus Left	Lateral Septal Nucleus Left	1,344	1,154
Medial Mamillary Nucleus Left	Medial Septal Nucleus Left	0,295	1,242
Medial Mamillary Nucleus Left	Nucleus Of The Horizontal Limb Of The Diagonal Band Left	0,756	0,803
Medial Mamillary Nucleus Left	Substantia Nigra Left	1,705	1,286
Medial Mamillary Nucleus Left	Medial Mamillary Nucleus Right	2,064	2,104
Medial Mamillary Nucleus Right	Lateral Septal Nucleus Right	1,502	1,414
Medial Mamillary Nucleus Right	Substantia Nigra Right	1,079	0,993
Medial Mamillary Nucleus Right	Pituitary Gland Right	1,235	1,002
Medial Septal Nucleus Left	Preoptic Hypothalamic Area Left	1,645	1,393
Medial Septal Nucleus Left	Nucleus Of The Horizontal Limb Of The Diagonal Band Left	1,009	1,581
Medial Septal Nucleus Left	Substantia Nigra Left	0,551	1,268
Medial Septal Nucleus Left	Caudate Left	0,253	0,218
Medial Septal Nucleus Left	Globus Pallidum Left	1,230	2,072
Medial Septal Nucleus Left	SubFornical Organ Right	0,540	0,456
Medial Septal Nucleus Left	Lateral Septal Nucleus Right	0,646	0,673
Medial Septal Nucleus Left	Medial Septal Nucleus Right	-0,039	0,861
Medial Septal Nucleus Left	Preoptic Hypothalamic Area Right	-0,213	0,185
Medial Septal Nucleus Right	Preoptic Hypothalamic Area Right	0,210	1,479
Medial Septal Nucleus Right	Substantia Nigra Right	-0,246	-0,336
Medial Septal Nucleus Right	Caudate Right	-1,551	0,448
Medial Septal Nucleus Right	Globus Pallidum Right	-0,243	1,625
Medial Septal Nucleus Right	Putamen Right	-1,611	0,781
Midbrain Left	Pineal Gland Right	1,446	1,172
Midbrain Left	Pons Right	1,269	-0,536
Midbrain Left	Hippocampus Right	1,305	0,155
Midbrain Left	Periaqueductal Grey Substance Right	1,311	-1,194
Nucleus Of The Horizontal Limb Of The Diagonal Band Left	Globus Pallidum Left	0,679	1,534
Nucleus Of The Horizontal Limb Of The Diagonal Band Left	Putamen Left	-0,790	0,040
Nucleus Of The Horizontal Limb Of The Diagonal Band Left	SubFornical Organ Right	1,741	1,597
Nucleus Of The Horizontal Limb Of The Diagonal Band Left	Bed Nucleus of Stria Terminalis Right	0,689	1,267
Nucleus Of The Horizontal Limb Of The Diagonal Band Left	Lateral Septal Nucleus Right	1,639	1,392
Olfactory Bulb Left	Gyrus Rectus Right	2,658	2,390
Orbital Gyrus Left	Orbitofrontal Gyrus Left	0,935	0,824
Orbital Gyrus Left	Precruciate Gyrus Left	0,657	-0,021
Orbital Gyrus Left	Gyrus Rectus Left	2,899	0,806
Orbital Gyrus Left	Claustrocortex(Insula) Left	0,824	2,944
Orbital Gyrus Right	Orbitofrontal Gyrus Right	0,362	-0,001
Orbital Gyrus Right	Precruciate Gyrus Right	1,012	1,563
Orbital Gyrus Right	Gyrus Rectus Right	0,967	1,447
Orbital Gyrus Right	Olfactory Bulb Right	0,333	0,547
Orbital Gyrus Right	Claustrocortex(Insula) Right	0,168	-0,086
Orbitofrontal Gyrus Left	Precruciate Gyrus Left	0,680	1,103
Orbitofrontal Gyrus Left	Claustrocortex(Insula) Left	1,596	2,134
Orbitofrontal Gyrus Right	Precruciate Gyrus Right	1,236	1,380
Orbitofrontal Gyrus Right	Claustrocortex(Insula) Right	1,170	0,891
Parahippocampal Cortex Left	Thalamus Left	0,160	1,725
Parahippocampal Cortex Left	Suprasylvian Gyrus Left	0,071	1,348
Parahippocampal Cortex Left	Sylvian Gyrus Left	1,144	1,953
Parahippocampal Cortex Left	Ectolateralis Gyrus Left	-1,481	1,166
Parahippocampal Cortex Left	Nucleus Of The Horizontal Limb Of The Diagonal Band Right	1,831	2,215

Parahippocampal Cortex Right	Substantia Nigra Right	0,353	-0,863
Parahippocampal Cortex Right	Suprasylvian Gyrus Right	1,003	1,346
Parahippocampal Cortex Right	Sylvian Gyrus Right	1,128	1,667
Periaqueductal Grey Substance Left	Midbrain Left	0,484	-1,438
Periaqueductal Grey Substance Left	Pons Right	1,159	0,518
Periaqueductal Grey Substance Left	Periaqueductal Grey Substance Right	1,084	2,084
Pineal Gland Left	Pons Left	-0,010	0,497
Pineal Gland Left	Cingulate Cortex Left	-0,045	0,549
Pineal Gland Left	Hippocampus Left	-0,236	1,357
Pineal Gland Left	Geniculate Nucleus Left	0,412	1,156
Pineal Gland Left	Periaqueductal Grey Substance Left	0,092	-0,240
Pineal Gland Left	Thalamus Left	0,542	0,987
Pineal Gland Left	Lateral Gyrus Left	1,494	1,237
Pineal Gland Left	Entolateral Gyrus Left	-0,625	1,246
Pineal Gland Left	Midbrain Left	0,762	1,728
Pineal Gland Left	Pineal Gland Right	1,881	2,681
Pineal Gland Left	Hippocampus Right	0,905	0,545
Pineal Gland Left	Periaqueductal Grey Substance Right	1,296	-0,870
Pineal Gland Right	Hippocampus Right	1,176	0,669
Pineal Gland Right	Periaqueductal Grey Substance Right	1,504	-0,585
Pituitary Gland Left	Pituitary Gland Right	2,314	2,184
Pons Left	Periaqueductal Grey Substance Left	1,573	1,460
Pons Left	Midbrain Left	0,343	0,017
Pons Left	Pons Right	1,044	1,526
Pons Left	Periaqueductal Grey Substance Right	0,817	1,364
Pons Right	Periaqueductal Grey Substance Right	1,849	0,564
PostCruciate Gyrus Left	Posterior Sygmoideus Gyrus Left	1,150	1,807
PostCruciate Gyrus Left	Septum Right	0,993	0,885
PostCruciate Gyrus Left	Preoptic Hypothalamic Area Right	0,376	0,876
PostCruciate Gyrus Right	Posterior Sygmoideus Gyrus Right	1,255	1,142
PostCruciate Gyrus Right	Sylvian Gyrus Right	1,030	0,823
Posterior Sygmoideus Gyrus Left	Sylvian Gyrus Left	0,864	0,986
Posterior Sygmoideus Gyrus Left	Posterior Sygmoideus Gyrus Right	0,766	0,446
Posterior Sygmoideus Gyrus Right	Sylvian Gyrus Right	1,355	1,173
Posterior Sylvian Gyrus Left	Hippocampus Left	1,009	0,836
Posterior Sylvian Gyrus Left	Parahippocampal Cortex Left	-0,483	-0,249
Posterior Sylvian Gyrus Left	Suprasylvian Gyrus Left	0,798	1,657
Posterior Sylvian Gyrus Left	Ectolateralis Gyrus Left	0,437	0,279
Posterior Sylvian Gyrus Right	Temporal Lobe Right	1,423	2,239
Posterior Sylvian Gyrus Right	Suprasylvian Gyrus Right	1,078	1,773
Precruciate Gyrus Left	Claustrocortex(Insula) Left	0,981	0,668
Precruciate Gyrus Left	Precruciate Gyrus Right	1,373	1,764
Precruciate Gyrus Right	Gyrus Rectus Right	0,480	1,524
Precruciate Gyrus Right	Claustrocortex(Insula) Right	1,020	0,722
Precruciate Gyrus Right	PostCruciate Gyrus Right	1,044	0,376
Preoptic Hypothalamic Area Left	Nucleus Of The Horizontal Limb Of The Diagonal Band Left	1,691	1,901
Preoptic Hypothalamic Area Left	Caudate Left	0,298	1,499
Preoptic Hypothalamic Area Left	Globus Pallidum Left	0,627	1,494
Preoptic Hypothalamic Area Left	Putamen Left	-0,081	1,118
Preoptic Hypothalamic Area Left	PostCruciate Gyrus Left	0,141	0,619
Preoptic Hypothalamic Area Left	Medial Mamillary Nucleus Right	-0,011	0,471
Preoptic Hypothalamic Area Left	SubFornical Organ Right	1,523	1,668
Preoptic Hypothalamic Area Left	Bed Nucleus of Stria Terminalis Right	0,845	1,355
Preoptic Hypothalamic Area Left	Lateral Septal Nucleus Right	1,056	1,406
Preoptic Hypothalamic Area Left	Medial Septal Nucleus Right	0,426	1,718
Preoptic Hypothalamic Area Left	Septum Right	0,079	0,627
Preoptic Hypothalamic Area Left	Preoptic Hypothalamic Area Right	1,662	1,834
Preoptic Hypothalamic Area Left	Caudate Right	-0,121	0,465
Preoptic Hypothalamic Area Left	Globus Pallidum Right	0,046	0,830
Preoptic Hypothalamic Area Right	Cingulate Cortex Right	-0,149	0,599
Preoptic Hypothalamic Area Right	Substantia Nigra Right	-0,064	0,370
Preoptic Hypothalamic Area Right	Caudate Right	0,525	1,290
Preoptic Hypothalamic Area Right	Globus Pallidum Right	0,497	1,647
Preoptic Hypothalamic Area Right	Putamen Right	0,405	1,669
Preoptic Hypothalamic Area Right	PostCruciate Gyrus Right	0,035	1,466
Putamen Left	Claustrocortex(Insula) Left	1,313	1,129
Putamen Left	PostCruciate Gyrus Left	0,294	-0,109
Putamen Left	Bed Nucleus of Stria Terminalis Right	-0,539	0,429
Putamen Left	Septum Right	1,212	0,013
Putamen Right	Claustrocortex(Insula) Right	0,999	1,157
Putamen Right	PostCruciate Gyrus Right	1,025	0,706
Putamen Right	Sylvian Gyrus Right	0,692	0,431
Septum Left	Preoptic Hypothalamic Area Left	1,030	1,526
Septum Left	Nucleus Of The Horizontal Limb Of The Diagonal Band Left	0,172	1,259
Septum Left	Caudate Left	1,230	1,777
Septum Left	Globus Pallidum Left	0,554	0,156
Septum Left	Putamen Left	1,126	1,397
Septum Left	PostCruciate Gyrus Left	0,750	1,134
Septum Left	SubFornical Organ Right	0,366	1,492
Septum Left	Bed Nucleus of Stria Terminalis Right	1,460	1,609
Septum Left	Lateral Septal Nucleus Right	-0,217	1,235
Septum Left	Medial Septal Nucleus Right	-0,383	0,888
Septum Left	Septum Right	1,631	2,003
Septum Left	Preoptic Hypothalamic Area Right	1,909	1,622
Septum Left	Caudate Right	1,054	1,662
Septum Left	Globus Pallidum Right	0,162	0,609
Septum Left	Putamen Right	0,953	1,309
Septum Right	Preoptic Hypothalamic Area Right	1,163	1,236
Septum Right	Caudate Right	1,320	1,918
Septum Right	Globus Pallidum Right	0,165	0,551
Septum Right	Putamen Right	1,248	1,385
SubFornical Organ Left	Bed Nucleus of Stria Terminalis Left	1,501	1,934
SubFornical Organ Left	Lateral Septal Nucleus Left	2,153	2,226
SubFornical Organ Left	Medial Septal Nucleus Left	1,178	1,707
SubFornical Organ Left	Septum Left	-0,013	1,324
SubFornical Organ Left	Preoptic Hypothalamic Area Left	1,836	2,001
SubFornical Organ Left	Nucleus Of The Horizontal Limb Of The Diagonal Band Left	2,280	2,176
SubFornical Organ Left	Caudate Left	-0,668	1,164
SubFornical Organ Left	Globus Pallidum Left	0,049	1,127
SubFornical Organ Left	Medial Mamillary Nucleus Right	0,813	0,308
SubFornical Organ Left	SubFornical Organ Right	2,676	2,205

SubFornical Organ Left	Bed Nucleus of Stria Terminalis Right	1,896	1,799
SubFornical Organ Left	Lateral Septal Nucleus Right	2,306	1,928
SubFornical Organ Left	Medial Septal Nucleus Right	1,501	1,644
SubFornical Organ Left	Septum Right	-0,558	0,896
SubFornical Organ Left	Preoptic Hypothalamic Area Right	1,509	1,775
SubFornical Organ Left	Globus Pallidum Right	-0,005	0,713
SubFornical Organ Right	Bed Nucleus of Stria Terminalis Right	2,571	2,014
SubFornical Organ Right	Lateral Septal Nucleus Right	2,459	2,110
SubFornical Organ Right	Medial Septal Nucleus Right	1,842	1,882
SubFornical Organ Right	Septum Right	-0,581	1,120
SubFornical Organ Right	Preoptic Hypothalamic Area Right	1,568	1,854
SubFornical Organ Right	Nucleus Of The Horizontal Limb Of The Diagonal Band Right	-0,588	-0,140
SubFornical Organ Right	Globus Pallidum Right	-0,135	1,102
Substantia Nigra Left	Globus Pallidum Left	0,643	1,423
Substantia Nigra Right	Globus Pallidum Right	0,262	-0,682
Suprasylvian Gyrus Left	Sylvian Gyrus Left	0,452	1,061
Suprasylvian Gyrus Left	Ectolateralis Gyrus Left	1,257	1,904
Suprasylvian Gyrus Left	Occipital Lobe Left	1,074	0,944
Suprasylvian Gyrus Right	Sylvian Gyrus Right	1,099	1,058
Temporal Lobe Left	Hippocampus Left	-0,132	1,036
Temporal Lobe Left	Parahippocampal Cortex Left	1,329	1,377
Temporal Lobe Left	Suprasylvian Gyrus Left	0,478	1,050
Temporal Lobe Left	Sylvian Gyrus Left	1,117	1,016
Temporal Lobe Left	Nucleus Of The Horizontal Limb Of The Diagonal Band Right	1,324	1,307
Temporal Lobe Right	Hippocampus Right	0,866	1,823
Temporal Lobe Right	Parahippocampal Cortex Right	0,647	1,359
Temporal Lobe Right	Suprasylvian Gyrus Right	0,977	1,320
Temporal Lobe Right	Sylvian Gyrus Right	1,124	1,638
Thalamus Left	Midbrain Left	0,631	0,983
Thalamus Left	Pineal Gland Right	0,591	0,787
Thalamus Left	Nucleus Of The Horizontal Limb Of The Diagonal Band Right	0,632	1,585
Thalamus Left	Thalamus Right	1,512	-0,166

Brain Region 1	Brain Region 2	Mean functionnal connectivity Male castrated (Z score)	Mean functionnal connectivity Female castrated (Z score)
Amygdala Left	Parahippocampal Cortex Left	1,151	0,229
Amygdala Left	Substantia Nigra Left	1,986	1,828
Amygdala Left	Globus Pallidum Left	1,519	1,450
Amygdala Right	Parahippocampal Cortex Right	0,955	1,265
Amygdala Right	Substantia Nigra Right	2,025	0,577
Amygdala Right	Globus Pallidum Right	1,151	-0,136
AnteriorSigmoideus Gyrus Left	Orbitofrontal Gyrus Left	0,899	2,907
AnteriorSigmoideus Gyrus Left	Precruciate Gyrus Left	1,270	1,522
AnteriorSigmoideus Gyrus Left	PostCruciate Gyrus Left	1,643	0,513
AnteriorSigmoideus Gyrus Right	Cingulate Cortex Right	1,106	0,836
AnteriorSigmoideus Gyrus Right	Orbital Gyrus Right	-0,446	0,401
AnteriorSigmoideus Gyrus Right	Orbitofrontal Gyrus Right	1,382	1,759
AnteriorSigmoideus Gyrus Right	Precruciate Gyrus Right	1,852	1,174
AnteriorSigmoideus Gyrus Right	Putamen Right	0,011	0,213
AnteriorSigmoideus Gyrus Right	Claustrocortex(Insula) Right	-0,775	1,323
AnteriorSigmoideus Gyrus Right	PostCruciate Gyrus Right	1,712	1,891
AnteriorSigmoideus Gyrus Right	Posterior Sygmoideus Gyrus Right	1,060	1,902
AnteriorSigmoideus Gyrus Right	Sylvian Gyrus Right	-0,290	0,801
Bed Nucleus of Stria Terminalis Left	Lateral Septal Nucleus Left	1,548	1,599
Bed Nucleus of Stria Terminalis Left	Medial Septal Nucleus Left	1,510	1,430
Bed Nucleus of Stria Terminalis Left	Septum Left	1,871	2,347
Bed Nucleus of Stria Terminalis Left	Preoptic Hypothalamic Area Left	1,725	2,130
Bed Nucleus of Stria Terminalis Left	Nucleus Of The Horizontal Limb Of The Diagonal Band Left	1,895	2,243
Bed Nucleus of Stria Terminalis Left	Caudate Left	1,023	1,906
Bed Nucleus of Stria Terminalis Left	Globus Pallidum Left	0,672	1,561
Bed Nucleus of Stria Terminalis Left	Putamen Left	0,628	1,166
Bed Nucleus of Stria Terminalis Left	SubFornical Organ Right	1,160	1,253
Bed Nucleus of Stria Terminalis Left	Bed Nucleus of Stria Terminalis Right	0,674	1,683
Bed Nucleus of Stria Terminalis Left	Lateral Septal Nucleus Right	0,815	0,452
Bed Nucleus of Stria Terminalis Left	Septum Right	0,829	1,310
Bed Nucleus of Stria Terminalis Left	Preoptic Hypothalamic Area Right	1,121	1,786
Bed Nucleus of Stria Terminalis Right	Lateral Septal Nucleus Right	1,851	1,622
Bed Nucleus of Stria Terminalis Right	Medial Septal Nucleus Right	1,735	2,407
Bed Nucleus of Stria Terminalis Right	Septum Right	0,480	1,670
Bed Nucleus of Stria Terminalis Right	Preoptic Hypothalamic Area Right	1,934	2,301
Bed Nucleus of Stria Terminalis Right	Caudate Right	0,604	0,704
Bed Nucleus of Stria Terminalis Right	Globus Pallidum Right	0,329	1,061
Bed Nucleus of Stria Terminalis Right	Putamen Right	-0,239	0,583
Caudate Left	Globus Pallidum Left	1,131	1,539
Caudate Left	Putamen Left	1,599	1,993
Caudate Left	Thalamus Left	0,212	0,142
Caudate Left	Claustrocortex(Insula) Left	1,502	0,480
Caudate Left	PostCruciate Gyrus Left	1,755	1,303
Caudate Left	Bed Nucleus of Stria Terminalis Right	1,222	0,843
Caudate Left	Septum Right	0,347	0,734
Caudate Left	Preoptic Hypothalamic Area Right	1,453	1,063
Caudate Left	Cingulate Cortex Right	0,640	0,188
Caudate Left	Caudate Right	1,026	0,352
Caudate Right	Globus Pallidum Right	1,365	2,068
Caudate Right	Putamen Right	2,242	2,444
Caudate Right	Claustrocortex(Insula) Right	0,457	2,147
Caudate Right	PostCruciate Gyrus Right	1,425	0,287
Caudate Right	Posterior Sygmoideus Gyrus Right	0,992	1,625
Caudate Right	Sylvian Gyrus Right	1,023	0,390
Cingulate Cortex Left	Orbital Gyrus Left	1,032	-0,108
Cingulate Cortex Left	Orbitofrontal Gyrus Left	0,824	-0,392
Cingulate Cortex Left	Hippocampus Left	1,069	0,263
Cingulate Cortex Left	Caudate Left	0,565	0,581
Cingulate Cortex Left	Precruciate Gyrus Left	1,347	1,104
Cingulate Cortex Left	Putamen Left	0,556	0,203
Cingulate Cortex Left	Gyrus Rectus Left	0,756	1,257
Cingulate Cortex Left	Geniculate Nucleus Left	0,038	-1,093
Cingulate Cortex Left	Thalamus Left	0,154	-0,522
Cingulate Cortex Left	Claustrocortex(Insula) Left	0,779	0,414
Cingulate Cortex Left	Lateral Gyrus Left	0,749	-0,309
Cingulate Cortex Left	PostCruciate Gyrus Left	1,210	0,965
Cingulate Cortex Left	Posterior Sygmoideus Gyrus Left	1,402	-0,454
Cingulate Cortex Left	Suprasylvian Gyrus Left	0,887	0,019
Cingulate Cortex Left	Sylvian Gyrus Left	0,037	-0,727
Cingulate Cortex Left	Ectolateralis Gyrus Left	0,750	-0,370
Cingulate Cortex Left	Entolateral Gyrus Left	1,809	0,731
Cingulate Cortex Left	Midbrain Left	0,413	0,200
Cingulate Cortex Left	Septum Right	0,624	0,682
Cingulate Cortex Left	AnteriorSigmoideus Gyrus Right	-0,213	1,076
Cingulate Cortex Left	Cingulate Cortex Right	1,854	1,689
Cingulate Cortex Left	Orbital Gyrus Right	0,773	-0,117
Cingulate Cortex Left	Orbitofrontal Gyrus Right	1,258	1,006
Cingulate Cortex Left	Nucleus Of The Horizontal Limb Of The Diagonal Band Right	0,648	0,057
Cingulate Cortex Left	Caudate Right	0,125	0,705
Cingulate Cortex Left	Precruciate Gyrus Right	0,107	1,094
Cingulate Cortex Left	Putamen Right	0,439	-0,015
Cingulate Cortex Left	Claustrocortex(Insula) Right	0,601	1,431
Cingulate Cortex Left	Lateral Gyrus Right	0,046	0,120
Cingulate Cortex Left	PostCruciate Gyrus Right	-0,408	1,267
Cingulate Cortex Left	Posterior Sygmoideus Gyrus Right	-0,308	0,190
Cingulate Cortex Left	Sylvian Gyrus Right	0,523	0,414
Cingulate Cortex Left	Entolateral Gyrus Right	0,612	0,800
Cingulate Cortex Right	Orbital Gyrus Right	0,250	0,954
Cingulate Cortex Right	Orbitofrontal Gyrus Right	1,485	0,833
Cingulate Cortex Right	Hippocampus Right	0,643	0,991
Cingulate Cortex Right	Caudate Right	0,727	0,600
Cingulate Cortex Right	Precruciate Gyrus Right	1,329	1,380
Cingulate Cortex Right	Putamen Right	0,640	-0,206
Cingulate Cortex Right	Periaqueductal Grey Substance Right	0,440	0,908
Cingulate Cortex Right	Claustrocortex(Insula) Right	0,000	1,130
Cingulate Cortex Right	Lateral Gyrus Right	1,330	0,945
Cingulate Cortex Right	PostCruciate Gyrus Right	0,888	1,840
Cingulate Cortex Right	Posterior Sygmoideus Gyrus Right	0,831	0,654
Cingulate Cortex Right	Suprasylvian Gyrus Right	1,086	0,628
Cingulate Cortex Right	Sylvian Gyrus Right	-0,079	1,163
Cingulate Cortex Right	Ectolateralis Gyrus Right	1,158	0,835
Cingulate Cortex Right	Entolateral Gyrus Right	1,442	1,453
Cingulate Cortex Right	Occipital Lobe Right	0,460	0,954
Claustrocortex(Insula) Left	Sylvian Gyrus Left	1,339	0,174
Claustrocortex(Insula) Left	Gyrus Rectus Right	0,306	-1,244
Claustrocortex(Insula) Right	PostCruciate Gyrus Right	-1,257	0,311
Claustrocortex(Insula) Right	Posterior Sygmoideus Gyrus Right	-1,668	0,485
Claustrocortex(Insula) Right	Sylvian Gyrus Right	1,262	0,109
Ectolateralis Gyrus Left	Entolateral Gyrus Left	1,437	1,544
Ectolateralis Gyrus Left	Occipital Lobe Left	1,144	1,391
Ectolateralis Gyrus Right	Entolateral Gyrus Right	2,633	1,226
Ectolateralis Gyrus Right	Occipital Lobe Right	1,282	1,255
Entolateral Gyrus Left	Entolateral Gyrus Right	1,902	1,293
Entolateral Gyrus Right	Occipital Lobe Right	0,894	1,183

Geniculate Nucleus Left	Thalamus Left	1,841	2,128
Geniculate Nucleus Right	Thalamus Right	2,113	1,617
Globus Pallidum Left	Putamen Left	1,808	1,553
Globus Pallidum Right	Putamen Right	2,096	2,359
Gyrus Rectus Left	Olfactory Bulb Left	2,738	1,484
Gyrus Rectus Left	Gyrus Rectus Right	2,850	1,757
Gyrus Rectus Left	Olfactory Bulb Right	2,339	-0,370
Gyrus Rectus Right	Olfactory Bulb Right	2,348	1,383
Hippocampus Left	Parahippocampal Cortex Left	1,608	1,460
Hippocampus Left	Geniculate Nucleus Left	1,324	-0,135
Hippocampus Left	Lateral Gyrus Left	1,104	0,134
Hippocampus Left	Suprasylvian Gyrus Left	1,962	1,211
Hippocampus Left	Ectolateralis Gyrus Left	1,157	-0,940
Hippocampus Left	Midbrain Left	1,379	1,457
Hippocampus Left	Nucleus Of The Horizontal Limb Of The Diagonal Band Right	1,933	1,351
Hippocampus Right	Parahippocampal Cortex Right	1,447	1,140
Hippocampus Right	Geniculate Nucleus Right	0,029	0,707
Hippocampus Right	Periaqueductal Grey Substance Right	1,265	1,459
Hippocampus Right	Thalamus Right	0,760	1,004
Hippocampus Right	Suprasylvian Gyrus Right	0,516	0,699
Hippocampus Right	Ectolateralis Gyrus Right	0,131	1,343
Hippocampus Right	Midbrain Right	1,478	1,477
Lateral Gyrus Left	Suprasylvian Gyrus Left	1,506	0,293
Lateral Gyrus Left	Ectolateralis Gyrus Left	1,968	2,743
Lateral Gyrus Left	Entolateral Gyrus Left	1,976	1,816
Lateral Gyrus Left	Occipital Lobe Left	-0,025	1,326
Lateral Gyrus Left	Lateral Gyrus Right	1,392	0,817
Lateral Gyrus Right	Suprasylvian Gyrus Right	1,392	0,833
Lateral Gyrus Right	Ectolateralis Gyrus Right	2,711	1,810
Lateral Gyrus Right	Entolateral Gyrus Right	2,844	1,974
Lateral Gyrus Right	Occipital Lobe Right	1,443	1,373
Lateral Septal Nucleus Left	Medial Septal Nucleus Left	2,009	1,313
Lateral Septal Nucleus Left	Preoptic Hypothalamic Area Left	1,800	0,993
Lateral Septal Nucleus Left	Nucleus Of The Horizontal Limb Of The Diagonal Band Left	2,010	2,145
Lateral Septal Nucleus Left	Substantia Nigra Left	0,779	0,129
Lateral Septal Nucleus Left	Globus Pallidum Left	1,221	0,695
Lateral Septal Nucleus Left	Medial Mamillary Nucleus Right	-0,127	0,451
Lateral Septal Nucleus Left	SubFornical Organ Right	1,665	0,960
Lateral Septal Nucleus Left	Bed Nucleus of Stria Terminalis Right	0,944	0,544
Lateral Septal Nucleus Left	Lateral Septal Nucleus Right	1,643	1,132
Lateral Septal Nucleus Left	Preoptic Hypothalamic Area Right	1,539	0,595
Lateral Septal Nucleus Right	Medial Septal Nucleus Right	1,894	1,916
Lateral Septal Nucleus Right	Preoptic Hypothalamic Area Right	1,562	1,518
Lateral Septal Nucleus Right	Nucleus Of The Horizontal Limb Of The Diagonal Band Right	-0,105	1,216
Lateral Septal Nucleus Right	Substantia Nigra Right	0,459	0,969
Lateral Septal Nucleus Right	Globus Pallidum Right	0,268	0,047
Medial Mamillary Nucleus Left	Lateral Septal Nucleus Left	1,162	1,682
Medial Mamillary Nucleus Left	Medial Septal Nucleus Left	1,166	-0,177
Medial Mamillary Nucleus Left	Nucleus Of The Horizontal Limb Of The Diagonal Band Left	0,951	1,205
Medial Mamillary Nucleus Left	Substantia Nigra Left	0,959	-0,462
Medial Mamillary Nucleus Left	Globus Pallidum Left	1,350	-0,582
Medial Mamillary Nucleus Left	Medial Mamillary Nucleus Right	0,390	1,526
Medial Mamillary Nucleus Left	Lateral Septal Nucleus Right	0,575	-0,159
Medial Mamillary Nucleus Right	SubFornical Organ Right	-0,957	0,043
Medial Mamillary Nucleus Right	Bed Nucleus of Stria Terminalis Right	-1,299	-0,255
Medial Mamillary Nucleus Right	Lateral Septal Nucleus Right	0,505	0,958
Medial Mamillary Nucleus Right	Medial Septal Nucleus Right	0,237	0,239
Medial Mamillary Nucleus Right	Preoptic Hypothalamic Area Right	-0,650	0,037
Medial Mamillary Nucleus Right	Substantia Nigra Right	1,888	1,594
Medial Mamillary Nucleus Right	Pituitary Gland Right	-1,985	1,360
Medial Septal Nucleus Left	Preoptic Hypothalamic Area Left	1,904	2,000
Medial Septal Nucleus Left	Nucleus Of The Horizontal Limb Of The Diagonal Band Left	1,736	1,643
Medial Septal Nucleus Left	Substantia Nigra Left	0,458	0,773
Medial Septal Nucleus Left	Caudate Left	1,322	1,286
Medial Septal Nucleus Left	Globus Pallidum Left	1,012	2,008
Medial Septal Nucleus Left	SubFornical Organ Right	1,807	1,322
Medial Septal Nucleus Left	Lateral Septal Nucleus Right	1,689	0,803
Medial Septal Nucleus Left	Medial Septal Nucleus Right	1,337	0,950
Medial Septal Nucleus Left	Preoptic Hypothalamic Area Right	1,589	1,488
Medial Septal Nucleus Right	Preoptic Hypothalamic Area Right	1,638	1,900
Medial Septal Nucleus Right	Substantia Nigra Right	0,585	0,110
Medial Septal Nucleus Right	Caudate Right	0,752	0,683
Medial Septal Nucleus Right	Globus Pallidum Right	1,684	1,266
Medial Septal Nucleus Right	Putamen Right	0,551	0,493
Midbrain Left	Pineal Gland Right	1,109	1,480
Midbrain Left	Pons Right	1,073	1,393
Midbrain Left	Hippocampus Right	1,091	1,672
Midbrain Left	Periaqueductal Grey Substance Right	1,924	1,486
Midbrain Left	Midbrain Right	1,588	1,531
Nucleus Of The Horizontal Limb Of The Diagonal Band Left	Substantia Nigra Left	0,742	-0,476
Nucleus Of The Horizontal Limb Of The Diagonal Band Left	Globus Pallidum Left	1,362	1,675
Nucleus Of The Horizontal Limb Of The Diagonal Band Left	Putamen Left	0,961	0,896
Nucleus Of The Horizontal Limb Of The Diagonal Band Left	SubFornical Organ Right	1,292	0,150
Nucleus Of The Horizontal Limb Of The Diagonal Band Left	Bed Nucleus of Stria Terminalis Right	0,659	0,536
Nucleus Of The Horizontal Limb Of The Diagonal Band Left	Lateral Septal Nucleus Right	0,870	-0,285
Olfactory Bulb Left	Gyrus Rectus Right	2,892	1,154
Orbital Gyrus Left	Orbitofrontal Gyrus Left	0,668	1,946
Orbital Gyrus Left	Precruciate Gyrus Left	1,728	1,149
Orbital Gyrus Left	Gyrus Rectus Left	1,681	0,430
Orbital Gyrus Left	Olfactory Bulb Left	1,911	0,784
Orbital Gyrus Left	Claustrocortex(Insula) Left	0,264	0,971
Orbital Gyrus Left	Gyrus Rectus Right	2,002	-1,310
Orbital Gyrus Right	Precruciate Gyrus Right	1,871	1,857
Orbital Gyrus Right	Gyrus Rectus Right	1,903	1,659
Orbital Gyrus Right	Olfactory Bulb Right	1,966	0,857
Orbitofrontal Gyrus Left	Precruciate Gyrus Left	0,777	1,469
Orbitofrontal Gyrus Left	Claustrocortex(Insula) Left	0,715	2,133
Orbitofrontal Gyrus Right	Precruciate Gyrus Right	-0,246	0,911
Orbitofrontal Gyrus Right	Claustrocortex(Insula) Right	0,262	1,429
Parahippocampal Cortex Left	Substantia Nigra Left	0,741	0,925
Parahippocampal Cortex Left	Thalamus Left	1,694	0,645
Parahippocampal Cortex Left	Nucleus Of The Horizontal Limb Of The Diagonal Band Right	2,155	1,731
Parahippocampal Cortex Right	Substantia Nigra Right	0,152	0,735
Parahippocampal Cortex Right	Caudate Right	1,449	0,617
Parahippocampal Cortex Right	Globus Pallidum Right	1,004	0,143
Parahippocampal Cortex Right	Putamen Right	1,655	0,314
Parahippocampal Cortex Right	Geniculate Nucleus Right	-1,083	-0,004
Parahippocampal Cortex Right	Thalamus Right	-0,905	0,264
Parahippocampal Cortex Right	Claustrocortex(Insula) Right	0,857	0,701
Parahippocampal Cortex Right	Lateral Gyrus Right	-0,545	0,222
Parahippocampal Cortex Right	Suprasylvian Gyrus Right	0,139	0,319
Parahippocampal Cortex Right	Sylvian Gyrus Right	1,414	0,160
Parahippocampal Cortex Right	Ectolateralis Gyrus Right	0,184	0,083
Parahippocampal Cortex Right	Occipital Lobe Right	-0,517	0,851
Parahippocampal Cortex Right	Midbrain Right	0,294	0,401
Periaqueductal Grey Substance Left	Pons Right	1,505	1,333
Periaqueductal Grey Substance Left	Periaqueductal Grey Substance Right	1,880	1,523

Periaqueductal Grey Substance Right	Midbrain Right	1,079	1,524
Pineal Gland Left	Hippocampus Left	1,684	0,835
Pineal Gland Left	Geniculate Nucleus Left	0,690	-0,182
Pineal Gland Left	Midbrain Left	0,925	0,887
Pineal Gland Left	Pineal Gland Right	3,477	1,567
Pineal Gland Left	Hippocampus Right	0,454	0,825
Pineal Gland Left	Midbrain Right	0,995	0,818
Pineal Gland Right	Hippocampus Right	0,355	1,276
Pineal Gland Right	Midbrain Right	0,368	1,304
Pituitary Gland Left	Pituitary Gland Right	2,126	2,046
Pons Left	Periaqueductal Grey Substance Left	2,554	1,781
Pons Left	Pons Right	2,007	1,691
Pons Right	Periaqueductal Grey Substance Right	0,937	1,584
PostCruciate Gyrus Left	Posterior Sygmoideus Gyrus Left	1,857	2,180
PostCruciate Gyrus Left	AnteriorSigmoideus Gyrus Right	-0,997	0,319
PostCruciate Gyrus Left	PostCruciate Gyrus Right	-0,363	-0,292
PostCruciate Gyrus Right	Posterior Sygmoideus Gyrus Right	1,940	2,105
PostCruciate Gyrus Right	Sylvian Gyrus Right	-0,016	1,122
Posterior Sygmoideus Gyrus Left	Suprasylvian Gyrus Left	-0,390	0,036
Posterior Sygmoideus Gyrus Left	Sylvian Gyrus Left	-0,417	0,330
Posterior Sygmoideus Gyrus Right	Sylvian Gyrus Right	-0,678	0,431
Posterior Sylvian Gyrus Left	Suprasylvian Gyrus Left	1,820	1,751
Posterior Sylvian Gyrus Right	Temporal Lobe Right	0,396	2,102
Posterior Sylvian Gyrus Right	Suprasylvian Gyrus Right	-0,996	1,365
Posterior Sylvian Gyrus Right	Ectolateralis Gyrus Right	-0,217	0,092
Precruciate Gyrus Left	Gyrus Rectus Left	1,076	-0,913
Precruciate Gyrus Left	Claustrocortex(Insula) Left	0,376	0,824
Precruciate Gyrus Left	Orbital Gyrus Right	1,376	-1,059
Precruciate Gyrus Left	Precruciate Gyrus Right	1,178	1,971
Precruciate Gyrus Right	Gyrus Rectus Right	0,470	1,239
Precruciate Gyrus Right	PostCruciate Gyrus Right	0,636	0,427
Preoptic Hypothalamic Area Left	Nucleus Of The Horizontal Limb Of The Diagonal Band Left	1,740	1,492
Preoptic Hypothalamic Area Left	Caudate Left	1,567	1,548
Preoptic Hypothalamic Area Left	Globus Pallidum Left	0,799	1,436
Preoptic Hypothalamic Area Left	Putamen Left	0,611	0,540
Preoptic Hypothalamic Area Left	Medial Mamillary Nucleus Right	0,247	0,099
Preoptic Hypothalamic Area Left	SubFornical Organ Right	1,803	1,576
Preoptic Hypothalamic Area Left	Bed Nucleus of Stria Terminalis Right	1,232	1,713
Preoptic Hypothalamic Area Left	Lateral Septal Nucleus Right	1,634	0,889
Preoptic Hypothalamic Area Left	Medial Septal Nucleus Right	1,461	1,548
Preoptic Hypothalamic Area Left	Septum Right	-0,370	0,527
Preoptic Hypothalamic Area Left	Preoptic Hypothalamic Area Right	1,908	2,433
Preoptic Hypothalamic Area Left	Substantia Nigra Right	-0,096	0,179
Preoptic Hypothalamic Area Left	Globus Pallidum Right	0,220	-0,248
Preoptic Hypothalamic Area Right	Nucleus Of The Horizontal Limb Of The Diagonal Band Right	-0,255	-0,039
Preoptic Hypothalamic Area Right	Substantia Nigra Right	-0,515	0,212
Preoptic Hypothalamic Area Right	Caudate Right	1,008	0,298
Preoptic Hypothalamic Area Right	Globus Pallidum Right	0,415	0,407
Preoptic Hypothalamic Area Right	Putamen Right	0,126	0,004
Putamen Left	Claustrocortex(Insula) Left	2,184	1,342
Putamen Left	Septum Right	0,609	0,087
Putamen Right	Claustrocortex(Insula) Right	1,379	1,469
Putamen Right	PostCruciate Gyrus Right	0,225	-0,985
Putamen Right	Posterior Sygmoideus Gyrus Right	-0,233	0,931
Putamen Right	Sylvian Gyrus Right	1,181	-0,288
Septum Left	Preoptic Hypothalamic Area Left	1,812	1,756
Septum Left	Nucleus Of The Horizontal Limb Of The Diagonal Band Left	1,454	1,625
Septum Left	Caudate Left	1,547	1,722
Septum Left	Putamen Left	0,836	0,694
Septum Left	SubFornical Organ Right	1,337	0,742
Septum Left	Bed Nucleus of Stria Terminalis Right	1,341	1,578
Septum Left	Lateral Septal Nucleus Right	1,088	0,253
Septum Left	Septum Right	1,552	2,189
Septum Left	Preoptic Hypothalamic Area Right	1,723	1,874
Septum Left	Caudate Right	1,341	1,210
Septum Right	Preoptic Hypothalamic Area Right	-0,187	0,828
Septum Right	Caudate Right	0,789	1,924
Septum Right	Putamen Right	0,851	1,655
SubFornical Organ Left	Bed Nucleus of Stria Terminalis Left	1,664	1,836
SubFornical Organ Left	Lateral Septal Nucleus Left	1,810	1,982
SubFornical Organ Left	Medial Septal Nucleus Left	1,964	1,961
SubFornical Organ Left	Septum Left	1,523	1,189
SubFornical Organ Left	Preoptic Hypothalamic Area Left	1,864	2,070
SubFornical Organ Left	Nucleus Of The Horizontal Limb Of The Diagonal Band Left	1,686	1,380
SubFornical Organ Left	Globus Pallidum Left	0,879	1,288
SubFornical Organ Left	Medial Mamillary Nucleus Right	-0,222	0,274
SubFornical Organ Left	SubFornical Organ Right	2,332	2,206
SubFornical Organ Left	Bed Nucleus of Stria Terminalis Right	1,645	1,905
SubFornical Organ Left	Lateral Septal Nucleus Right	1,989	1,794
SubFornical Organ Left	Medial Septal Nucleus Right	1,567	1,492
SubFornical Organ Left	Septum Right	-0,738	0,263
SubFornical Organ Left	Preoptic Hypothalamic Area Right	1,888	1,968
SubFornical Organ Right	Bed Nucleus of Stria Terminalis Right	2,019	2,354
SubFornical Organ Right	Lateral Septal Nucleus Right	2,304	2,120
SubFornical Organ Right	Medial Septal Nucleus Right	1,709	1,936
SubFornical Organ Right	Septum Right	-0,960	0,561
SubFornical Organ Right	Preoptic Hypothalamic Area Right	1,936	2,157
SubFornical Organ Right	Globus Pallidum Right	-0,253	-0,148
Substantia Nigra Left	Globus Pallidum Left	1,557	0,780
Substantia Nigra Right	Globus Pallidum Right	0,908	-0,197
Suprasylvian Gyrus Left	Sylvian Gyrus Left	0,557	1,659
Suprasylvian Gyrus Left	Ectolateralis Gyrus Left	1,921	-0,031
Suprasylvian Gyrus Right	Ectolateralis Gyrus Right	2,095	1,129
Temporal Lobe Left	Parahippocampal Cortex Left	1,797	1,003
Temporal Lobe Right	Hippocampus Right	0,226	-0,041
Temporal Lobe Right	Parahippocampal Cortex Right	1,336	0,436
Temporal Lobe Right	Suprasylvian Gyrus Right	-0,979	0,279
Temporal Lobe Right	Ectolateralis Gyrus Right	-0,816	-0,081
Thalamus Left	Midbrain Left	1,757	-0,094
Thalamus Left	Nucleus Of The Horizontal Limb Of The Diagonal Band Right	1,872	0,223
Thalamus Right	Midbrain Right	0,886	0,803

Regions Of Interest	Baseline	Gonadectomized	Mean Diff,	95,00% CI of diff	t	Individual P Value	Summary
Amygdala Left	0,5747	0,5947	-0,02003	-0,0394 to -0,0006694	2,033	0,0426	*
Amygdala Right	0,6125	0,6351	-0,02259	-0,04195 to -0,003222	2,293	0,0224	*
Cerebellum Left	0,4168	0,3852	0,03157	0,0122 to 0,05093	3,204	0,0015	**
Claustrum Left	0,4534	0,3776	0,07577	0,05641 to 0,09514	7,692	<0,0001	****
Claustrum Right	0,4363	0,3628	0,07348	0,05412 to 0,09284	7,459	<0,0001	****
Ectolateralis Gyrus Left	0,6395	0,4975	0,1421	0,1227 to 0,1614	14,42	<0,0001	****
Ectolateralis Gyrus Right	0,6409	0,5043	0,1366	0,1173 to 0,156	13,87	<0,0001	****
Fornix Left	0,4503	0,4237	0,02661	0,007247 to 0,04597	2,701	0,0072	**
Fornix Right	0,4793	0,4462	0,03301	0,01365 to 0,05237	3,351	0,0009	***
Geniculate Nucleus Left	0,179	0,1576	0,02133	0,001967 to 0,04069	2,165	0,0309	*
Hippocampus Left	0,5206	0,5416	-0,02107	-0,04043 to -0,001703	2,138	0,033	*
Medial Mamillary Nucleus Left	0,3783	0,3503	0,02796	0,008596 to 0,04732	2,838	0,0048	**
Medial Mamillary Nucleus Right	0,3745	0,3433	0,03117	0,01181 to 0,05053	3,164	0,0017	**
Medial Septal Nucleus Right	0,4452	0,4234	0,02187	0,002503 to 0,04123	2,22	0,027	*
Medulla Oblongata Left	0,2755	0,211	0,06453	0,04516 to 0,08389	6,55	<0,0001	****
Medulla Oblongata Right	0,3083	0,2387	0,06954	0,05017 to 0,0889	7,059	<0,0001	****
Midbrain Left	0,234	0,1787	0,05531	0,03594 to 0,07467	5,614	<0,0001	****
Midbrain Right	0,2313	0,1792	0,05206	0,0327 to 0,07143	5,285	<0,0001	****
Orbital Gyrus Left	0,468	0,492	-0,024	-0,04337 to -0,004639	2,436	0,0152	*
Periaqueductal Grey Substance Left	0,6429	0,538	0,1049	0,08554 to 0,1243	10,65	<0,0001	****
Periaqueductal Grey Substance Right	0,5522	0,4744	0,07781	0,05845 to 0,09717	7,898	<0,0001	****
Pons Left	0,4104	0,2825	0,1279	0,1086 to 0,1473	12,98	<0,0001	****
Pons Right	0,3971	0,2762	0,1209	0,1015 to 0,1402	12,27	<0,0001	****
Preoptic Hypothalamic Area Left	0,442	0,4189	0,02306	0,003696 to 0,04242	2,341	0,0197	*
Preoptic Hypothalamic Area Right	0,4748	0,4432	0,03164	0,01228 to 0,051	3,212	0,0014	**
SubFornical Organ Right	0,5848	0,559	0,02578	0,006419 to 0,04515	2,617	0,0092	**
Suprasylvian Gyrus Right	0,3862	0,4068	-0,02064	-0,04 to -0,001274	2,095	0,0368	*
Thalamus Left	0,3032	0,2707	0,03245	0,01309 to 0,05182	3,294	0,0011	**
Thalamus Right	0,3102	0,2793	0,03091	0,01155 to 0,05028	3,138	0,0018	**

Regions Of Interest	Baseline	Gonadectomized	Mean Diff,	95,00% CI of diff	t	Individual P Value	Summary
Claustrum Left	0,4085	0,3737	0,03473	0,02561 to 0,04385	7,489	<0,0001	****
Claustrum Right	0,4046	0,3703	0,03427	0,02515 to 0,0434	7,391	<0,0001	****
Ectolateralis Gyrus Right	0,4411	0,4165	0,02462	0,0155 to 0,03374	5,31	<0,0001	****
Subfornical Organ Left	0,4372	0,4115	0,0257	0,01658 to 0,03482	5,541	<0,0001	****
Subfornical Organ Right	0,4431	0,4166	0,02647	0,01734 to 0,03559	5,707	<0,0001	****
Globus Pallidum Left	0,2584	0,2484	0,01006	0,0009362 to 0,01918	2,169	0,0308	*
Globus Pallidum Right	0,2473	0,2372	0,01018	0,001057 to 0,0193	2,195	0,0289	*
Medial Mamillary Nucleus Left	0,3348	0,3135	0,02131	0,01219 to 0,03043	4,595	<0,0001	****
Medial Mamillary Nucleus Right	0,3335	0,3116	0,02195	0,01283 to 0,03107	4,733	<0,0001	****
Medulla Oblongata Right	0,1898	0,1649	0,02496	0,01584 to 0,03409	5,383	<0,0001	****
Midbrain Left	0,2078	0,1805	0,02727	0,01815 to 0,03639	5,881	<0,0001	****
Midbrain Right	0,2595	0,2321	0,02736	0,01824 to 0,03648	5,9	<0,0001	****
Nucleus Of The Horizontal Limb Of The Diagonal Band Left	0,2834	0,2678	0,01566	0,006534 to 0,02478	3,376	0,0008	***
Nucleus Of The Horizontal Limb Of The Diagonal Band Right	0,3093	0,2903	0,01902	0,009901 to 0,02814	4,102	<0,0001	****
Parahippocampal Cortex Right	0,3541	0,323	0,03116	0,02204 to 0,04028	6,719	<0,0001	****
Pituitary Gland Left	0,04898	0,06561	-0,01663	-0,02575 to -0,007506	3,586	0,0004	***
Pituitary Gland Right	0,05069	0,06808	-0,01739	-0,02651 to -0,008265	3,749	0,0002	***
Preoptic Hypothalamic Area Left	0,4288	0,4038	0,02504	0,01592 to 0,03416	5,4	<0,0001	****
Preoptic Hypothalamic Area Right	0,4189	0,394	0,02485	0,01573 to 0,03397	5,358	<0,0001	****
Putamen Right	0,328	0,3159	0,01215	0,003031 to 0,02127	2,621	0,0092	**
Substantia Nigra Right	0,1451	0,1353	0,009719	0,0005973 to 0,01884	2,096	0,0368	*
Thalamus Left	0,3341	0,3113	0,0228	0,01368 to 0,03192	4,916	<0,0001	****

Brain Region 1	Brain Region 2	Mean functionnal connectivity Male baseline (Z score)	Mean functionnal connectivity Male castrated (Z score)
AnteriorSigmoideus Gyrus Left	Caudate Left	0,022	0,900
AnteriorSigmoideus Gyrus Left	Gyrus Rectus Left	0,879	0,181
AnteriorSigmoideus Gyrus Left	Gyrus Rectus Right	0,391	0,293
Bed Nucleus of Stria Terminalis Left	Orbital Gyrus Right	0,105	-0,923
Bed Nucleus of Stria Terminalis Left	Orbitofrontal Gyrus Right	0,211	-0,207
Bed Nucleus of Stria Terminalis Right	AnteriorSigmoideus Gyrus Right	0,727	-0,791
Bed Nucleus of Stria Terminalis Right	Orbital Gyrus Right	-0,741	-2,185
Bed Nucleus of Stria Terminalis Right	Orbitofrontal Gyrus Right	0,729	-1,148
Bed Nucleus of Stria Terminalis Right	Precruciate Gyrus Right	-0,134	-1,563
Caudate Left	Occipital Lobe Left	0,488	-1,465
Cingulate Cortex Left	Bed Nucleus of Stria Terminalis Right	0,542	-0,209
Gyrus Rectus Left	Entolateral Gyrus Left	-1,063	-1,000
Gyrus Rectus Left	Lateral Septal Nucleus Right	-0,430	-1,212
Gyrus Rectus Left	Pineal Gland Right	-0,554	-2,254
Gyrus Rectus Left	Periaqueductal Grey Substance Right	-0,088	-2,178
Hippocampus Left	Lateral Gyrus Left	1,104	0,524
Hippocampus Left	Thalamus Right	0,935	-0,579
Lateral Gyrus Left	Suprasylvian Gyrus Left	1,506	0,877
Medial Septal Nucleus Left	PostCruciate Gyrus Left	1,009	-0,131
Medial Septal Nucleus Left	PostCruciate Gyrus Right	0,287	-0,464
Medial Septal Nucleus Right	Orbital Gyrus Right	0,223	-0,890
Occipital Lobe Left	Thalamus Right	-0,014	-1,364
Orbital Gyrus Right	Globus Pallidum Right	0,936	-0,657
Parahippocampal Cortex Left	Periaqueductal Grey Substance Left	0,484	-0,113
Parahippocampal Cortex Left	Cerebellum Left	-0,686	-0,987
Parahippocampal Cortex Left	Lateral Gyrus Left	1,258	-1,429
Parahippocampal Cortex Left	Pons Right	0,886	-0,569
Parahippocampal Cortex Left	Geniculate Nucleus Right	1,582	-0,500
Parahippocampal Cortex Left	Lateral Gyrus Right	1,138	0,177
Parahippocampal Cortex Left	Suprasylvian Gyrus Right	0,970	0,286
Parahippocampal Cortex Left	Ectolateralis Gyrus Right	0,668	0,493
Periaqueductal Grey Substance Left	Periaqueductal Grey Substance Right	1,880	1,084
Periaqueductal Grey Substance Right	Midbrain Right	1,079	1,294
Pituitary Gland Left	Thalamus Left	-0,054	-0,006
Pituitary Gland Left	Entolateral Gyrus Left	0,330	-0,179
Pituitary Gland Left	Septum Right	0,031	-0,589
Pituitary Gland Left	Putamen Right	0,614	-0,440
Pituitary Gland Left	Claustrocortex(Insula) Right	0,073	-0,661
Pituitary Gland Left	Lateral Gyrus Right	-0,111	-0,555
Pituitary Gland Left	Ectolateralis Gyrus Right	0,326	-0,731
Pituitary Gland Left	Medulla Oblongata Right	0,428	0,144
Pons Left	Pons Right	2,007	1,044
PostCruciate Gyrus Left	Medulla Oblongata Left	0,198	-0,112
PostCruciate Gyrus Left	Medulla Oblongata Right	0,007	0,141
Posterior Sygmoideus Gyrus Left	Medulla Oblongata Right	0,362	1,138
Posterior Sylvian Gyrus Left	Substantia Nigra Left	0,153	-2,259
Posterior Sylvian Gyrus Left	Septum Right	0,323	-1,120
Posterior Sylvian Gyrus Left	Orbitofrontal Gyrus Right	0,341	-0,673
Posterior Sylvian Gyrus Left	Ectolateralis Gyrus Right	-0,392	-0,094
Preoptic Hypothalamic Area Right	Orbital Gyrus Right	-0,522	-0,748
Preoptic Hypothalamic Area Right	Orbitofrontal Gyrus Right	0,517	-0,010
Septum Left	Nucleus Of The Horizontal Limb Of The Diagonal Band Left	1,454	0,172
Septum Left	PostCruciate Gyrus Left	1,290	0,750
Septum Left	Orbital Gyrus Right	0,147	-0,865
Septum Left	Orbitofrontal Gyrus Right	0,713	0,414
Septum Right	AnteriorSigmoideus Gyrus Right	0,605	0,763
Septum Right	Orbital Gyrus Right	0,195	-1,094
SubFornical Organ Left	Orbital Gyrus Right	-0,705	-0,449
SubFornical Organ Left	Orbitofrontal Gyrus Right	0,576	-0,881
SubFornical Organ Right	Orbital Gyrus Right	-0,825	-0,944
SubFornical Organ Right	Orbitofrontal Gyrus Right	0,744	-1,245
Substantia Nigra Left	Posterior Sylvian Gyrus Right	1,244	-1,712
Temporal Lobe Left	Periaqueductal Grey Substance Left	0,725	0,428
Temporal Lobe Left	Pons Right	1,263	0,006
Temporal Lobe Left	Gyrus Rectus Right	-0,660	-0,144
Temporal Lobe Left	Periaqueductal Grey Substance Right	0,429	-0,023

Brain Region 1	Brain Region 2	Mean functionnal connectivity Female baseline (Z score)	Mean functionnal connectivity Female castrated (Z score)
Amygdala Left	Globus Pallidum Left	1,450	1,805
AnteriorSigmoideus Gyrus Left	Gyrus Rectus Left	-1,753	0,239
AnteriorSigmoideus Gyrus Left	Orbitofrontal Gyrus Right	-0,017	0,569
AnteriorSigmoideus Gyrus Right	Nucleus Of The Horizontal Limb Of The Diagonal Band Right	0,258	0,273
Bed Nucleus of Stria Terminalis Left	Lateral Septal Nucleus Left	1,599	1,913
Bed Nucleus of Stria Terminalis Left	Pituitary Gland Left	-1,046	-0,106
Bed Nucleus of Stria Terminalis Left	Medial Mamillary Nucleus Right	-0,408	0,313
Bed Nucleus of Stria Terminalis Left	Pituitary Gland Right	-1,004	-0,466
Bed Nucleus of Stria Terminalis Left	Midbrain Right	-0,529	-0,096
Bed Nucleus of Stria Terminalis Right	Pituitary Gland Right	-0,560	0,057
Caudate Left	Gyrus Rectus Left	0,147	-0,087
Cingulate Cortex Left	Orbital Gyrus Right	-0,117	0,374
Cingulate Cortex Left	Orbitofrontal Gyrus Right	1,006	1,375
Cingulate Cortex Left	Claustrocortex(Insula) Right	1,431	1,079
Cingulate Cortex Left	Sylvian Gyrus Right	0,414	1,002
Cingulate Cortex Right	Orbital Gyrus Right	0,954	1,582
Cingulate Cortex Right	Orbitofrontal Gyrus Right	0,833	1,517
Cingulate Cortex Right	Precruciate Gyrus Right	1,380	1,673
Claustrocortex(Insula) Left	Pineal Gland Right	-1,819	-0,527
Ectolateralis Gyrus Left	Suprasylvian Gyrus Right	-0,335	0,272
Geniculate Nucleus Left	Olfactory Bulb Right	-0,632	0,543
Gyrus Rectus Left	Olfactory Bulb Left	1,484	2,483
Gyrus Rectus Left	Periaqueductal Grey Substance Left	-0,037	0,782
Gyrus Rectus Left	PostCruciate Gyrus Left	0,173	-1,528
Gyrus Rectus Left	Orbital Gyrus Right	0,604	1,130
Gyrus Rectus Left	Precruciate Gyrus Right	0,657	0,784
Lateral Gyrus Left	Olfactory Bulb Right	-0,732	-0,374
Lateral Septal Nucleus Left	SubFornical Organ Right	0,960	1,703
Medial Mamillary Nucleus Left	AnteriorSigmoideus Gyrus Right	-0,397	-0,404
Medial Septal Nucleus Left	Medulla Oblongata Right	-0,925	-0,949
Medial Septal Nucleus Right	Pituitary Gland Right	0,346	-0,483
Medulla Oblongata Left	Pineal Gland Right	0,849	0,099
Midbrain Left	Olfactory Bulb Right	-0,560	-0,482
Nucleus Of The Horizontal Limb Of The Diagonal Band Left	Midbrain Left	-1,287	-0,321
Nucleus Of The Horizontal Limb Of The Diagonal Band Left	Pituitary Gland Right	-1,293	-0,716
Nucleus Of The Horizontal Limb Of The Diagonal Band Left	Midbrain Right	-1,303	0,564
Nucleus Of The Horizontal Limb Of The Diagonal Band Right	Claustrocortex(Insula) Right	-0,644	0,332
Olfactory Bulb Left	Periaqueductal Grey Substance Left	-1,022	0,373
Olfactory Bulb Left	Orbital Gyrus Right	-1,102	1,148
Orbital Gyrus Left	Olfactory Bulb Left	0,784	0,780
Orbitofrontal Gyrus Left	Suprasylvian Gyrus Left	-1,883	-0,474
Orbitofrontal Gyrus Left	Cingulate Cortex Right	-2,575	-0,288
Orbitofrontal Gyrus Left	Orbital Gyrus Right	-1,481	1,601
Orbitofrontal Gyrus Left	Orbitofrontal Gyrus Right	-0,935	0,861
Orbitofrontal Gyrus Left	Precruciate Gyrus Right	-0,624	1,118
Orbitofrontal Gyrus Right	Nucleus Of The Horizontal Limb Of The Diagonal Band Right	-1,614	0,049
Orbitofrontal Gyrus Right	Entolateral Gyrus Right	-0,748	0,735
Parahippocampal Cortex Left	Putamen Left	-0,318	-0,225
Parahippocampal Cortex Left	Claustrocortex(Insula) Left	-0,677	1,192
Parahippocampal Cortex Left	PostCruciate Gyrus Left	-1,375	0,197
Parahippocampal Cortex Left	Posterior Sygmoideus Gyrus Left	-0,916	1,433
Parahippocampal Cortex Left	Bed Nucleus of Stria Terminalis Right	-0,574	-0,465
Parahippocampal Cortex Left	Septum Right	-1,430	-0,317
Parahippocampal Cortex Left	AnteriorSigmoideus Gyrus Right	0,556	-0,735
Parahippocampal Cortex Left	Orbitofrontal Gyrus Right	-1,258	0,102
Parahippocampal Cortex Left	Caudate Right	-1,275	0,276
Parahippocampal Cortex Left	Claustrocortex(Insula) Right	-0,818	-0,413
Parahippocampal Cortex Left	PostCruciate Gyrus Right	0,632	-0,639
Parahippocampal Cortex Left	Posterior Sygmoideus Gyrus Right	-0,588	0,989
Periaqueductal Grey Substance Left	Olfactory Bulb Right	-0,388	0,598
Pineal Gland Left	Pineal Gland Right	1,567	2,681
Pituitary Gland Left	Posterior Sylvian Gyrus Right	-1,618	0,084
Pituitary Gland Left	Medial Septal Nucleus Right	-0,724	-1,003
Pituitary Gland Left	Sylvian Gyrus Right	-0,107	-0,194
Pituitary Gland Right	Suprasylvian Gyrus Right	-1,205	0,823
Pons Right	Gyrus Rectus Right	0,227	0,592
Pons Right	Olfactory Bulb Right	-0,091	1,389
Posterior Sygmoideus Gyrus Left	Thalamus Right	-1,079	0,282
Precruciate Gyrus Left	Olfactory Bulb Left	1,339	1,082
Preoptic Hypothalamic Area Left	Gyrus Rectus Left	-0,201	-0,290
Preoptic Hypothalamic Area Left	Medulla Oblongata Left	-0,600	-0,107
Preoptic Hypothalamic Area Left	Medulla Oblongata Right	-1,066	0,564
Preoptic Hypothalamic Area Right	Pituitary Gland Right	-0,026	0,041
Preoptic Hypothalamic Area Right	Cerebellum Right	-0,957	1,223
Preoptic Hypothalamic Area Right	Medulla Oblongata Right	-1,287	1,184
Putamen Left	Gyrus Rectus Left	-0,020	-0,348
Putamen Left	Substantia Nigra Right	-1,607	1,091
Putamen Left	Gyrus Rectus Right	-0,218	-0,535
Septum Left	Amygdala Left	-0,073	-0,751
Septum Left	Parahippocampal Cortex Left	-1,055	-0,384
Septum Left	Gyrus Rectus Left	-0,005	-0,062
Septum Left	Pituitary Gland Left	-1,204	0,739
Septum Left	Pituitary Gland Right	-0,880	0,087
Septum Left	Midbrain Right	-0,887	-0,194
Septum Right	Nucleus Of The Horizontal Limb Of The Diagonal Band Right	-1,401	0,646
Septum Right	Periaqueductal Grey Substance Right	-1,765	0,544
Septum Right	Midbrain Right	-1,555	-0,130
SubFornical Organ Left	Pituitary Gland Right	-0,240	-0,374
SubFornical Organ Right	Pituitary Gland Right	-0,102	-0,056
Temporal Lobe Left	Septum Right	-1,371	-0,233
Temporal Lobe Left	Precruciate Gyrus Right	-1,495	-0,235
Thalamus Left	Posterior Sylvian Gyrus Right	-1,023	-0,824
Thalamus Left	Putamen Right	-0,639	0,336
Thalamus Left	Claustrocortex(Insula) Right	-1,006	-0,675

Conflict of interest :

The authors state that they have no conflict of interest.

Nature Research Editing Service Certification

This is to certify that the manuscript titled In vivo magnetic resonance imaging reveals the effect of gonadal hormones on morphological and functional brain sexual dimorphisms in adult sheep. was edited for English language usage, grammar, spelling and punctuation by one or more native English-speaking editors at Nature Research Editing Service. The editors focused on correcting improper language and rephrasing awkward sentences, using their scientific training to point out passages that were confusing or vague. Every effort has been made to ensure that neither the research content nor the authors' intentions were altered in any way during the editing process.

Documents receiving this certification should be English-ready for publication; however, please note that the author has the ability to accept or reject our suggestions and changes. To verify the final edited version, please visit our verification page. If you have any questions or concerns over this edited document, please contact Nature Research Editing Service at support@as.springernature.com.

Manuscript title: In vivo magnetic resonance imaging reveals the effect of gonadal hormones on morphological and functional brain sexual dimorphisms in adult sheep.

Authors: BARRIERE, ELLA, ADRIAENSEN, ROSELLI, CHEMINEAU & KELLER

Key: 9AD2-968E-8BFA-F291-9D32

This certificate may be verified at **secure.authorservices.springernature.com/certificate/verify**.

Nature Research Editing Service is a service from Springer Nature, one of the world's leading research, educational and professional publishers. We have been a reliable provider of high-quality editing since 2008.

Nature Research Editing Service comprises a network of more than 900 language editors with a range of academic backgrounds. All our language editors are native English speakers and must meet strict selection criteria. We require that each editor has completed or is completing a Masters, Ph.D. or M.D. qualification, is affiliated with a top US university or research institute, and has undergone substantial editing training. To ensure we can meet the needs of researchers in a broad range of fields, we continually recruit editors to represent growing and new disciplines.

Uploaded manuscripts are reviewed by an editor with a relevant academic background. Our senior editors also quality-assess each edited manuscript before it is returned to the author to ensure that our high standards are maintained.